الجمهورية الجزائرية الديمقراطية الشعبية
REPUBLIQUE ALGERIENNE DEMOCRATIQUE ET POPULAIRE
وزارة التعليم العالي و البحث العلمي
MINISTERE DE L'ENSEIGNEMENT SUPERIEUR ET DE LA RECHERCHE SCIENTIFIQUE
جامعة عمّار ثليجي بالأغواط
UNIVERSITE AMAR TELIDJI LAGHOUAT

كلية العلوم والتكنولوجيا
FACULTE DE SCIENCE TECHNIQUE

DEPARTEMENT D'ELECTRONIQUE

Mémoire de MASTER

Domaine : Sciences et techniques
Filière : Télécommunication
Option : Systèmes de Télécommunication

Par:

- Latar Kaouthar
- Fechkeur Meriem

THEME

Design of metamaterials biosensor antenna for the rapid detection of coronaviruses COV-19 (SARS2)

Soutenu publiquement devant le jury composé de:

Mr. Chaker Saleh	*Président*
Mr. Birane Mohoub	*Examinateur*
Mr. Bensafieddine Djalal Eddine	*Rapporteur*

Année Universitaire 2020/2021

بسم الله الرحمن الرحيم

والصلاة والسلام على اشرف المرسلين

Acknowledgments

Above all, our warmful thanks at the first place goes to Allah our lord who blessed us with grace of health ,courage , ability and patience to manage to finish this modest work within a perfect time.

Firstly, we would like to thank in particular our beloved parents they been and still the roots to our growth, and evolution, our success is considered to be the fruit of their long years of sacrifices and hardship.

We are greatly indebted to our supervisor Dr.Bensafieddine Djalal Eddine who contributed a lot in the fulfillment of this dissertation with his advice, help, continual support and encouragements.

Same thanks extend to our teachers who've helped us directly and indirectly during the years of study

Last but not least, we would like to thank gratefully the jury members whose agreed to be a part of our humble work.

Without forgetting to share thanks with everyone else who contributed to complete our happiness

Finally, to all those we love.

ملخص

تتمثل أطروحتنا في إقتراح تقنية جديدة لاستخدام هوائي للإستشعارالحيوي قائم على المواد الخارقة من أجل التشخيص السريع و المبكر لفيروس كورونا المستجد SARS-COV-2 في عينة دم مأخوذة من جسم الإنسان. تم تصميم هذا المستشعر الحيوي عدديًا من خلال تقييم التغيرات في معامل الانعكاس (S11) وفي عوامل أخرى مثل الكسب المحقق (Gain) وعرض النطاق الترددي (bandwidth). لقد استخدمنا موصلان معدنيان مختلفان لهيكل المواد الفوقية لتحليل حساسية جهاز هوائي الاستشعار الحيوي المقترح . بالنسبة للمادة الفوقية القائمة على النحاس، لقد أظهرنا أنه في حالة دم حامل للفيروس COVID-19 تحول تردد الرنين نحو نطاق تردد أعلى بحوالي 100 ميجاهرتز مقارنة بالدم الطبيعي. بينما يبلغ الحد الأقصى لفقد العودة حوالي 3.64 ديسيبل في الدم الطبيعي والدم الحامل للفيروس. أما بالنسبة للمواد الفوقية التي تعتمد على الجرافين كموصل معدني ، هناك تباين يبلغ حوالي 6.78 ديسيبل في حجم خسارة العودة بين الدم الطبيعي و الدم الذي يحمل الفيروس COVID-19.

من المأمول أن تساعد هذه الدراسة والنتائج المتحصل عليها الأطباء وعلماء الأحياء الدقيقة السريرية على مواجهة التحدي المتمثل في الكشف الفعال عن COVID-19.

الكلمات المفتاحية: SARS-COV-2، المواد الفوقية، هوائي للاستشعار الحيوي، عينة الدم، نموذج ديباي.

Abstract

Our thesis consist of proposing a new technique of utilizing metamaterials biosensor antenna for rapid diagnosis of coronavirus SARS-COV-2 in human blood samples. This biosensor was designed numerically by evaluating the variations in the reflection coefficient (S_{11}) and others parameters such as the realized gain and the bandwidth. Two different metallic conductor of our metamaterials structure has been used for analyses the sensibility of our biosensor antenna devices. For the metamaterials based on copper as a metallic conductor, we showed that in the case of COVID-19 blood, the resonance frequency shifted towards higher frequency band by about 100 MHz compared to the normal blood filled sensor. The maximum return loss contrast between the normal blood and COVID-19 blood filled sensor is about 3.64 dB. For the metamaterials based on graphene as a metallic conductor, there was a contrast of about 6.78 dB in the magnitude of the return loss between the normal blood and COVID-19 blood filled sensor.

These results are hoped to help physicians and clinical microbiologists to address the challenge for effective detection of COVID-19.

Keywords: SARS-COV-2, Metamaterials, Biosensor antenna, Blood samples, Debye model.

Résumé

Notre thèse consiste à proposer une nouvelle technique pour utiliser une antenne de biodétection basée sur des métamatériaux pour un diagnostic rapide et précoce du SRAS-COV-2 dans un échantillon de sang prélevé sur le corps humain. Ce biocapteur a été conçu numériquement en évaluant les variations du coefficient de réflexion (S11) et d'autres paramètres tels que le gain réalisé et la bande passante. Deux conducteurs métalliques différents de notre structure de métamatériaux ont été utilisés pour analyser la sensibilité de nos dispositifs d'antenne biocapteur. Pour les métamatériaux à base de cuivre en tant que conducteur métallique, nous montrons que dans le cas du sang porteur le virus COVID-19, la fréquence de résonance s'est déplacée vers une plage de fréquence plus élevée d'environ 100 MHz par rapport au capteur rempli de sang normal. Le contraste de perte de retour maximal entre le sang normal et le capteur rempli de sang COVID-19 est d'environ 3,64 dB. En ce qui concerne les métamatériaux à base de graphène en tant que conducteur métallique, il existe un contraste d'environ 6,78 dB dans l'amplitude de la perte de retour entre le sang normal et le capteur rempli de sang COVID-19.

On espère que ces résultats aideront les cliniciens et les microbiologistes cliniques à relever le défi d'une détection efficace du COVID-19.

Mots clé : SARS-COV-2, Métametriaux, Antenne de biocapteur, échantillons de sang, Modél de Debye.

Table of contents

Chapter 1

Chapter 2

Chapter 3

List of Figure

Chapter 1

Chapter 2

Chapter 3

List of table

Chapter 3

Introduction

In late 2019, severe acute respiratory syndrome coronavirus 2 (SARS-CoV-2) was first discovered and quickly transmitted via humans to humans, which proved itself as a tricky illness that can emerge in various forms and levels of severity ranging from mild to severe with the risk of organ failure and death. With the progress of the pandemic and rising number of the confirmed cases and patients who experience severe respiratory failure and cardiovascular complications, Subsequently, the World Health Organization (World Health Organization 2020) classified this coronavirus disease 2019 (COVID-19) outbreak as a global pandemic, as of now, over 168 million infected cases with approximately 3.5 million deaths worldwide have been reported (27/05/2021), Unfortunately there is no specific vaccine or drug yet available for this ongoing pandemic.

Currently, real-time polymerase chain reaction (RT-PCR) is being used widely to detect COVID-19 from various types of biological specimens, which is time-consuming, labor-intensive, this might lead to hindrance in acquiring realistic data of infectivity and community spread of SARS-CoV-2 in the population, antibody-based techniques (IgG/IgM)), on the other hand, can provide quantitative, accurate, and sensitive results, but it involves complicated and expensive instruments and long assay time. In addition, samples need to be sent to centralized labs, which significantly increase the turn-around time. Therefore, the development of biosensors is important for rapid diagnosis of COVID-19.

We are interested in this work, by the design of biosensors antenna to use as an electro-medical devices for rapid detection and diagnosis of COVID-19within few seconds, through electromagnetic-stimulated analysis of the blood drawn from the patient.

This work is divided into three chapters. The first one presents an overview of coronavirus COVID-19, then summarize the structure of the SARS-CoV-2 virus, its origin and his genome characteristics, and the current progression of SARS-CoV-2 , antibodies, diagnosis and different methodologies for early detection like biosensors which hold promising potential for point-of-care detection of COVID-19 even in asymptomatic conditions with high reliability and low cost.

The second chapter interests with characterization of homogenization metamaterials. One of the goals of this chapter is to outline a definition of metamaterial, discuss homogenization of metamaterials, and illustrate its successful implementation in diverse application such as the sensing. It also includes the effective parameters extraction methods. Finally this approach is illustrated to design and characterized our metamaterial unit cell by using Ansoft (HFSS).

In the third chapter, a metamaterial based biosensor antenna operating in the GHz frequency band is presented .The design and analysis of this biosensor antenna was performed using (HFSS) simulation software to detect the presence of COVID-19 in patient blood samples.

The electromagnetic response of our proposed biosensor antenna depends only if that the electrical properties of human blood, such as dielectric permittivity, refractive index are changed, due to the existence of COVID-19 viruses. These electrical changes could be detected from the changes of reflection coefficient (S_{11}), especially the shift in the resonance frequency of the biosensor antenna.

1. Biosensors for COVID-19 detection

1.1 Introduction

The novel Coronavirus designated SARS-CoV-2 appeared in December 2019 to initiate a pandemic of respiratory illness known as COVID-19 which caused by a novel strain of coronavirus that recognized as Sever Acute Respiratory Syndrome Coronavirus 2 (SRAS-CoV-2), it can be transmitted both by air and via direct and indirect contact; and proved itself as a tricky illness that can emerge in various forms and levels of severity ranging from mild to severe with the risk.

The virus is a member of Coronaviridae family, which contains enveloped single stranded RNA viruses. The SRAS-CoV-2 primarily attacks the respiratory system of human and occasionally causes severe pneumonia. The sever cases is also followed by multi-organ dysfunctions, respiratory failure and death.

The outbreak of Coronavirus was first reported from Wuhan, Hubei, China on the end month of 2019. Due to its rapid outbreak and quick transmission, the World Health Organization (WHO) declared it as an ongoing pandemic. The available viral influenza medicines are found to be ineffective to treat COVID-19, so there is a need of strong technology to detect and monitor public health. Early notification on symptoms of the disease is necessary and can be control up to some extent from this dreadful disease. If monitored in early stage, the infected person can undergo different therapeutic approaches. In order to scan the early symptoms of COVID-19, different techniques have been applied. Use of sensor is considered as one of the method.

Up to 23rd June 2020, about 9 million cases and almost half a million deaths were reported globally, in view of the rapid spread of COVID-19, countries across the World have adopted several public health measures intended to prevent its spread, including social distancing ,and mass gatherings have been prohibited, and lockdown measures have been imposed in many of them , allowing travel only for essential needs, and extreme antiviral disinfection measures and protocols in coping with infected patients.

This chapter provides an overview of the COVID-19 pandemic with nanomaterials and metamaterials enabled biosensing approaches that have been recently reported for the diagnosis of SARS-CoV-2.

1.2 Origin of the COVID-19 SARS-2 virus

In late December 2019, several health facilities in Wuhan, in Hubei province in China, reported clusters of patients with pneumonia of unknown cause [1]. Similarly to patients with SARS and MERS, these patients showed symptoms of viral pneumonia, including fever, cough and chest discomfort, and in severe cases dyspnea and bilateral lung infiltration[1]. Among the first 27 documented hospitalized patients, most cases were epidemiologically linked to Huanan Seafood Wholesale Market, a wet market located in downtown Wuhan, which sells not only seafood but also live animals, including poultry and wildlife[3]. According to a retrospective study, the onset of the first known case dates back to 8 December 2019[4]. On 31 December, Wuhan Municipal Health Commission notified the public of a pneumonia outbreak of unidentified cause and informed the World Health Organization (WHO).

By met genomic RNA sequencing and virus isolation from bronchoalveolar lavage fluid samples from patients with severe pneumonia, independent teams of Chinese scientists identified that the causative agent of this emerging disease is a beta coronavirus that had never been seen before[5].

This novel coronavirus pneumonia soon spread to other cities in Hubei province and to other parts of China. Within 1 month, it had spread massively to all 34 provinces of China. The number of confirmed cases suddenly increased, with thousands of new cases diagnosed daily during late January. On 30 January 2020[6], the WHO declared the novel coronavirus outbreak a public health emergency of international concern. On 11 February, the International Committee on Taxonomy of viruses named the novel coronavirus SARS-CoV-2, and the WHO named the disease COVID-19 [7].

The outbreak of COVID-19 in China reached an epidemic peak in February. According to the National Health Commission of China, the total number of cases continued to rise sharply in early February at an average rate of more than 3,000 newly confirmed cases per day. To control COVID-19, China implemented unprecedentedly strict public health measures. The city of Wuhan was shut down on 23 January, and all travel and transportation connecting the city was blocked. In the following couple of weeks, all outdoor activities and gatherings were restricted, and public facilities were closed in most cities as well as in countryside [8].

On 11 March 2020, the WHO officially characterized the global COVID-19 outbreak as a pandemic. Since March, while COVID-19 in China has become effectively controlled, the case numbers in Europe, the USA and other regions have jumped sharply. According to the COVID-19 dashboard of the Center for System Science and Engineering at Johns Hopkins University, as of 11 August 2020, 216 countries and regions from all six continents had reported more than 20 million cases of COVID-19, and more than 733,000 patients had died[9].

Although genetic evidence suggests that SARS-CoV-2 is a natural virus that likely originated in animals, there is no conclusion yet about when and where the virus first entered humans. As some of the first reported cases in Wuhan had no epidemiological link to the seafood market [10], it has been suggested that the market may not be the initial source of human infection with SARS-CoV-2. One study from France detected SARS-CoV-2 by PCR in a stored sample from a patient who had pneumonia at the end of 2019, suggesting SARS-CoV-2 might have spread there much earlier than the generally known starting time of the outbreak [11].

1.3 Diagnosis

Early diagnosis is crucial for controlling the spread of COVID-19. Molecular detection of SARS-CoV-2 nucleic acid is the gold standard. Many viral nucleic acid detection kits targeting ORF1b, N, E or S genes are commercially available. The detection time ranges from several minutes to hours depending on the technology [12] . The molecular detection can be affected by many factors. Although SARS-CoV-2 has been detected from a variety of respiratory sources, including throat swabs, posterior or opharyngeal saliva, nasopharyngeal swabs, sputum and bronchial fluid, the viral load is higher in lower respiratory tract samples [13] . In addition, viral nucleic acid was also found in samples from the intestinal tract or blood even when respiratory samples were negative. Lastly, viral load may already drop from its peak level on disease onset. Accordingly, false negatives can be common when oral swabs and used, and so multiple detection methods should be adopted to confirm a COVID-19 diagnosis. Other detection methods were therefore used to overcome this problem. Chest CT was used to quickly identify a patient when the capacity of molecular detection was overloaded in Wuhan. Patients with COVID-19 showed typical features on initial CT, including bilateral multilobar ground-glass opacities with a peripheral or posterior distribution. Thus, it has been suggested that CT scanning combined with repeated swab tests should be used for individuals with high clinical suspicion of COVID-19 but who test negative in initial nucleic acid screening[14]. Finally, SARS-CoV-2 serological tests detecting antibodies to N or S protein could complement molecular diagnosis, particularly in late phases after disease onset or for retrospective studies. However, the extent and duration of immune responses are still unclear, and available serological tests differ in their sensitivity and specificity, all of which need to be taken into account when one is deciding on serological tests and interpreting their results or potentially in the future test for T cell responses.

1.4 Testing and Pharmacological Approach

Appropriate and specific diagnostic techniques are important to detect the presence of the SARS-CoV-2 virus in the human body early. Although many laboratory tests have been implemented, screening protocols should be adapted to the local situation and the guideline reviewed and update on the basis of the last information available.

In this regard, the World Health Organization reviewed and published a paper containing guidelines to follow and practice. Together, along with the ordinary tests, these provide further and specific information about the real existence of this specific virus in the samples analyzed.

1.5 COVID-19 (Coronavirus) Molecular (Swab) Test

This test uses a long swab to collect material, including physical pieces of coronavirus, from the back of the nose where it meets the throat. A positive result indicates that viral genetic material is present, but it does not indicate that bacterial or other infections also are present. A negative result indicates that the SARS-CoV-2 virus that causes the COVID-19 disease was not found. It is possible to have a very low level of the virus in the body with a negative test result.

This test is needed to identify the presence of the SARS-CoV-2 virus that causes the COVID-19 disease.

1.6 COVID-19 (Coronavirus) Antibody (Serology) Tests

1.6.1 Spike Protein IgG Antibody Test

This is a blood test. It is designed to detect IgG antibodies specific for nucleocapsid protein of the coronavirus that causes the disease called COVID-19. Antibodies are proteins produced by the immune system in response to an infection and are specific to that particular infection. They are found in the liquid part of blood specimens, which is called serum or plasma. Nucleocapsid Protein and IgG Spike Protein IgG antibody tests may either be ordered together or separately.

Having the nucleocapsid protein antibody test is helpful if :

This test detects IgG antibodies that develop in most patients within seven to 10 days after symptoms of COVID-19 begin. IgG antibodies remain in the blood after an infection has passed. These antibodies indicate that you may have had COVID-19 in the recent past and have developed antibodies that may protect you from future infection. It is unknown at this point how much protection antibodies might provide against reinfection.

1.6.2 Spike Protein IgM Antibody Test

This test detects IgM antibodies. IgM is usually the first antibody produced by the immune system when a virus attacks. A positive IgM test indicates that you may have been infected or that you have recently been vaccinated and your immune system has started responding to the vaccination and that your immune system has started responding to the virus. When IgM is detected you may still be infected, or you may have recently recovered from a COVID-19 infection.

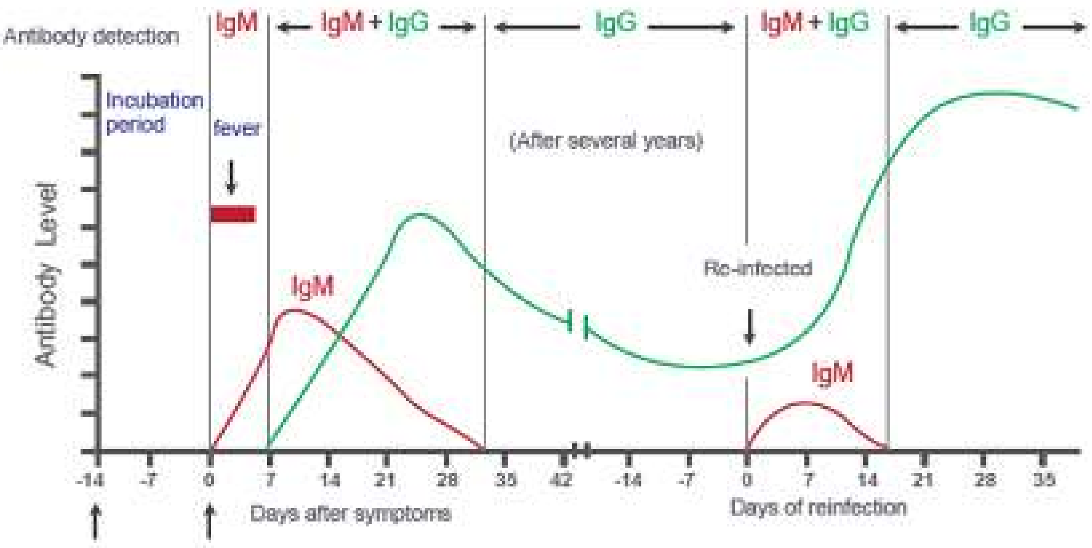

Figure 1-1:Variation-of-the-Levels-of-SARS-CoV-2-RNA-and-Antigen-IgM-and-IgG-after-infection.

The level of IgM antibody begins to rise after 1 week after the initial infection, while the IgG appears later than IgM (usually in 14 days after infection) and can last for 6 months or even several years, which means that the IgG serves as an indicator of previous infection.

Suspected patients that are infected by SARS-CoV-2 can be rapidly identified by simultaneous monitoring of IgM and IgG.

1.7 Biosensors for COVID-19 detection

We are currently facing the COVID-19 pandemic which is the consequence of severe acute respiratory syndrome coronavirus (SARS-CoV-2). Since no specific vaccines or drugs have been developed till date for the treatment ofSARS-CoV-2 infection, early diagnosis is essential to further combat this pandemic. In this context, the reliable, rapid, and low-cost technique for SARS-CoV-2 diagnosis is the foremost priority. At present reverse transcription polymerase chain reaction (RT-PCR) is the reference technique presently being used for the detection of SARS-CoV-2 infection. However, in a number of cases, false results have been noticed in COVID-19 diagnosis. To develop advanced techniques, researchers are continuously working and in the series of constant efforts, nanomaterial senabled biosensing approaches can be a hope to offer novel techniques that may perhaps meet the current demand of fast and early diagnosis of COVID-19 cases.

1.7.1 Biosensors

Biosensors are analytical techniques that could be used as simple, real-time and effective devises for the detection of various infectious diseases, that convert biological reactions into measurable signals, and can be broadly defined as devices that are used to detect the presence or concentration of a biological analyte [15], This may take the form of a biomolecule, a biological structure or even larger structures such as cells and microorganisms Where Bio-receptors act as sensing elements Due to their biochemical properties making them sensitive and selective for biomarkers detection with minimum interference with other microorganisms or molecules present in the tested sample , they are essential in many areas, such as disease diagnostics, environmental monitoring, and food safety, and they are also vital tools in the investigation of biological phenomena. Fluorescence-based methods have proven useful in analyzing both genomic and proteomic microarrays [16,17] and in imaging, including single molecule detection inside living cells [18].

The biosensors research field began in 1962 with the designing of glucose oxidase biosensor, which was introduced by Clark and Lyons. After that, numerous applications of sensors and biosensors have been described [19]. Biosensors have been invented over decades ago by biotechnologists to detect bacteria and viruses by recognizing biomarkers or characteristics of the targets.

1.7.2 Biosensor Applications

Since their development in the early 1950's, Biosensors have become very important in the fields of medicine, clinical analysis and in general health monitoring. The advantages of biosensors over lab based equipment are as follows:

- Small size.
- Low cost.
- Quick results.
- Very easy to use.

Apart from the desired medicine and health based applications, Biosensors have also found critical applications in several other fields like industrial processing, agriculture, food processing, pollution control etc.

So, the following is a small list of the potential fields where Biosensors are frequently used.

- Medicine, Clinical and Diagnostic Applications.
- Environmental Monitoring.
- Industrial Applications.
- Food Industry.
- Agriculture Industry.

These sensors have become very popular, and they are applicable in different fields which are mentioned below:

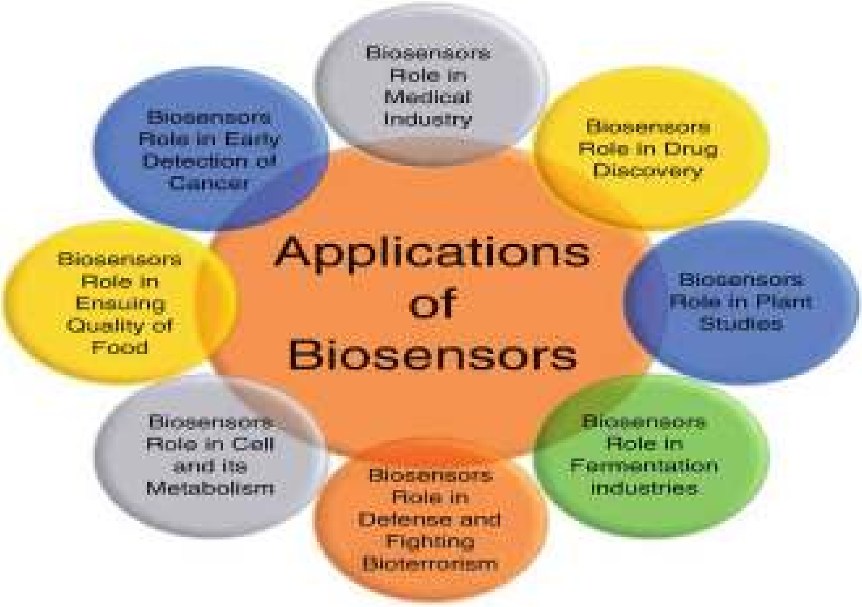

Figure 1-2: Applications of biosensors in different facets.

1.7.3 Biosensors Role in Medical Industry:

The flared up of COVID-19 throughout the globe has terrified people and attract more attention towards health. It made a challenge to the researchers in development of medicines and vaccines or advanced methods to prevent the spreading out of the virus. A thermal scanner is used to detect the body temperature but unable to detect the virus.

A biosensing device too utilized in form of a smart band and have the functional properties to detect body temperature. An optical sensor which is designed by combining two different kind of effect i.e., a visual and a thermal is use to detect the virus. A powerful biosensor like cell-based biosensor have the ability to detect some species and amplification of those species, molecular biosensors to monitor the virus in the environment and also plays a vital role in the pharmaceutical industry, environmental and monitoring of food analysis etc. As a matter of fact, scientists have focus on working of new technology and produce a rapid diagnostic sensor that can detect the SARS-CoV-2 within a minute. Jing Wang, along with his fellow researchers, developed a new sensor in the form of an optical sensor whose receptor acts as a complementary sequence for the RNA sequence and detect the virus. Biosensor with plasmonic photothermal effect also developed, which inhibits the binding of non-complementary sequence to the sensor's DNA strands by promoting local temperature. Cell-based biosensors are also used to detect the species and their amplification into an optical and electrical signal through a processor [14]. It also used in wide range conditions like pH values and temperature.

Moreover the Studies also revealed that SARS-CoV-2 could transmit through the air, and the cell-based biosensor may detect it, but these sensors have not been proven till now. Many more techniques should develop to diagnose the virus at less cost. Thus, tools like biosensor which can diagnose rapidly are necessary to prevent the rapid spreading of the virus. Biosensor and other technology should improve with high sensitivity, reproducibility, etc.

1.8 SARS-CoV-2 and its consequences on COVID-19 pandemic

1.8.1 Structure of the SARS-CoV-2

SARS-CoV-2, a β-coronavirus has been identified as a single positive strand RNA genome [21].It consists of four different structural proteins namely spike (S), envelope (E), matrix (M), and nucleocapsid (N) [figure 1-3]. Through the phylogenetic analysis of SARS-CoV-2, the genomic similarities about 80% and 50% have been noticed with severe acute respiratory syndrome virus (SARS-CoV) and middle east respiratory syndrome virus (MERS-

CoV), respectively, More importantly, SARS-CoV-2 expresses the genomic similarity of about 96% with the bat coronavirus RaTG13, and hence itis a matter of intense debate that SARS-CoV-2 may perhaps have originated from the bat[21]. Many studies have explored that SARS-CoV-2 exploits the angiotensin converting enzyme-II (ACE2), as a receptor for the cellular entry. Further, ACE2 has been recognized for high affinity of the spike protein (S) of SARS-CoV-2[22].

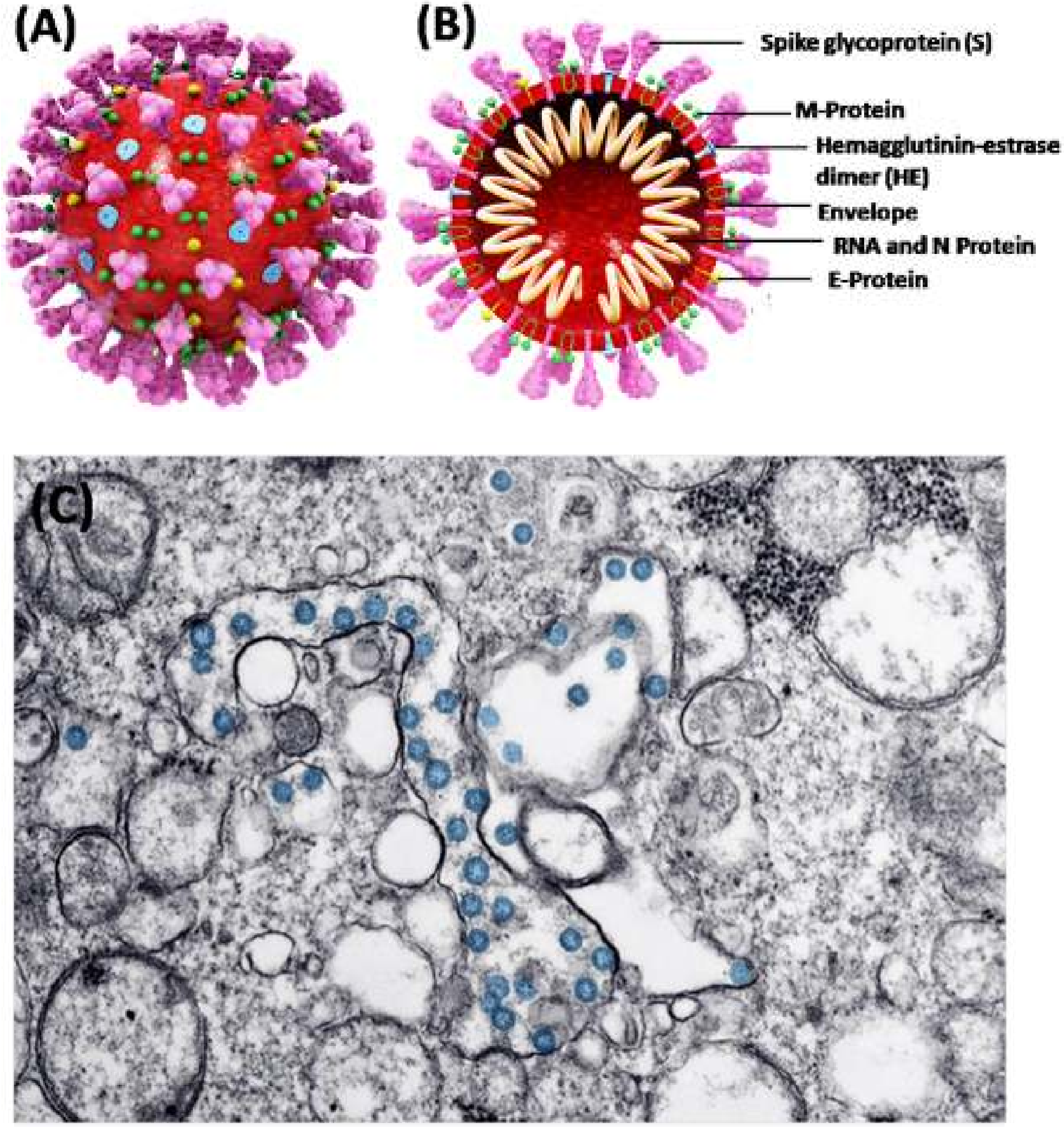

Figure 1-3 : (A) 3D structure of SARS-CoV-2, (B) Cross sectional representation of the viral structure with its proteins, (C) Transmission electron microscope image of SARS-CoV-2.

Respiratory droplets and fomites are the possible medium and are responsible to transmit COVID-19 diseases. As per the clinical studies conducted on COVID-19, it has been estimated that SARS-CoV-2 canhave the incubation period of up to 24 days. Whereas, a high basic reproductive number has been determined to be ~3.77[23]. In most of the clinical cases, this virus has been detected in the upper respiratory tract, suggesting nasopharynx as the main site of replication. Nevertheless, the gastrointestinal symptoms have been noticed in a number of patients suffering from COVID-19 [24]. Moreover, even when the nasopharyngeal sample was found to be negative, the RNA trace of SARS-CoV-2 could be detected in rectal swabs [25]. These observations clearly suggest that transmission of SARS-CoV-2 through fecal-oral is also possible. It has been reported that usually, lungs are the most affected organs by SARS-CoV-2, but other organs like brain may also be severely infected. Gandhi et al, have reported that through the olfactory bulb, the central nervous system (CNS) is most likely to be infected by SARS-CoV-2 (Gandhi et al ,2020). Consequently, SARS-CoV-2 can easily target the thalamus and brain stem, leading to infection in the respiratory center of the brain.

Thus, it is possible that SARS-CoV-2 can infect the respiratory center of the brain and is therefore, responsible for the respiratory break down in patients suffering from COVID-19. Besides this, the spectrum of this disease is partly recognized in patients. And, both the symptomatic and asymptomatic cases have been noticed. In asymptomatic case, no specific symptoms have been identified. Some of the symptoms may include respiratory issues, pneumonia, fever, cough and dyspnea. On the other hand, an asymptomatic patient is capable of transmitting this disease. However, technically one can say that the asymptomatic individuals are more dangerous since they can spread the disease unknowingly. Therefore, the development of a lowcost and rapid diagnosis technique is imperative and is urgently needed to identify the infected patients to further prevent and control this pandemic.

In this context, nanomaterials enabled biosensing approaches can be imperative and are expected to fulfill the current demand for early, rapid and low-cost point- of- care diagnostic techniques for COVID-19 detection. As discussed in the next section chemical properties of nanomaterials can be a potential to design ultra-sensitive biosensing techniques for respiratory viral infections. In the meantime, to avoid the infection through SARS-CoV-2, the only options that an individual should follow are the precautionary measures.

1.9 Nanomaterials-enabled biosensing of respiratory viral infection (MERS-CoV, SARS-CoV, SARS-CoV-2)

Recent advancements in the field of nano-biotechnology have given birth to advanced techniques for diagnosis and therapeutic applications [26]. In particular, properties of nanomaterials including high surface-to-volume ratio, quantum size effects, high adsorption and reactive capacity as compared to their bulk form are imperative to design biosensing techniques. Moreover, the size and shape of nanomaterials can be easily tailored, and, therefore, surface modification/immobilization with numerous biological species via covalent or non-covalent bonding are possible to enhance the biosensing characteristics in terms of low-detection limit (in creased up to several order of magnitudes), high sensitivity, selectivity and rapid response towards the sample analytes.

Nevertheless, one of the biggest challenges in designing of biosensors (e.g. DNA/RNA) is to capture signal of very low magnitude which takes place between the biological species (bio-receptors and analytes).

To overcome this issue, nanomaterials can be used as labels to achieve the significant enhancement of signal, high enough to be easily detectable.

Labeling can be done using metal nanoparticles (Au NPs/Ag NPs) and quantum dots (Cd/Pb) by attaching on the targeted DNA/bio recognizing probe [27]. The synergic effect due to nano-labeling results in significant amplification of the electrochemical signal and therefore, it is possible to develop ultra sensitive and highly selective labeled-bio-sensing techniques.

In this context, biosensors for the diagnosis of viral infected diseases are being developed. Biosensors can be utilized to determine the virus-mediated infections that have been categorized into four major groups including (i) nucleic acid (ii) anti-body (iii) aptamer and (iv) antigen-dependent[28]. Thus, taking the advantages of the numerous physicochemical properties of nano-dimensions specifically electrical, optical, magnetic, and optomagnetic, attempts have been made to develop nano-enabled biosensing techniques for detection of virus, responsible for respiratory infections (MERS-CoV, SARS-CoV and SARS-CoV-2).

Layqah et al [29], reported an electrochemical immune-sensor prepared by using AuNPs modified carbon electrode and the recombinant spike protein S1 as the biomarker for the detection of MERS-CoV. This immune-sensor has been found to be capable of simultaneous detection of different coronavirus (CoVs) including MERS-CoV and human corona virus (HCoVs). This biosensor exhibits liner response as 0.001 to 100 ng.mL−1 and 0.01 to 10,000 ng.mL−1 for the detection of MERS-CoV and HCoV, respectively. And the detection limit was determined to be 1.0 and 0.4 pg.mL−1 for MERS-CoV and HCoV, respectively. This assay can be performed within 20min and successfully employed to detect MERS-CoV and HCoVs protein in spiked nasal samples. Using AuNPs a label-free colorimetric biosensing approach has been reported for the detection of MERS-CoV. This colorimetric assay is based on the detection of DNA that employs disulfide induced self-assembly and the MgCl2 salt-induced aggregation and prevention of AuNPs in the absence and presence of the target, respectively. The MgCl2 induced aggregation of AuNPs leads to change in the optical properties and thereby detects the presence of MERS-CoV. The LOD of the colorimetric assay was calculated to be1 pmol/μL (6 × 1011 copies/μL), and the detection of MERS-CoV could be done within 10 min.

Ishikawa et al [30], reported a label-free In2O3 nanowires based FET biosensor that employed antibody mimic proteins (Fibronectin, Fn) to detect N protein, a biomarker of SARS. This FET biosensor worked on the impedimetric effect and was capable of detecting the N protein concentration at subnanomolar having a response time ~10 min. Martinez-Paredes et al, designed a genosensor using AuNPs modified screen-printed carbon electrodes for the detection of SARS virus. This genosensor exhibited a linear response in the range of 2.5 to 50 pmol/L having LOD2.5 pmol/L and sensitivity as 1.76 mA/pmol/L towards the biotinylated target. A technique based on the localized surface plasmon coupled fluorescence (LSPCF) fiber-optic enabled biosensing of the recombinant N protein (SARS-CoV-N) using AuNPs has been reported [Huang et al ,2009]. This LSPCF fiber-optic enabled biosensor exhibited LOD of1 pg/mL in the human serum with a linear response, 0.1 pg/mL to1 ng/mL. Moreover, compared to the enzyme-linked immunosorbentassay (ELISA), the LSPCF fiber-optic biosensor exhibited 104-fold enhanced LOD and thus may be helpful for the early diagnosis of SARS infection.

And it is anticipated that using such fiber optics based nanoenabled biosensing can detect the viral load as small as 106 particles/ mL within 15 min. These studies suggest that nanomaterials-enabled biosensing can be potential approach for the early and rapid detection of the virus originated respiratory infections.

1.10 Biosensors for COVID-19 diagnosis

1.10.1 Gold nanostructures enabled-biosensing

Owing to exceptional physicochemical properties, gold-based nanostructures have been widely employed for biomedical applications. Particularly, gold nanostructures have been exploited as the signal transducers in terms of optical signal amplifier, current amplifier, and resonance light scattering to fabricate biosensors for virus detection [31]. A unique dual-functional biosensing platform based on plasmonic effect for the sensing of SARS-CoV-2 has been developed by Qiu et al [32]. The developed biosensor exploits the combination of plasmonic photothermal (PPT) and the localized surface plasmon resonance (LSPR) effect. This biosensor was designed using two-dimensional gold nano-islands (AuNIs) [2D-AuNIs] chip following the self-assembly of thermally de-wetted gold (Au) nanofilmon the BK7 glass surface, wherein the Au-film was firstly prepared by magnetron-sputtering. Further, 2D-AuNIs were functionalized with the complementary DNA receptors, leading to sensitive detection ofSARS-CoV-2 facilitated by nucleic acid hybridization. To enhance the sensing properties laser beam was allowed to fall at two different angles and hence it was possible to excite the plasmonic resonances of PPT and LSPR at two different wavelengths. In addition, the in situ PPT enhancement was recorded to significantly improve the hybridization kinetics and thus specific detection of nucleic acid, resulting in accurate discrimination between the different gene sequences. Thus, the developed biosensor was capable of real-time as well as label-free detection of desired virus sequences. The detection limit for the biosensor was calculated to be 0.22 pM [entire RNA strands ~2.26 × 104 copies].

The colorimetric assay can be a simple and reliable approach for the naked-eye detection of viral infectious diseases, requiring no sophisticated technique. Using AuNPs capped with thiol-modified antisense oligonucleotides (ASOs) [AuNPs-ASOs], a colorimetric biosensing approach has been reported for the detection of SARS-CoV-2 (Moitra et al., 2020). The AuNPs-ASOs enabled biosensing was specific for the nucleocapsid phosphor protein (N-gene) from the RNA sample (oropharyngeal swab) and, therefore, can be utilized to detect the SARS-CoV-2 infection within 10 min. The colorimetric detection involved a phenomenon wherein AuNPs-ASOs nanostructures were selectively agglomerated in the presence of the targeted RNA sequence of SARS-CoV-2, leading to a red-shift in the UV-absorbance spectrum owing to the SPR effect. Further, it was found that the addition of RNaseH was responsible for cleaving the RNA strand from the RNA–DNA hybrid. And it was thus possible to visually detect precipitation from the solution due to additional agglomeration of

AuNPs. Figure 1-, shows a schematic representation of the mechanism for the selective naked-eye detection of SARS-CoV-2. Moreover, the selectivity of the developed colorimetric assay was investigated towards the MERS-CoV viral RNA and the detection limit of 0.18 ng/µL for SARS-CoV-2 RNA were determined along with the dynamic range of 0.2–3 ng/µL (Moitra et al., 2020). In another study, a similar colorimetric dependent biosensing has been reported to detect RdRp gene of SARS-CoV-2. This assay exhibited LOD of 0.5 ng for the SARS-CoV-2 RNA and was capable to detect SARS-CoV-2 infection in the human nasopharyngeal sample within30 min. Moreover, the specificity of this colorimetric assay was investigated using a cervical DNA sample [obtained from Human papillomavirus infected women] exhibited selective detection of SARS-CoV-2.

A lateral flow immunoassay (LFIA) prepared by using AuNPs which simultaneously detected immunoglobulin M (IgM) and IgG antibodies of SARS-CoV-2 was reported (Li et al., 2020b). In this assay, the testing strip was prepared using the NC membrane, where anti-human-IgM, anti-human-IgG, and anti-rabbit-IgG (control) were immobilized at three different test lines. Thereafter, conjugation padwas sprayed using the mixture of AuNPs-COVID-19 recombinant antigen conjugate and AuNPs rabbit-IgG. This LIFA could detect the SARS-CoV-2 infection within 15 min using the human blood sample. Besides, owing to the capability of simultaneous detection of IgM and IgG, it is possible to diagnose COVID-19 cases in patients at different infection stages. Further, using the blood sample of the COVID-19 patients, it was noticed that the LIFA exhibited good clinical detection sensitivity (88.66%) and specificity (90.63%), and therefore may be helpful to rapid detection of COVID-19 infections.

Mahari et al [33], reported Au-NPs based electrochemical biosensor to detect COVID-19 (spikeS1 protein) antigen. This biosensor was prepared using fluorine-doped tin oxide (FTO) based substrate wherein Au-NPs were used as signal amplifier owing to very high electrical conductivity. To prepare the biosensing platform, firstly Au-NPs having size ~29 nm were drop cast, and subsequently, the monoclonal antibodies of COVID-19 [COVID-19Ab] were immobilized to fabricate FTO/AuNPs/COVID-19Ab immune-sensor. The biosensing performance of the FTO/AuNPs/COVID-19Ab was also compared with COVID-19Ab immobilized screen-printed carbon electrode (SPCE). Further, electrochemical performances of both types of immune-sensors were determined towards the specific COVID-19 antigen (spike protein) [COVID-19Ag]. The specific interaction between COVID-19 antibody (Ab) and COVID-19Ag led to the change in electrical conductivity and therefore increase in current was measured for varying concentrations of COVID-19Ag [1 f. to 1 μM]. The detection limit of FTO/AuNPs/COVID-19Ab immune-sensor was determined to be 10 f. for COVID-19Ag detection. The interference study was also performed in the presence of different viral antigen (Ag) including HIV, JEV, or AIV and the observed results revealed that FTO/AuNPs/COVID-19Abimmune-sensor had good selectivity towards the COVID-19Ag (spike protein). In addition, the repeatability test revealed that the FTO/AuNPs/COVID-19Ab immune-sensor could be used up to 3 times, and could be utilized to detect COVID-19Ag concentration up to 120 fM. This immune-sensor was found to be stable up to 21 days. Apart from this, the performance of the screen-printed carbon electrode (SPEC) based biosensor [SPCE/COVID-19Ab] was investigated using COVID-19Ag (spike protein) in spiked saliva sample. The SPCE/COVID-19Abelectrode-based sensing device exhibited limit of detection as 90 f. and the rapid response time of ~1 min. Thus, it could be used for the rapid diagnosis of COVID-19 patient.

Similarly, Xiang et al[34] in their study evaluated the biosensing efficiency of colloidal gold-immuno-chromatographic (GICA) and enzyme-linked immunoassay (ELISA) kit for the detection SARS-CoV-2 infection. It was noticed that the GICA kit that relied on the combined detection of GICA-IgM and GICA-IgG (IgM and IgG antibodies) was 82.4% sensitive. On the other hand, ELISA kit showed a sensitivity of 87.3%.

Moreover, both the GICA and ELISA kits were 100% specific in case of normal patients and no significant difference between these two kits could be noticed. This study suggests the feasibility of colloidal gold NPs to prepare immuno-chromatographic kit that may assist to relieve huge pressure of the clinical diagnosis of COVID-19 cases through rRT-PCR based technique.

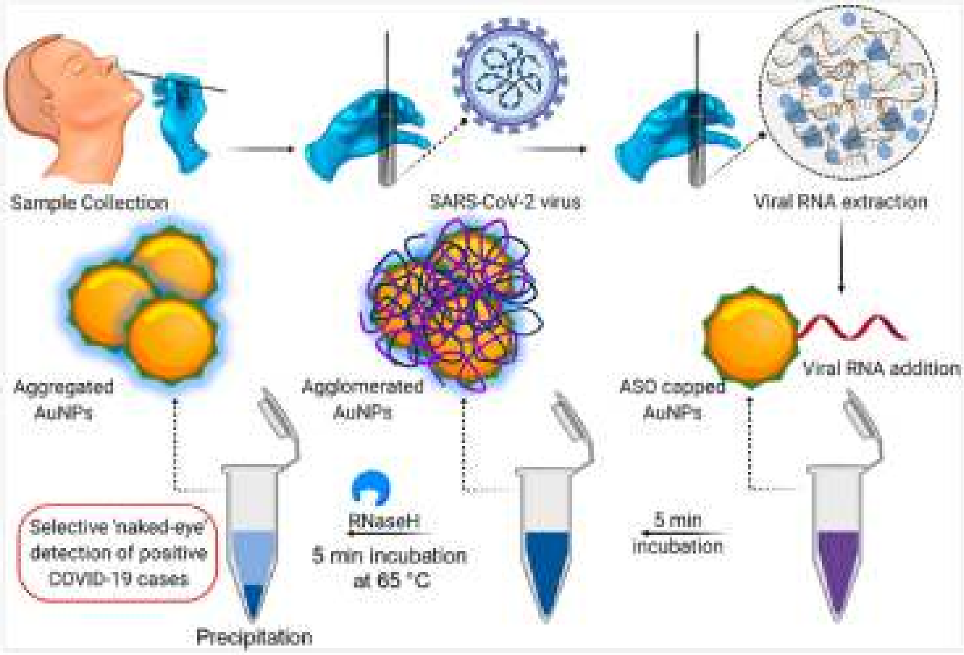

Figure 1-4 : Schematic representation for the Selective Naked-Eye Detection of SARS-CoV-2 RNA Mediated by the Suitably Designed ASO-Capped AuNPs.

1.10.2 Lanthanide-doped polysterene NPs enabled biosensing

Lanthanides possess unique electronic configuration, enablel anthanide-doped NPs numerous interesting optical characteristics including long luminescence life-times, large and sharp emission bands.

Specially, owing to their long luminescence life-times, lanthanide doped NPs have been widely used for highly sensitive biosensing applications[35]. Using lanthanide-doped NPs, LFIA based biosensor has been reported as the point of care diagnostic for infectious agents. In a study, LFIA based biosensing for the diagnosis of SARS-CoV-2 has been developed by Chen el al [36].

The developed LFIA relies on the principle to detectanti-SARS-CoV-2 IgG in human serum sample. This biosensing platform was fabricated using lanthanide-doped polystyrene nanoparticles (LNPs), prepared by mini-emulsion polymerization method. Further, surface modifications of LNPs that acted as the fluorescent probe was done using mouse anti-human IgG antibody (MH-IgG) and rabbit IgG (R-IgG) following EDC/NHS chemical reaction.

A nitrocellulose membrane was used as the template to immobilize a recombinant nucleocapsidphospho-protein of SARS-CoV-2, responsible to confine the specific IgG. figure 1-, illustrates a schematic diagram, showing sequential steps for the fabrication process of LFIA. The fabricated LIFA could detect anti-SARS-CoV-2 IgG in human serum approximately in 10 min. Further, to validate the clinical application of LIFA, these authors compared results of the anti-SARS-CoV-2 IgG detection through the RT-PCR technique.

Itwas noticed that the results through LIFA were the same as obtained through RT-PCR technique except for one sample, which showed the contrary result. Thus, the authors affirmed that though the developed LFIA did not yield accurate quantitative results due to non-availability of any anti-SARS-CoV-2 IgG standard, it can be of high interest for rapid diagnosis of the suspicious COVID-19 cases.

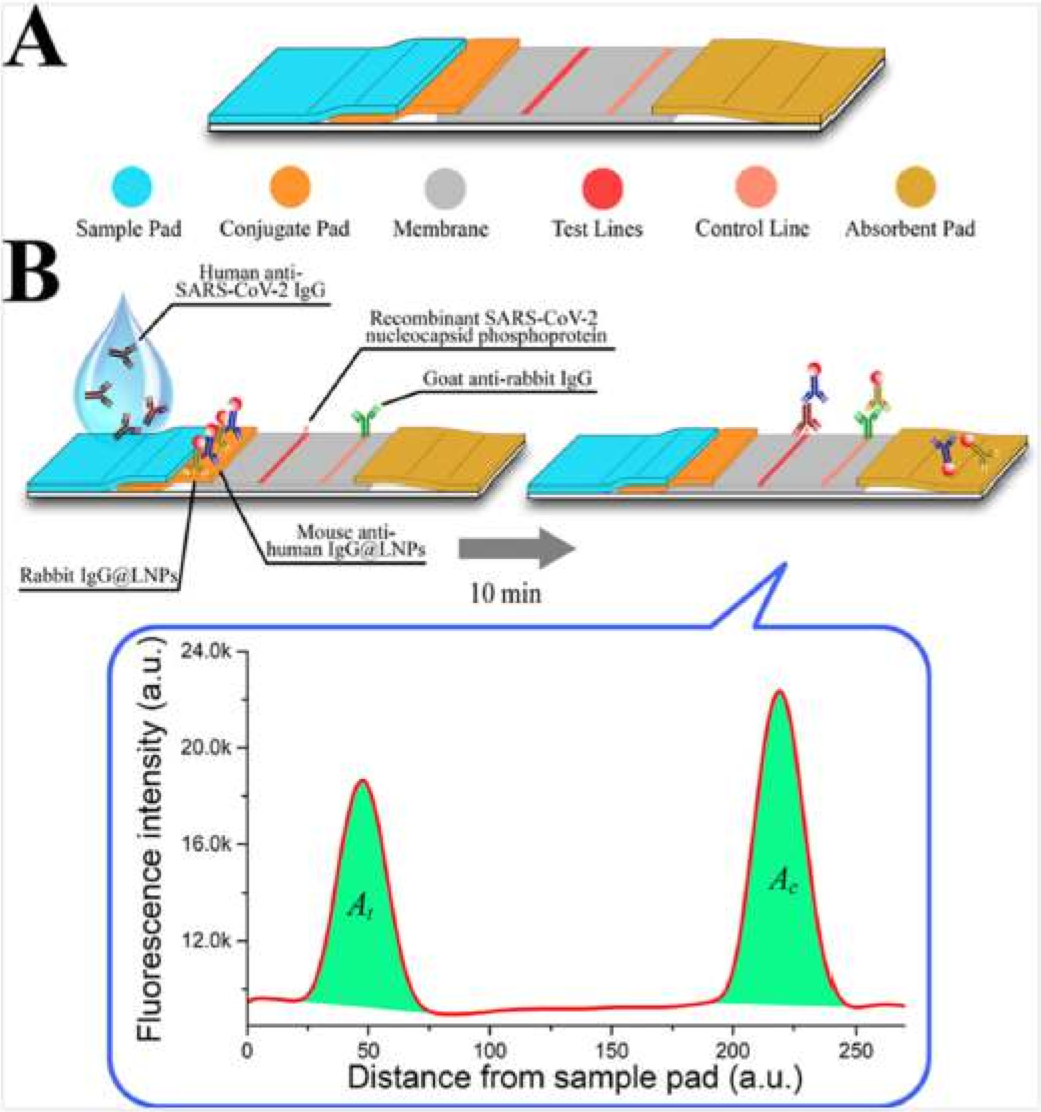

Figure 1-5 : Design and fabrication of the developed LFIA assay. (A) Lateral flow test strip. (B) Assay.

1.10.3 Graphene enabled-biosensing

Graphene, 2D hexagonally arranged carbon based single atom thick layer has proven its worth towards the development of advanced biosensing platforms[37]. This is mainly because of numerous exceptional properties such as high specific surface area, high electrical, and ionic mobility, thus, it has the potential to develop ultra sensitive biosensors [38]. By exploiting these properties of graphene, Seo et al[39] developed a field-effect transistor (FET) based biosensing platform to detect SARS-CoV-2 in human nasopharyngeal swabs. The FET-based biosensing platform was developed by transferring graphene into the SiO2/Si substrate following the wet-transfer method. Further, this graphene based-FET device was possible to develop by using the photolithography technique. Subsequently, the graphene surface was coated with a specific antibody of SARS-CoV-2 spike protein to finally prepare the FET-based biosensing device. The clinical application of the FET-based biosensing device was investigated using different sample analytes e.g. antigen protein, cultured virus, and nasopharyngeal swab of COVID-19 patients. Detection of SARS-CoV-2 spike protein was measured at the concentration of1 fg/mL in phosphate-buffered saline whereas 100 fg/mL in case of the universal transport medium. This graphene-based FET sensor exhibited LOD, 1.6 × 101 pfu/mL, and 2.42 × 102 copies/mL in case of SARS-CoV-2 spiked culture and clinical samples, respectively [figure 1-6]. It may be noted that there was no measurable interference that could be detected with MERS-CoV antigen, suggesting practical application for diagnosis of COVID-19 patients[39].

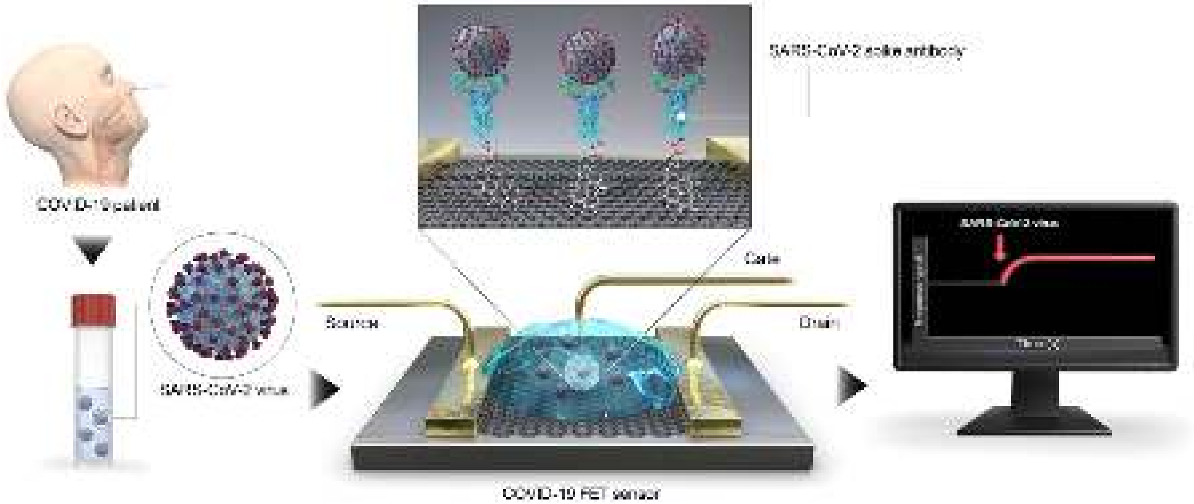

Figure 1-6 : Schematic diagram of COVID-19 FET sensor.

In addition, the California Institute of technology (Caltech) researchers have developed a standalone unit that uses a test to combine multiple data to help detect and diagnose individuals suspected of being infected with COVID-19. The device integrates a multiplexed test along with a low-cost sensor which could be used for the at-home diagnosis of a COVID-19 infection.

The researchers say that only a small volume of saliva or blood needs to be used in order to receive a rapid analysis and result within 10 minutes. Additionally, the design and usability of this technology means that there is no need for medical professionals to be involved to use it.

Figure 1-7 : The SARS-CoV-2 RapidPlex.

The new sensor was developed within the lab of Assistant Professor, Wei Gao, in the Andrew and Peggy Cherng Department of Medical Engineering. Previous work by Gao and his research team was centered on the development of wireless sensors that could monitor health conditions such as gout. Stress levels could also be measured with these devices through the detection of specific biological components in blood, sweat, or saliva. Previous models of the sensor, now adapted to detect COVID-19, were impregnated with antibodies for the hormone cortisol. This hormone is associated with stress and uric acid, which can cause gout at high concentrations.

Gao's latest sensor, the SARS-CoV-2 RapidPlex, is made up of graphene structures along with antibodies and proteins that help with the detection of coronavirus. An antibody is a large Y-shaped protein that is produced by the immune system to identify and neutralize foreign matter entering the body such as viruses and bacteria. In particular, antibodies recognize a specific molecule of a particular pathogen (such as coronavirus), known as an antigen. The graphene structures of the sensor have very small pores that take up a large surface area. This enables accurate detection of low levels of certain compounds and matter such as the antigens of coronavirus. Data collected with the RapidPlex can be wirelessly transmitted to a mobile user interface.

1.10.4 Metamaterial enabled-biosensing

Metamaterials are man-made materials, composed of artificially structured unit cells that are designed of conventional materials and usually (but not necessarily) arranged in periodic fashion.

A potential application field of metamaterials is on biosensing. Conventional biosensors (such as those based on electro-mechanical transduction, fluorescence, nanomaterials, and surface plasmon resonance) often involve labor-intensive sample preparation and very sophisticated equipment.

In recent years, researchers have proposed to use metamaterials as candidates for detection of highly sensitive chemical, biochemical and biological analytes. For example, Lee et al[40] studied the possibility of using split-ring resonators (SRRs) for biosensors. The basic principle is based on the fact that SRR can be considered to be a simple LC circuit with a response frequency of $f = 1/2\pi\sqrt{LC}$, which shows that the resonant frequency varies in terms of the changes in the inductance L and/or capacitance C. Hence the resonant frequency of the SRR shall be shifted before and after the introduction of biomaterials. Planar metamaterials were proposed to serve as thin-film sensors recently by O’Hara et al[41]. They found that a resonant frequency response can be tuned through metamaterial designs. Though their metamaterial design can only detect thin films having a thickness less than 100 nm, their work presents a promising utlook for THz sensing technology.

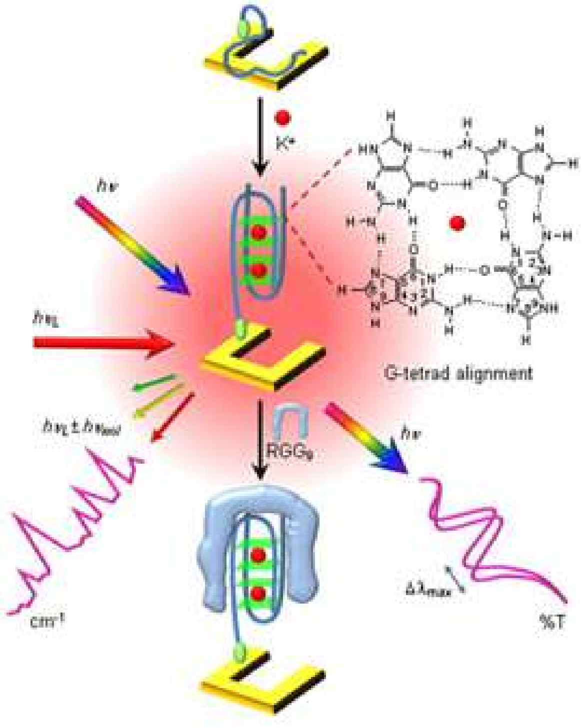

Figure 1-8 : Schematic illustration of Vis-NIR SRR metamaterials as dual transducing mode nanosensor for the detection and identification of biomolecules.

Yadgar et al [42], proposed a new technique of utilizing metamaterials-based sensor for rapid diagnosis ofcovid-19 through electromagnetic-stimulated analysis of the blood drawn from the patient. The sensor was inspired by a coronavirus in plane-shaped design with presume that its circular structure might produce abroader interaction of the electromagnetic waves with the blood sample. The sensor was designed numerically and tested experimentally by evaluating variations in the reflection coefficient (S_{11}) and transmission coefficient (S_{21}) of the waves at resonant frequency. Results of covid-19 relevant blood sample showed a pronounced shift in the main resonant frequency of about 740 MHz compared to that of the control blood sample.

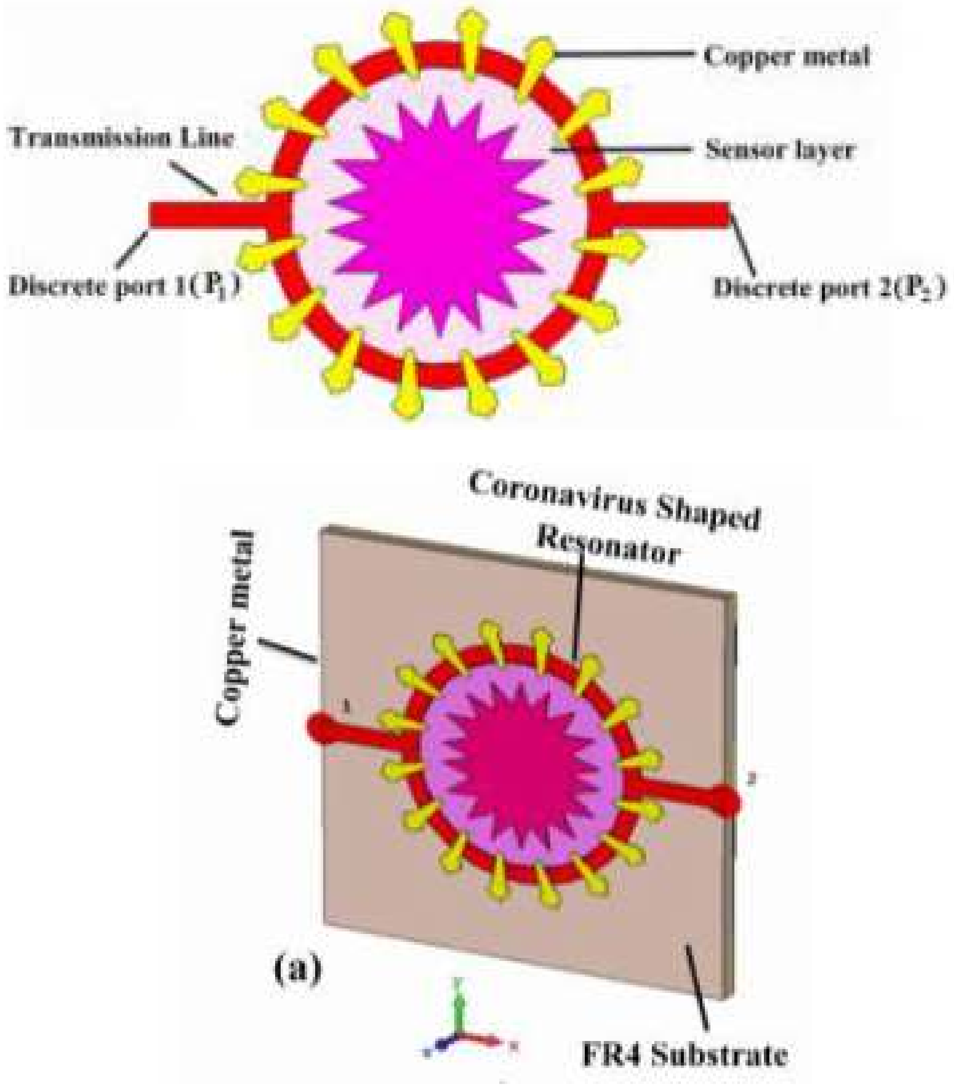

Figure 1-9 : Prospective view of the proposed metamaterials-based sensor [42].

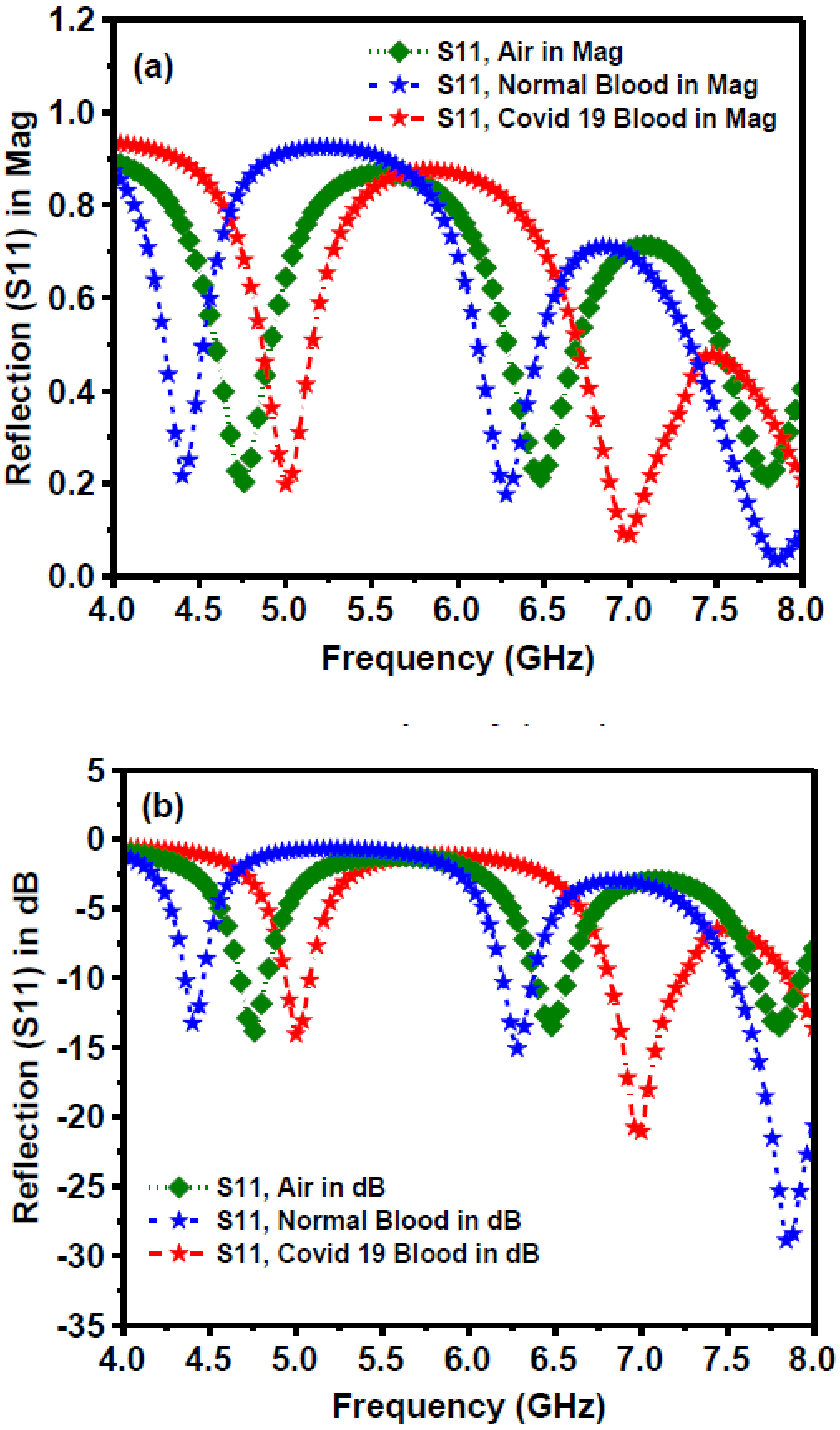

Figure 1-10 : results for air, normal blood and COVID-19 blood samples: (a) reflection (S11) in magnitude and (b) reflection (S11) in decibel[42].

Regarding the blood of COVID-19 patient (COVID-19 blood henceforth), data of dielectric constant and loss tangent was calculated based on their decrement by 5%compared to that of the normal blood at high frequency, i.e. the plateau region. It was evidenced from literature that dielectric permittivity of blood is decreased when the count of lymphocytes is increased[42][43]. Ermolina et. al. used different mixture formulas to conclude that the relationship between static dielectric permittivity of blood as functions of volume fraction of cells is almost linear from 0% to about 20% of cells volume fraction[43]. It was reported that in most cases of COVID-19, lymphocyte percentage (LYM %) was reduced to lower than 5% [33]. Furthermore, when the immunoglobulin/antibody proteins are just started to produce by the immune system in response to theCOVID-19 antigen, the dielectric permittivity is further lowered. This is because it was evidenced that the increase of IgG and IgM immunoglobulins has led to the decreased capacitance and dielectric permittivity of blood [43].

Hence, 5% smaller values of dielectric permittivity and loss tangent compared to those of the normal blood were imported into the CST software to represent the electrical response of COVID-19 blood. Figure 1-, shows the reflection coefficient for air, normal blood and COVID-19 blood samples. It can be seen that the resonant frequency has three different peaks at 4.38 GHz, 6.26 GHz and 7.82 GHz corresponding to the reflection -13 dB, -15.2 and -29 dB, respectively. Interestingly, for the covid-19 samples, there sonant frequency presented two peaks at 5.1 GHz and 7 GHz, with a pronounced shift of about 720 MHz and 740 MHz, respectively. This proposed sensor can be achieved for rapid diagnosis of COVID-19 within few seconds.

1.11 Conclusion

The pandemic of COVID-19 has motivated researchers to make efforts towards the development of an advanced approach that must be highly efficient and should be capable of responding to the present demand of early diagnosis to manage this global issue. Since there is no explicit technique currently available for the treatment of COVID-19, therefore the management of this pandemic is only possible through detection, monitoring, and prevention of SARS-CoV-2 infection in time. Moreover, the asymptomatic cases of COVID-19 have made this issue more complex and, therefore, it is necessary to invent a rapid and low-cost technique for the early diagnosis of this suspicious infection at mass levels to discriminate against the infected and non-infected cases.

In this context, since the metamaterials-based biosensors have already shown their potential towards the diagnosis of numerous viral infections and hence may perhaps fulfill the current demand for early diagnosis of COVID-19 cases.

2. Characterization of homogenized metamaterial unit cell

2.1 Introduction

In recent decades, scientists have spent a lot of time and effort in researching new materials and physical phenomena in order to cater to modern life. There are many new artificial materials that have been found to replace the earlier natural materials, which have brought significant benefits in various areas of life. Metamaterials are among those new materials that are made up of the arrangement of metal structures on the surface of dielectric substrates. Therefore, the physical properties of metamaterials depend on their structures more than the component that makes up them. Now we must ask two questions: Is a metamaterial structure with sub-wavelength unit cell equivalent to a homogenous effective medium? How to determine the effective medium parameters once the periodic structure is known? The answers to these questions are key points for the homogenization of artificial particles and effective medium theory.

This chapter is divided into two parts. In the first part we present a brief overview of the homogenization of composite materials and the effective electromagnetic parameters extraction methods. These methods use either the *S* parameter's method or the field averaging method. The second part deals with the characterization of metamaterial unit cell.

2.2 Metamaterials

The term of metamaterial was synthesized by Rodger M. Walser, University of Texas at Austin, in 1999 [44], which was originally defined as "Macroscopic composites having a synthetic, three-dimensional, periodic cellular architecture designed to produce an optimized combination, not available in nature, of two or more responses to specific excitation", the metamaterial is defined as "a material which gains its properties from its structure rather than directly from its composition" this material called left-handed substances.

Metamaterials (MTMs) are well known for their singular and periodic structure which is able to show a negative permittivity and permeability [45]. By appropriate designing, The physical properties of MTMs are largely dependent on the shape, design, orientation and dimensions of their constituted unit cells, the shape, geometry, orientation, and properly excited electric/magnetic field determine their behavior. For instance, a proper choice of metamaterials can determine whether the sensor is sensitive to electric or magnetic fields or both, and at what operating frequency the resonance should occur, MTM has found itself in various applications including biosensors[46], antennas, signal absorbers, energy harvesting and microwave lenses [47],

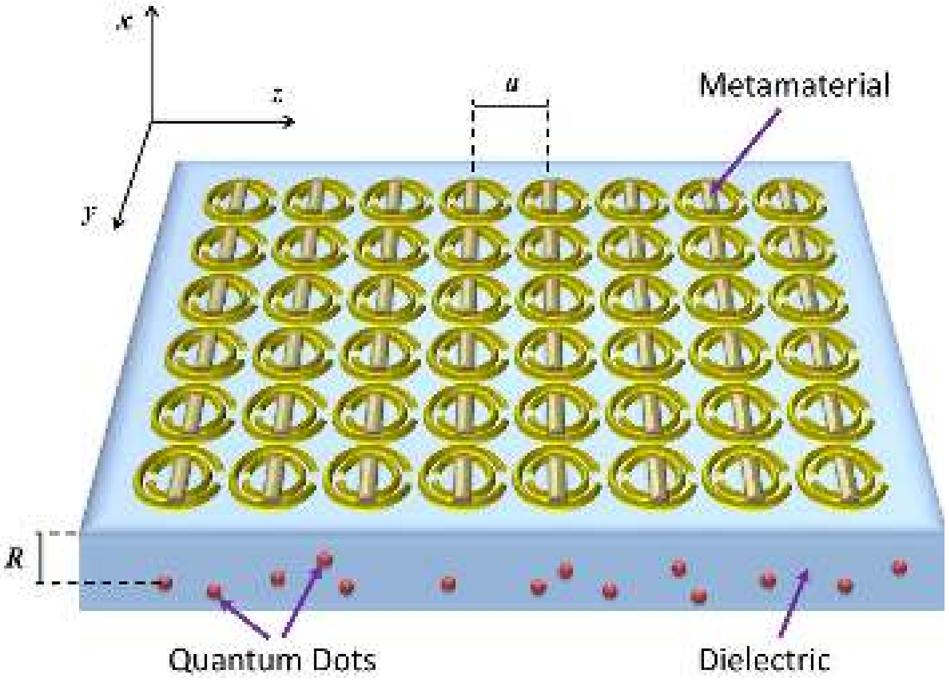

Figure 2-1 : Metamaterial.

2.3 Metamaterial applications

Due to the special physical properties that natural materials do not exist, nowadays, the metamaterials are very attractive materials and are applied in many areas of life, such as the microwave invisibility cloaks, the invisible submarines, the revolutionary electronics, the negative refractive-index lenses, the microwave components, as the filters, compact, and efficient antennas, applying metamaterials to design of antennas is one of its most important applications [48].

2.3.1 Superlenses

For left-handed metamaterial, the most attractive feature is the superlens which can be widely used in super resolution medical imaging, optical imaging, and nondestructive detections [49]. A super lens or perfect lens is a lens which uses metamaterials to go beyond the diffraction limit [50]. The diffraction limit is an inherent limitation in conventional optical devises or lenses. In 2000, a type of lens was proposed, consisting of a metamaterial that compensates for wave decay and reconstructs images in the near field and most importantly the both propagating and evanescent waves contribute to the resolution of the image. In 2004, the first superlens with a negative refractive index provided resolution three times better than the diffraction limits and was demonstrated at microwave frequencies. In 2005, the first near field superlens which exceeded the diffraction limit was demonstrated [51]. The higher focusing resolution will be provided by flat LHM lens if compared to convex dielectric lens and elliptical reflector focusing system. The LHM lens has the potential to acquire higher imaging resolution and easy in-depth scanning, which will simplify the detection system design.

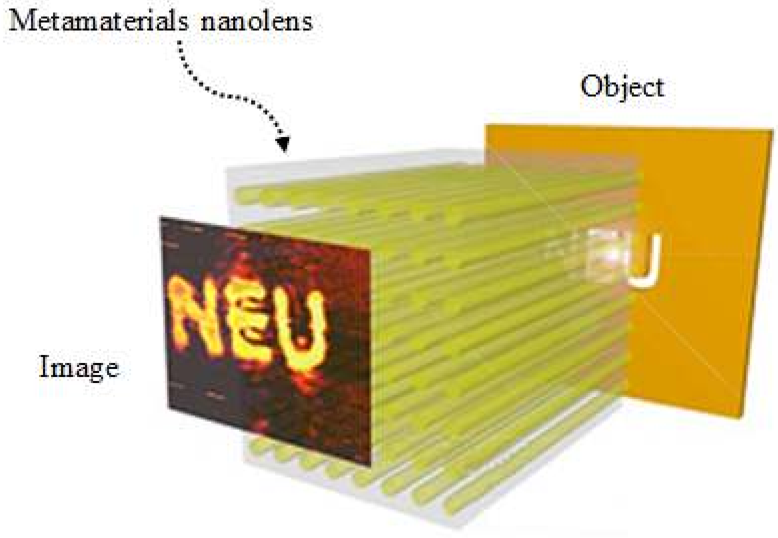

Figure 2-2:Super-resolution imaging using a three-dimensional metamaterials nanolens.

For example, in biological domain, microwaves are used to destroy or ablate diseased soft-tissue by heating it to a temperature that causes cell death. This procedure is called hyperthermia. The generator produces microwave energy which is transmitted through the antennas into the patient. Elevating the temperature of tumor cells causes cell membrane damage, which leads to the destruction of the cancer cells. Hyperthermia treatment of cancer requires directing a carefully controlled dose of heat to the cancerous tumor and surrounding body tissue. The most prominent property of metamaterial lens is the ability of negative-refractive index (NRI) to focus the electromagnetic field of a source. Hence, it can generate appropriate focusing spot in biological tissue as required in microwave hyperthermia treatment.

2.3.2 Antennas

Metamaterial antennas are a class of antennas which use metamaterials to enhance or increase the antenna performances. The metamaterial could enhance the radiated power of an antenna. Materials with negative magnetic permeability could possibly allow for properties such as an electrically small antenna size, high directivity, and tunable operational frequency. Furthermore, metamaterial based antennas can demonstrate improved efficiency and high bandwidth performance.

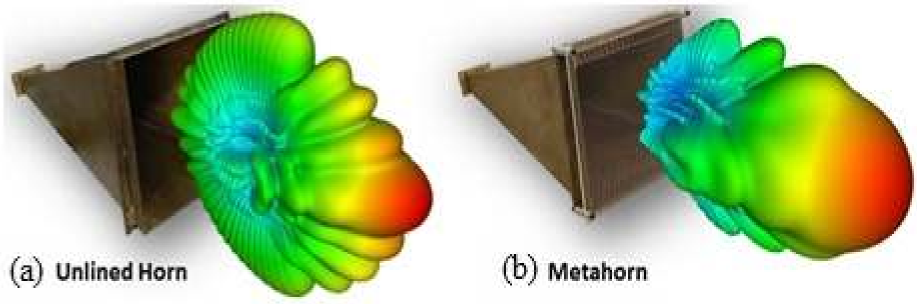

Figure 2-3: rectangular horn antenna (a)-alone (b)-with metamaterial.

Metamaterials employed in the ground plane surrounding antennas offers improved isolation between radio frequency or microwave channels of (multiple-input multiple-output) (MIMO) antenna arrays. Metamaterial, high-impedance ground planes can also be used to improve the radiation efficiency, and axial radio performance of low-profile antennas located close to the ground plane surface.

Metamaterials have also been used to increase the beam scanning range by using both the forward and backward waves in leaky wave antennas. Various metamaterial antenna systems can be employed to support surveillance sensors, communication links, navigation systems, command and control systems [52].

The gradient refractive index metamaterials are also utilized to produce beam-bending lens and beam-focusing lenses. Based on such properties, high-gain and broadband gradient planar lens antennas and Luneberg like lens antennas have been proposed and realized [52]. The Industrial, Scientific and Medical (ISM) radio bands are portions of the radio spectrum reserved internationally for the use of radio frequency (RF) energy for industrial, scientific and medical purposes other than communications.

2.3.3 Microwave devices

The waveguided or planar metamaterials which are composed of complimentary structures like CSRR have been used to design microwave components like filters, power dividers, and phase shifters. Narrowband and broadband polarizers have been realized using three-dimensional (3D) anisotropic metamaterials [52].

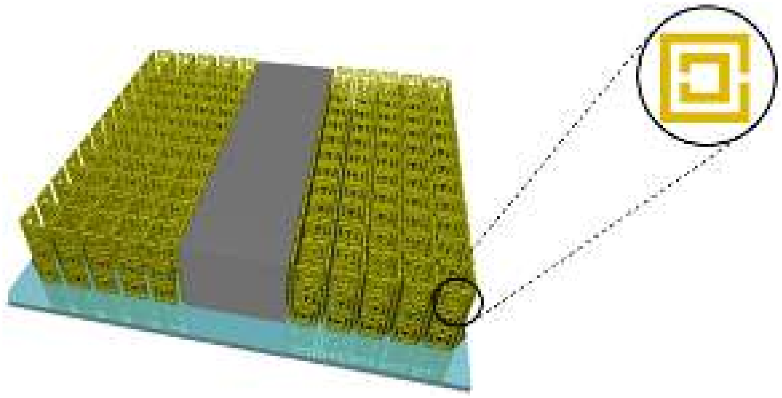

Figure 2-4: planar waveguides with double SRR metamaterials.

Superconducting metamaterials have been achieved in addition to superconducting split rings and wires. They have been utilized to realize a number of unique applications. The combination of left-handed and right-handed propagation media creates opportunities for new types of resonant structures. By laminating two materials with opposite sense of phase, it is possible to create a new class of resonant structures [53]. For example, two flat conducting plates separated by a sandwich of left-handed and right-handed metamaterials constitutes such a new resonator. A wave propagating in the direction normal to the plates will suffer a combination of forward and reverse phase windings before reaching the other reflecting boundary. Under these conditions the wave could undergo a net phase shift of 0 radians and still create a resonance condition. The net phase shift could also be a positive or negative multiple of 2π radians as well, each creating a resonant condition. The result is an ultra-compact resonator whose overall dimension is no longer constrained by the wavelength of the resonant wave.

Superconductors are particularly attractive for use in ultra-compact resonators and showed resonances with indices between +2 and -6, including zero, over the broad frequency range from about 5 to 24 GHz [54]. Quality factors of the negative order resonances were on the order of 3000 at 30 K, while those for positive order resonances were below 400.

2.3.4 Circuit Applications

SRR and CSRR-based transmission lines are useful for device miniaturization, and find their applications in microwave passive components such as impedance inverters, power dividers [55], couplers, and filters. SRRs are also useful particles in many other applications such as magneto inductive and electro inductive wave components [56] frequency selective surfaces [57].

2.3.5 Cloaking

Cloaking devices are advanced stealth technologies that can make objects partially or wholly invisible to some portions of the electromagnetic spectrum. Generally speaking, there are several major approaches to render objects invisible. For example, Alu and Engheta [58] proposed to use plasmonic coatings to cancel the dipolar scattering. But this technique is limited to the sub-wavelength scale of the object, and the coating depends on the geometry and material parameters of the object. Milton and Nicorovici [59] discovered that using a metamaterial coating would cloak polarizable line dipoles. But the coating is affected by the objects placed inside. Leonhardt [60] and independently Pendry, Schurig and Smith [61] discovered a coordinate transformation mechanism for electromagnetic cloaking.

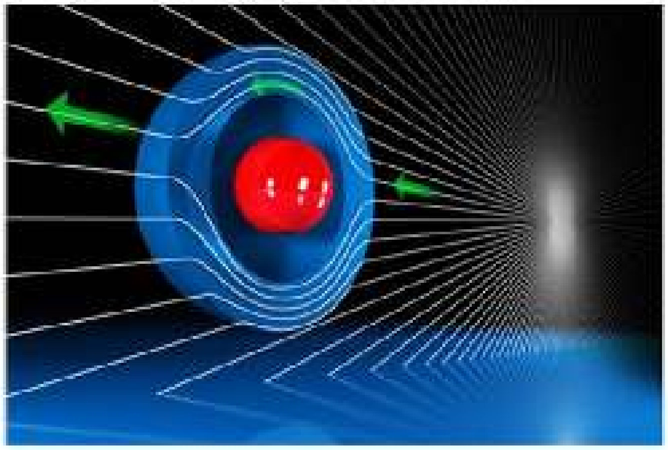

Figure 2-5: Invisibility cloaks.

Their mechanism was quite similar to that of Greenleaf et al. [62] introduced for conductivity. Their main idea is to guide electromagnetic wave around the cloaked region, and many later work has adopted this technique. In May 2006, the first full wave numerical simulations on cylindrical cloaking was carried out by Cummer et al.[63]. A few months later, the first experiment of such a cloak at microwave frequencies was successfully demonstrated by Schuriget al.[64], where the cloak surrounding a 25-mm-radius Cu cylinder was measured. After 2006, numerous studies have been devoted to cloaking, mainly inspired by [63]. For example, in 2008, Liang et al [65] performed a time-dependent simulation for the cylindrical cloak using finite-difference time-domain method.

2.3.6 Biosensing

One of the most important applications of metamaterals is their use as sensors in different frequency regions such as far infrared (FIR), mid infrared (MIR), near infrared (NIR), visible, and THz. In 2008 [66] demonstrated a metamaterals sensor made of a metal and a dielectric has also designed a sensor, by a thin metallic film on a dielectric substrate which had better sensitivity and figure of merit (FOM) in comparison with other similar works. Afterwards, the researchers conducted many significant works in this field by using semiconductors [10], and graphene materials in their structures.

Recently, it has been shown that the sensitivity and resolution of a sensors are enhanced in nanoscale MMs [66], thus, many works used nanoscale metamaterals as biosensors, thin film sensors, strain sensors, temperature sensors, displacement sensors and thermos-optic sensor, The useful application of THz biosensing MM is as virus detection.

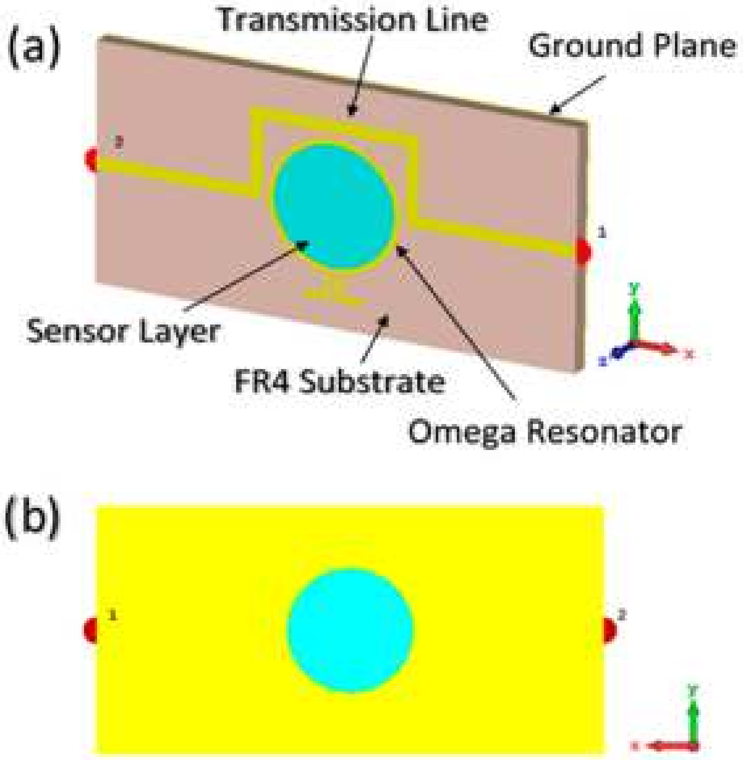

Figure 2-6 : Omega resonator based transmission line biosensors [80].

2.4 Metamaterial classes

Permittivity ε and permeability μ are two parameters used to characterize the electric and magnetic properties of materials interacting with electromagnetic fields.

The permittivity is a measure of how much a medium changes to absorb electrical energy when it is subjected to an electric field[67]. It is defined as the ratio of the electric displacement $\vec{D}$ and the electric field $\vec{E}$. The common term dielectric constant is the ratio of permittivity of the material to that of free space ε_0. It is also termed as the relative permittivity. The permeability is also defined as the ratio of the magnetic induction $\vec{H}$ and magnetic field $\vec{B}$. The free-space permeability μ_0 is approximately 1.257×10^{-6} H/m. Recently, Ziolkowski [68] has categorized metamaterials by their constitutive parameters as shown in figure 2-7. Most of the materials in nature have positive permittivity and permeability, and hence, they are referred to as 'double-positive' (DPS' medias or right-handed materials (RHM). In contrast, if both of these quantities are negative, these medias are called 'double-negative' (DNG) and are also referred to as left-handed materials (LHM). Finally, materials with one negative parameter are named 'single-negative' (SNG) and are further classified into two subcategories, namely, 'epsilon-negative' (ENG) an 'mu-negative' (MNG). Interestingly, natural materials such as cold plasma and silver exhibit negative permittivities at microwave and optical frequencies, respectively, and ferromagnetic materials exhibit a negative permeability behavior in the VHF and UHF regimes [68]. However, to date, no materials that exhibit simultaneous negative permittivity and permeability have been found in nature, and hence they must be produced artificially.

The first comprehensive review of the history of negative refraction and metamaterials was given by Moroz [69]. He indicated that some of metamaterial research started long before Veselago's work and went back to as far as 1905, when Lamb [70] suggested the existence of backward waves, which are associated with waves in which the phase propagates in a direction opposite to that of the energy flow. Moroz's on-line article first appeared in 2003, tracing the roots of research on backward waves, negative refraction, and LHM. Only recently, Veselago and Narimanov [71], Shivola [72], and Shamonina [73] have linked LHMs, and more generally metamaterials, to the earlier works.

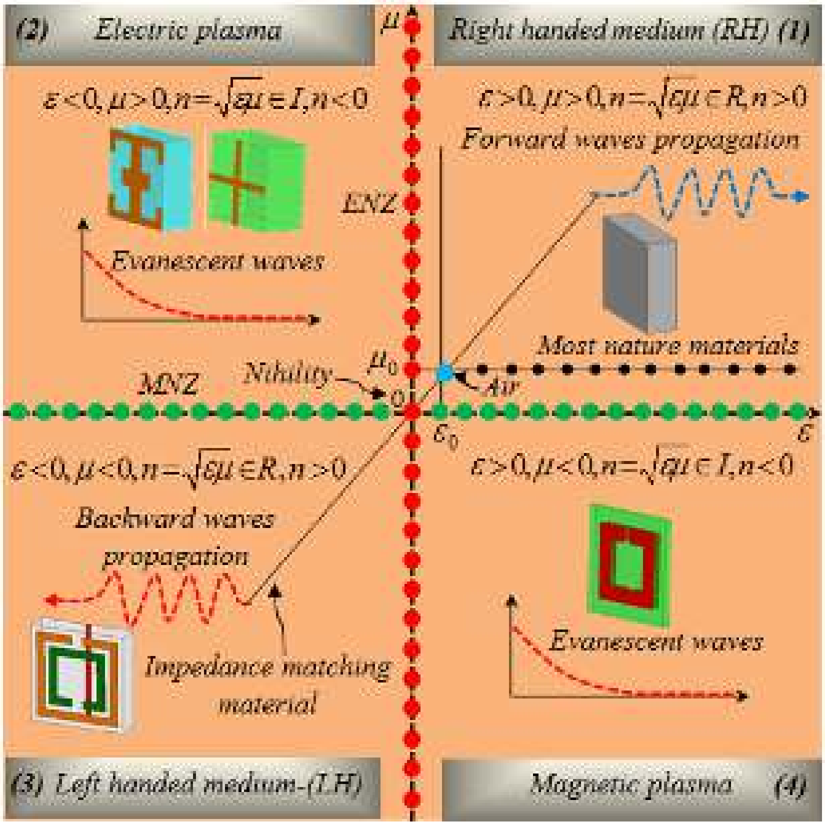

Figure 2-7: Metamaterial classes.

From figure 2-7 four possible quadrants can be taken:

- Quadrant 1: double-positive media or right-handed materials $\varepsilon > 0$ and $\mu > 0$.

This quadrant represents (RHM), which support the forward propagating waves. It is well know that the constitutive parameters ε and μ are related to the refractive index *n* by:

$$n = \sqrt{\varepsilon_r \mu_r} \qquad (2\text{-}1)$$

We have $\varepsilon > 0 \Rightarrow \varepsilon = |\varepsilon|$ and $\mu > 0 \Rightarrow \mu = |\mu|$.

From (2-1) we obtain:

$$n = \sqrt{|\varepsilon_r||\mu_r|} = +\sqrt{|\varepsilon_r||\mu_r|} \qquad (2\text{-}2)$$

$$k = \omega\sqrt{|\varepsilon_r||\mu_r|} = k_0 n \qquad (2\text{-}3)$$

$$\gamma = jk = j\omega\sqrt{|\varepsilon_r||\mu_r|} = \alpha + j\beta \qquad (2\text{-}4)$$

$$\gamma = j\omega\sqrt{|\varepsilon_r||\mu_r|} = \alpha + j\beta \Rightarrow \alpha = 0 \text{ and } \beta = \omega\sqrt{|\varepsilon_r||\mu_r|} = \gamma \qquad (2\text{-}5)$$

We have clearly propagating waves (propagating medium $\alpha = 0$). The expression of a propagating plane wave in such media is written as:

$$\vec{E} = \overrightarrow{E_0}\exp(-jkz) = \overrightarrow{E_0}\exp(-jnk_0 z) \tag{2-6}$$

- Quadrant 2: epsilon-negative medium or electric plasma $\varepsilon < 0, \mu > 0$

In certain frequency regimes many plasmas exhibit this characteristic. For example, noble metals (e.g., silver, gold) behave in this manner in the infrared (IR) and visible frequency domains. This quadrant supports evanescent waves.

We have $\varepsilon < 0 \Rightarrow \varepsilon = -|\varepsilon|$ and $\mu > 0 \Rightarrow \mu = |\mu|$.

From (2-1) we have:

$$n = \sqrt{-|\varepsilon_r||\mu_r|} = j\sqrt{|\varepsilon_r||\mu_r|} \tag{2-7}$$

$$k = \omega j\sqrt{|\varepsilon_r||\mu_r|} = k_0 n \tag{2-8}$$

$$\gamma = jk = j\omega j\sqrt{|\varepsilon_r||\mu_r|} = \alpha + j\beta \tag{2-9}$$

$$\gamma = j\omega j\sqrt{|\varepsilon_r||\mu_r|} = \alpha + j\beta \Rightarrow \beta = 0 \text{ and } \alpha = -\omega\sqrt{|\varepsilon_r||\mu_r|} < 0 \tag{2-10}$$

And then from (2-7) the expression of a propagating plane wave in such media is written as:

$$\vec{E} = \overrightarrow{E_0}\exp(-\alpha z) \tag{2-11}$$

Since α is negative the term $\exp(-\alpha z)$ is divergente when $z \to +\infty$. The evanescent waves are amplified in an ENG media.

- Quadrant 3:double-negative media or left-handed materials $\varepsilon < 0, \mu < 0$

This third case was proposed by Veselago in 1968, supporting the backward propagating waves. We have:

$$\varepsilon_r < 0 \Rightarrow \varepsilon_r = -|\varepsilon_r| \text{ and } \mu_r < 0 \Rightarrow \mu_r = -|\mu_r|$$

From equation (2-1) we obtain:

$$n = \sqrt{-|\varepsilon_r| \times -|\mu_r|} = \sqrt{|\varepsilon_r||\mu_r|} \tag{2-12}$$

$$k = \omega\sqrt{\varepsilon_r\mu_r} = \omega\sqrt{|\varepsilon_r||\mu_r|} \tag{2-13}$$

Comparing equations (2-9) and (2-13), then we obtain :

$$\alpha = 0 \text{ and } \beta = \omega\sqrt{|\varepsilon_r||\mu_r|} = \gamma \tag{2-14}$$

Then, the expression of the electric field corresponds to the propagating waves and can be written as:

$$\vec{E} = \overrightarrow{E_0}\exp(-jkz) = \overrightarrow{E_0}\exp(-jkn_0 z) \qquad (2\text{-}15)$$

- Quadrant 4: mu-negative medium or magnetic plasma $\varepsilon > 0, \mu < 0$.

In certain frequency regimes some gyrotropic materials exhibit this characteristic. This quadrant supports also evanescent waves.

$\varepsilon_r > 0 \Rightarrow \varepsilon_r = |\varepsilon_r|$ and $\mu_r < 0 \Rightarrow \mu_r = -|\mu_r|$

From equation (2-1):

$$n = \sqrt{-|\varepsilon_r||\mu_r|} = j\sqrt{|\varepsilon_r||\mu_r|} \qquad (2\text{-}16)$$

$$k = \omega\sqrt{\varepsilon_r\mu_r} = j\omega\sqrt{|\varepsilon_r||\mu_r|} \qquad (2\text{-}17)$$

Comparing equations (2-9) and (2-17), we find

$$\beta = 0 \text{ and } \alpha = -\omega\sqrt{|\varepsilon_r||\mu_r|} = \gamma \qquad (2\text{-}18)$$

From equation (2-6), the expression of the propagating plane wave in such medium is :

$$\vec{E} = \overrightarrow{E_0}\exp(-\alpha z) \qquad (2\text{-}19)$$

Metamaterials have much broader scope than LHM, as shown in figure 2-7. In the $\varepsilon - \mu$ domain, there are several special lines and points indicating special material properties. For example, the point $\mu = -\mu_0$ and $\varepsilon = -\varepsilon_0$ represents an antiair in the LHM region, which will produce a perfect lens; the point $\mu = 0$ and $\varepsilon = 0$ represents a nihility, which can yield a perfect tunneling effect; the line $\mu = -\varepsilon$ in both RHM and LHM regions represents impedance-matching materials, which have perfect impedance matching with air, resulting no reflections. Also, the vicinity of $\mu = 0$ is called as μ near zero (MNZ) material, and the vicinity of $\varepsilon = 0$ is called as ε-near zero (ENZ) material, which has special properties applied in in perfect lens [52].

2.5 Homogenization of Metamaterials

Metamaterials composed of artificial subwavelength structures, namely meta-atoms, can exhibit extraordinary optical properties not found in natural materials. The basic characterization of such metamaterials is the homogenization of the meta-atoms such that the effective parameters of the homogenization describe the overall optical response of the particular collection of meta-atoms [74],When the size of the meta-atoms is sufficiently small compared to the wavelength of light, such a homogenization of the metamaterial well describes its optical properties, The Nicholson-Ross-Weir (NRW)-type parameter retrieval methods, which are easy to implement for the numerical design of metamaterials, are now used as the standard to determine effective metamaterial parameters .

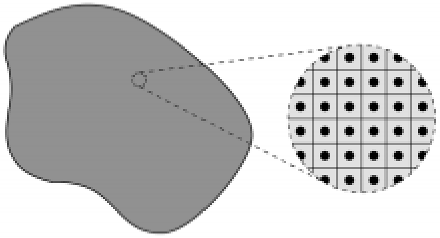

Figure 2-8: Homogenizaed materials

Field averaging method aims to obtain the average value of the field in the unit cell instead of the field that varies throughout the unit cell. In this method, averaged electric and magnetic field Ē and H̄ can be described as:

$$\hat{E} = d^{-1}\int E.dx_i \qquad (2\text{-}20)$$

$$\hat{H} = d^{-1}\int H.dx_i \qquad (2\text{-}21)$$

Where d is the length of the side of unit cell. In another words, E and H can be calculate from line integral of local field in the area of unit cell.

2.6 Effective parameters extraction

If the spacing between scattering elements is much smaller than the operating wave length, so we can consider that the metamaterial is homogenous and it responds to electromagnetic waves in a similar way [75]. It is possible to describe the metamaterials as continuous materials [77] . In these conditions, they can be characterized by effective parameters without considering the local field distribution. This part of the chapter treats classical and numerical homogenization approaches, which are the *S* parameters extraction method (Fresnel inversion method) and the field summation method which is an averaging approach.

2.6.1 Fresnel inversionextraction method

Smith et al[74] proposed a method to extract the constitutive parameters byusing scattering parameters *S*, which is suitableto be applied for both numerical simulation and experimentalmeasurements. Several reports have been published [75]; most of them deal with the isotropic parameters of permittivity and permeability. However, it has already been demonstrated[77] that most metamaterials are intrinsically bianisotropic due to the asymmetry of the compositecomponents such as split-ring resonators. For a bianisotropic metamaterial, the propagation wave vector isrelated not only to permittivity and permeability but also to the magnetoelectric coupling coefficient[77]. Moreover, there are some special metamaterial designs that take advantage of the property of bianisotropy. Consequently, in order to obtaina true picture for these metamaterials, it is important topresent not only the effective parameters of permittivity andpermeability but also some other important parameters, such as the magnetoelectric coupling coefficient ζ_0. Only then one can provide true data for the effective parameters. Figure 2-9, shows the schematics of a homogeneous bianisotropic material slab.

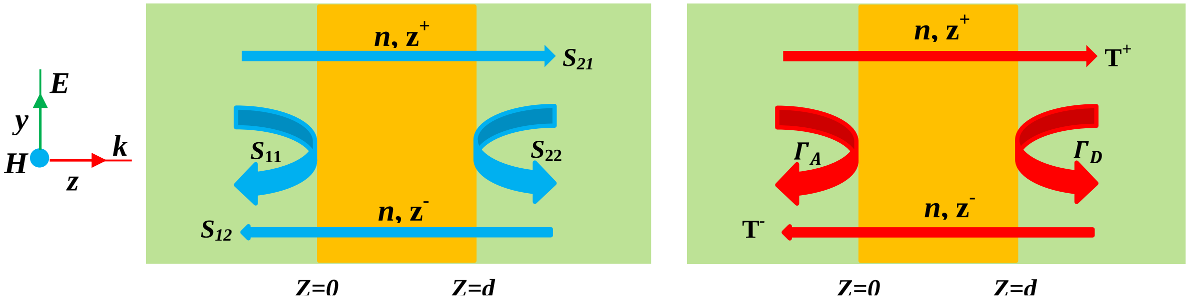

Figure 2-9: Transmission and reflection coefficients in bianisotropic metamaterial.

The metamaterial effective parameters extraction requires two steps[77][79]:

1- Computation of the homogenized metamaterial forward and backward wave impedance (z^+, z^-) and complex refractive index (*n*) (Figure 2-9)which are expressed in terms of reflection and transmission coefficients (S_{ij}).

2- Retrieval of the electromagnetic constitutive parameters (permittivity, permeability and magnetoelectric coupling coefficient) from the S_{ij} parameters.

2.6.2 Metamaterialwave impedances and refractive index computation

In Figure 2-9, a plane wave polarized in the *y* axis propagates along the zdirection and is incident up on the structure. We suppose that the configuration in Figure 2-9 has a bianisotropic property; the electric field in the *y* direction induces a magnetic dipole in the *x* direction, while the magnetic field in the *x* direction also induces an electric dipole in the *y* direction [75].

By assuming that the medium is reciprocal [76] and that the harmonic time dependence is $e^{-j\omega t}$, implying that $\varepsilon^{"} > 0$ and $\mu^{"} > 0$ simultaneously at all frequencies. We use primes and double primes for denoting real and imaginary parts of a complex quantity. The constitutive relations can be written ($\vec{E}$ - $\vec{H}$ or Tellegen representation [77]) as:

$$\vec{D} = \overline{\overline{\varepsilon}}.\vec{E} + \overline{\overline{\xi}}\,\vec{H} \qquad (2\text{-}22)$$

$$\vec{B} = \overline{\overline{\mu}}.\vec{H} + \overline{\overline{\varsigma}}.\vec{E} \qquad (2\text{-}23)$$

Where:

$$\overline{\overline{\varepsilon}} = \varepsilon_0 \begin{pmatrix} \varepsilon_{xx} & 0 & 0 \\ 0 & \varepsilon_{yy} & 0 \\ 0 & 0 & \varepsilon_{zz} \end{pmatrix} \qquad (2\text{-}24)$$

$$\overline{\overline{\mu}} = \mu_0 \begin{pmatrix} \mu_{xx} & 0 & 0 \\ 0 & \mu_{yy} & 0 \\ 0 & 0 & \mu_{zz} \end{pmatrix} \qquad (2\text{-}25)$$

$$\overline{\overline{\xi}} = \frac{1}{c} \begin{pmatrix} 0 & 0 & 0 \\ \text{-j}\zeta_0 & 0 & 0 \\ 0 & 0 & 0 \end{pmatrix} \qquad (2\text{-}26)$$

$$\overline{\overline{\varsigma}} = \frac{1}{c} \begin{pmatrix} 0 & \text{j}\zeta_0 & 0 \\ 0 & 0 & 0 \\ 0 & 0 & 0 \end{pmatrix} \qquad (2\text{-}27)$$

In equations (2-22) to (2-27) $\vec{E}$, $\vec{H}$, $\vec{D}$, and $\vec{B}$ are, respectively, the electric and magnetic field intensities and flux densities; and ε_0 and μ_0 are, respectively, the permittivity and permeability of the vacuum; *c* is the speed of light in vacuum; and $(\overline{\overline{\xi}},\ \overline{\overline{\zeta}})$ are the tensors quantities of the magnetoelectric coupling coefficient. In the present study, we will only deal with the determination of forward and backward wave impedances entailed by ε_{yy}, μ_{xx}, and ζ_0, since other unknown four quantities ($\varepsilon_{xx}, \varepsilon_{zz}, \mu_{yy}$,and μ_{zz}) are not related to the bianisotropic structure in figure 2-9 when a plane wave with a polarization in the *y* direction is incident in the *z* direction.

From Maxwell's curl equations and using equations (2-24) to (2-27), we find:

$$\frac{\partial^2 E_y}{\partial z^2} + k_z^2 E_y = 0 \tag{2-28}$$

$$\frac{\partial^2 H_x}{\partial z^2} + k_z^2 H_x = 0 \tag{2-29}$$

$$Z^+ = \frac{-E_y^+}{H_x^+} = \frac{z_0 \mu_x}{(n + j\zeta_0)} \tag{2-30}$$

$$Z^- = \frac{+E_y^-}{H_x^-} = \frac{z_0 \mu_x}{(n - j\zeta_0)} \tag{2-31}$$

$$z^+ = Z^+ / z_0 \text{ and } z^- = Z^- / z_0 \tag{2-32}$$

$$k_z = nk_0 \text{ and } n = \pm\sqrt{\varepsilon_y \mu_x - \zeta_0^2} \tag{2-33}$$

Here, E_y and H_x are, respectively, the *y* and *x* components of $\vec{E}$ and $\vec{H}$; k_z and k_0 are, respectively, the wave number of the wave propagating in the *z* direction and in free-space; Z^+ and Z^- are, respectively, the wave impedances inside the medium for forward (+*z*) and backward (-*z*) propagations, z^+ and z^- are normalized wave impedances, z_0 is the wave impedance (or intrinsic impedance) in air; and *n* is the refractive index of the sample. It is seen from equations (2-30) and (2-31) that the important feature of a bianisotropic metamaterial is that wave impedances are different for waves propagating in forward and backward directions.

For the derivation of *S*-parameters, we utilize the schematics of a homogeneous bianisotropic material slab with thickness *d* suspending in air as shown in figure 2-9, we derive the forward and backward reflection and transmission *S*-parameters in compact form as:

$$S_{11} = \frac{\Gamma_A (1 - T^2)}{1 - \Gamma_B T^2} \tag{2-34}$$

$$S_{21} = S_{12} = \frac{\Gamma_C T}{1 - \Gamma_B T^2} \tag{ 2-35 }$$

$$S_{22} = \frac{\Gamma_D (1 - T^2)}{1 - \Gamma_B T^2} \tag{ 2-36 }$$

Such as:

$$\Gamma_A = \frac{z^+ - 1}{z^+ + 1} \tag{ 2-37 }$$

$$\Gamma_B = \Gamma_A \Gamma_D \tag{ 2-38 }$$

$$\Gamma_C = 1 - \Gamma_B \tag{ 2-39 }$$

$$\Gamma_D = \frac{z^- - 1}{z^- + 1} \tag{ 2-40 }$$

$$T = e^{jk_0 nd} \tag{ 2-41 }$$

Where Γ_A, Γ_D are the reflection coefficients in the reference planes $Z = 0$ and $Z = d$, respectively, Γ_B, Γ_C are related into Γ_A, Γ_D, and T is the transmission coefficient.

Substituting equations (2-34), (2-35) and (2-36) into equations (2-37), (2-38), (2-39), (2-40) and (2-41) to obtain the following variables:

$$z^+ = \frac{-\Lambda_2 \pm \sqrt{\Lambda_2^2 - 4\Lambda_1 \Lambda_3}}{2\Lambda_1} \tag{ 2-42 }$$

$$z^- = \frac{\Lambda_4 z^+ + 1}{z^+ + \Lambda_4} \tag{ 2-43 }$$

Where

$$\Lambda_1 = S_{21}^2 - (1 - S_{11})(1 - S_{22}) \tag{ 2-44 }$$

$$\Lambda_2 = 2(S_{11} - S_{22}) \tag{ 2-45 }$$

$$\Lambda_3 = (1 + S_{11})(1 + S_{22}) - S_{21}^2 \tag{ 2-46 }$$

$$\Lambda_4 = \frac{S_{11} + S_{22}}{S_{11} - S_{22}} \tag{ 2-47 }$$

And

$$n = \frac{1}{k_0 d}\left[\mp(\ln T)'' \mp 2\pi m - j(\ln T)'\right] \tag{2-48}$$

Where (m = 1, 2, 3,…) denotes the branch index value. It is seen from equation (2-48) that the index n have multiple solutions depending on m values, the correct choice of m for unique retrieval of n can be realized by different technique [78][79].

Note that the correct sign of z^+, z^- and n corresponds to that for which the passivity conditions are satisfied: $(z^+)' > 0$, $(z^-)' > 0$, and $(n)'' \geq 0$.

2.6.3 Calculation of the constitutive electromagnetic parameters

From equations (2-42), (2-43), (2-48) and (2-37) (2-41).We deduce the effective parameters expressions [79]:

$$\zeta_0 = \frac{(2-\Gamma_C)^2 - (4\Gamma_A^2 + \Gamma_C^2)}{4i\Gamma_A\Gamma_C / n} \tag{2-49}$$

$$\mu_x = \frac{\Gamma_C(n^2 + \zeta_0^2)}{n(2-\Gamma_C) - 2n\Gamma_A - i\Gamma_C\zeta_0} \tag{2-50}$$

$$\varepsilon_y = \frac{n^2 + \zeta_0^2}{\mu_x} \tag{2-51}$$

2.7 Metamaterial characteristics

The structural units of metamaterials can be tailored in shape, size, and the composition. The inclusions composition and morphology can be designed and artificially tuned, and placed in a predetermined manner to achieve prescribed functionalities.

The dependence of metamaterial properties on the unit cell architecture provides great flexibility to control metamaterials electromagnetic responses which are described by the electric permittivity and the magnetic permeability. So, by varying the different unit cell geometry parameters, we can create an agile metamaterial which electromagnetic response is unavailable in nature and can be tailored in practice to a reach desired profile. Metamaterial tailoring is one of the important advantages of metamaterials.

2.8 Metamaterial unit cell characterization

Our metamaterial unit cell is shown in Figure 2-10, it is a “capacitively loaded loop (CLL)-shape”, which we will use as a resonator to design an antenna for bio-sensing application. This CLL unit cell behaves similarly to the SRRs but greatly simplify fabrication issues. The inner radius of the ring for the capacitively loaded loop unit cell (CLL) is *La* = 3.4 mm, and the gap *g* is 1 mm. The metallic thickness *t*=0.035 mm made of copper and printed on a Rogers RO3010 slab of thickness *h*=1.27 mm.

The representation of the unit cell with all the geometrical parameters is shown infigure2-10. The incident wave is a plane wave with its wave vector *k* in the x-direction and the *E*-field polarized in the *y*-direction, while the magnetic field vector *H* oriented along the *z*-direction.

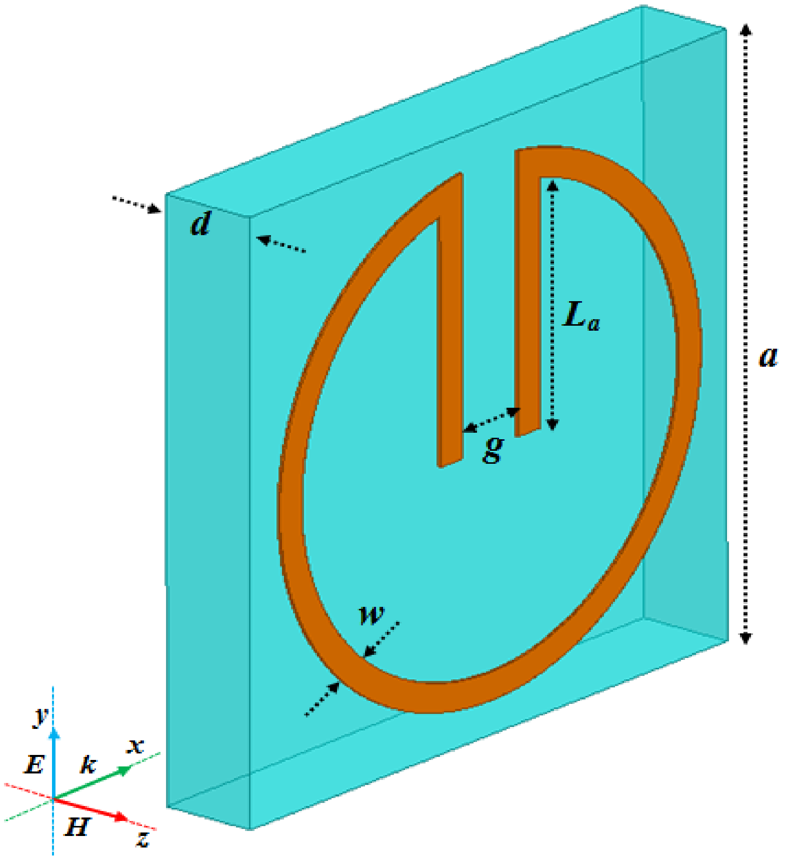

Figure 2-10: Capacitively loaded loop metamaterial unit cell, w=0.4 mm, a=8 mm, d=1.27 mm, La=3.4 mm, g=1 mm

We have seen early, the method used to calculate all the material parameters for a general bianisotropic structure based on numerical simulation of wave propagation in periodic media. We can easily verify the bianisotropic character of a structure, if there reflection scattering parameters are different ($S_{11} \neq S_{22}$).

The simulation results of effective permeability μ_{eff}, effective permittivity ε_{eff}, magneto-electric coupling coefficient ζ , impedances *Z*, and powers, are shown in Figure 2-11 to Figure 2-16.

It can be seen from Figure 2-11 and Figure 2-12, that the real parts of effective parameters (ε_{eff} , and μ_{eff}) of the metamaterial unit cell exhibits a resonant behavior in the frequency band (1.9–2.2 GHz). The resonance frequency f_0 of the structure is 2.11 GHz.

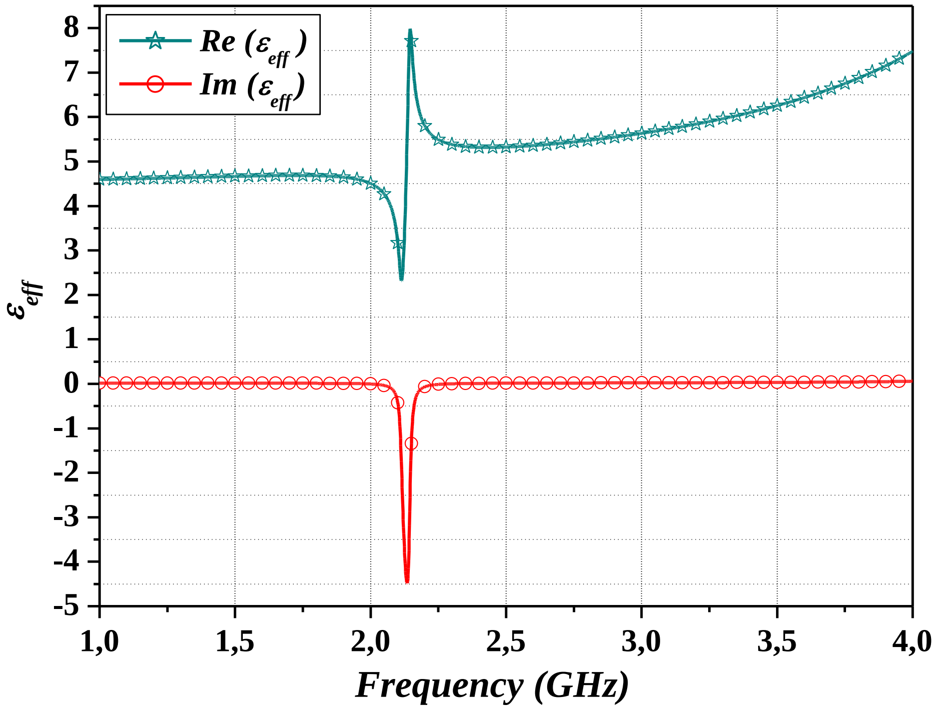

Figure 2-11: Real and imaginary parts of effective permittivity

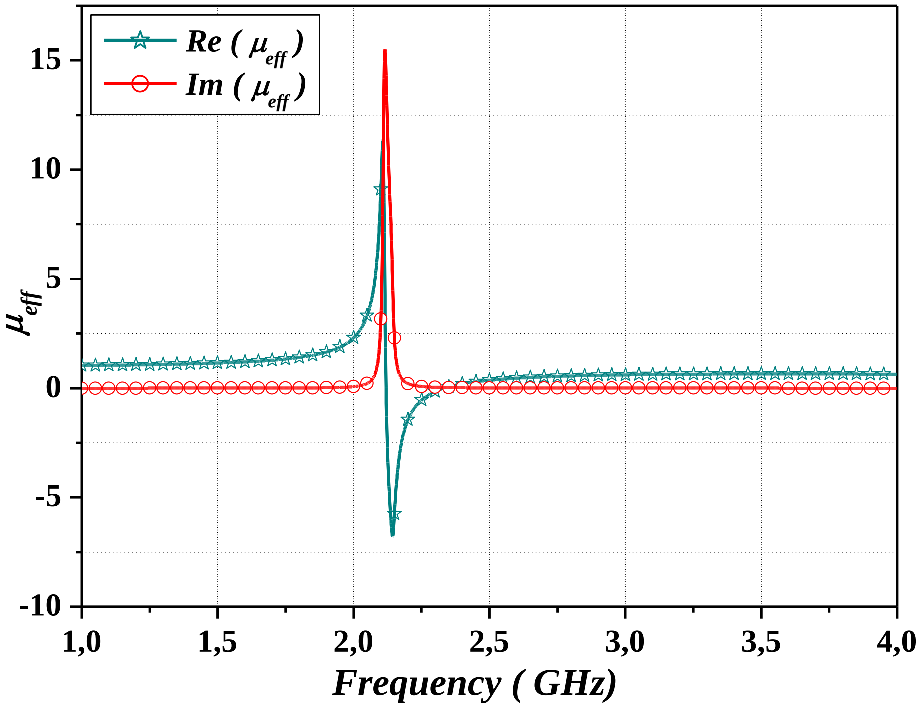

Figure 2-12: Real and imaginary parts of effective permeability.

The imaginary parts of (ε_{eff} , and μ_{eff}) account for losses in the structure caused by the electric and magnetic damping and the finite conductivity of conductors.

The magneto-electric coupling coefficient ζ of the structure is close to zero. Indeed, in general the values of ζ depend strongly on how the surface of the composite is terminated.

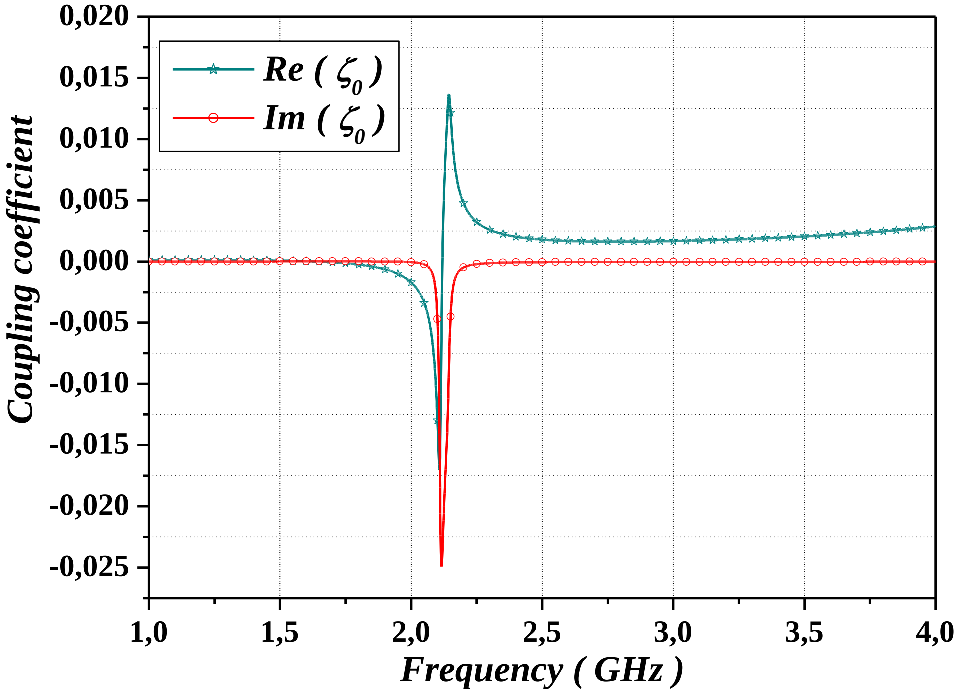

Figure 2-13 : Real and imaginary parts of magnetoelectric coupling coefficients

It is clear from the Figure 2-14, that the real part of the wave impedance Z is positive in concordance with the passivity conditions.

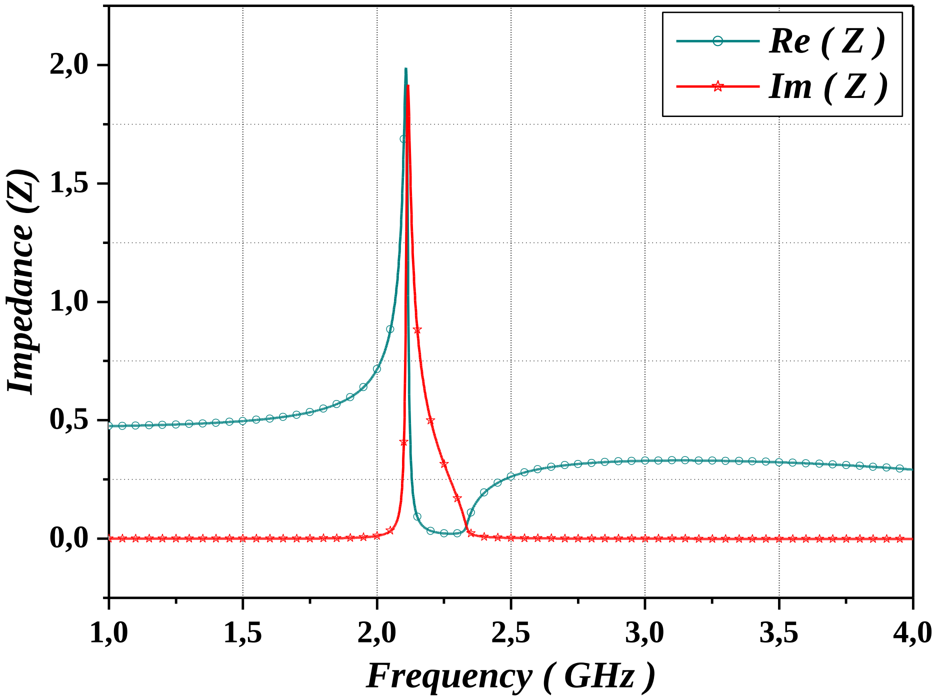

Figure 2-14: Real and imaginary parts of impedance Z.

It can be seen from Figure 2-15, that the real and the imaginary parts of the refractive index n is greater than zero for almost all analyzed frequencies.

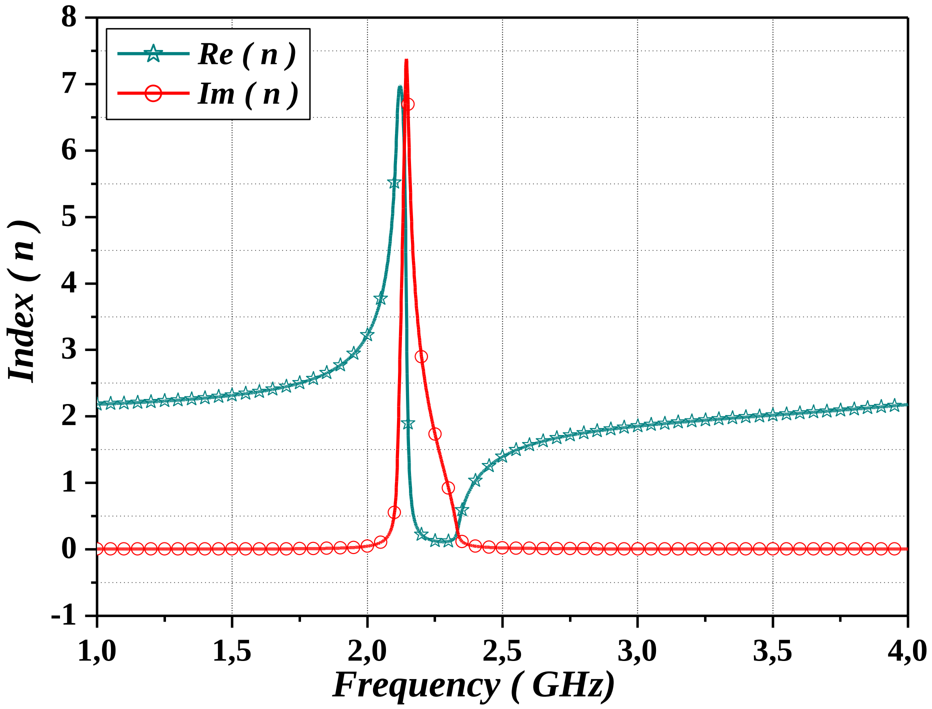

Figure 2-15: Real and imaginary parts of refractive index n.

In this section we are concerned with the power properties of the wave propagation in the capacitively loaded loop metamaterial unit cell (CLL).

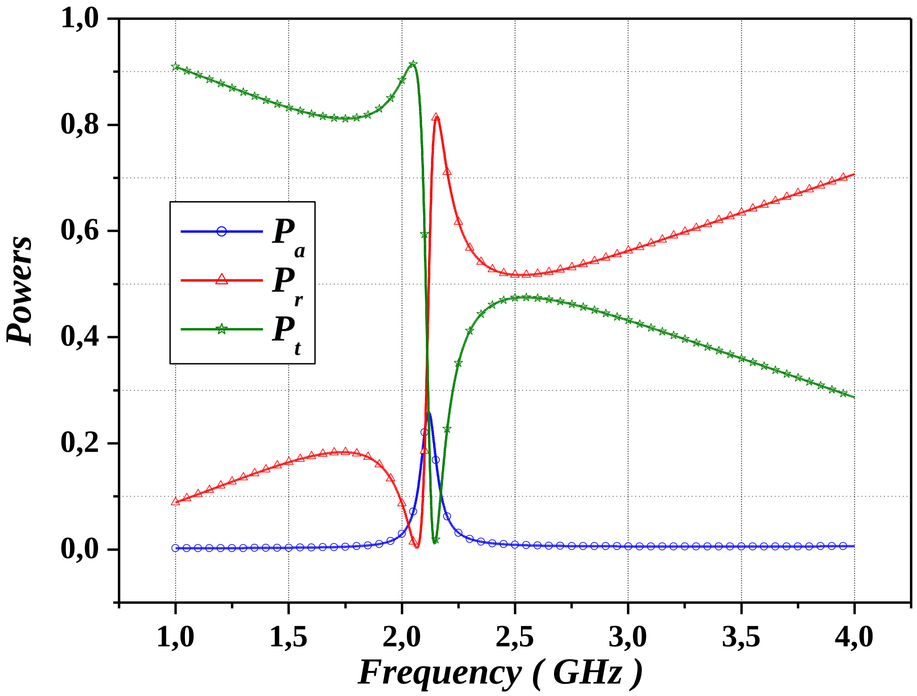

Figure 2-16: Absorbed powers (Pa), Transmitted powers (Pt), and Reflected powers (Pr)

We observe that the maximum absorbed power corresponding to f_0 = 2.11 *GHz,* is in the order of 25.4 %.

This figure also demonstrates that at the resonance frequency f_0 = 2.11 GHz, we observe a symmetric behavior between the transmitted and reflected powers (normal resonance behaviors for the transmitted power, and anti- resonance behaviors for the reflected power). When the reflected power is maximum the transmitted power is minimum and vice versa.

2.9 Conclusion

Homogenization theories are typically valid when the unit-cell size is much small compared to the wavelength.

We have used the Fresnel inversion method to extract the electromagnetic properties of metamaterials unit cell. This method is based on *S*-parameter which is suitable to be applied for both numerical simulation and experimental measurements.

The use metamaterials as bio-electromagnetic sensors is of great interest in many application fields, such as medicine, microbiology, physics, and environmental. Sensors suitable for biomedical applications are characterized by specific performance requirements. Considering the wide range of applications involving detection and characterization of organic materials, a biosensor should be simultaneously highly sensitive and selective, possibly biocompatible, and immune to external disturbances, such as pressure or temperature changes.

We have characterized a capacitively loaded loop metamaterial unit cell (CLL) which is exhibit a resonance behaviors in the frequency band (1.9–2.2 GHz).This metamaterial unit cell is used after that to design a biosensors antenna for the rapid detection of coronaviruses SARS-CoV-2.

3. Design of metamaterials biosensor antenna

3.1 Introduction

Comprehensive understanding of dielectric properties of biological tissues is crucial for understanding the effect of an electromagnetic field having on the human body. The study of the dielectric properties of biological systems and their components has shown to be important not only for fundamental scientific knowledge but also for applications in medicine, biology, biotechnology, and physiology, because the dielectric spectroscopy of the human blood is a powerful and convenient non-invasive testing technique that can be used to diagnose diseases such as diabetes and leukemia, even detecting some viruses such as COVID-19.

In this chapter, we have analyses the human blood in two different frequencies ranges (GHz and THz). The dielectric permittivity, the absorption, refractive index, and other parameters of whole human blood have also been calculated over those frequency ranges.

Then we have design a biosensor antenna for the rapid detection of coronavirus COVID-19-SARS-2. This antenna operating in frequency band (1-4 GHz).

3.2 The human Blood

Blood is the key biologic fluid of the human organism. Blood tests are very important, since they allow a quick determination of various changes in the organism. Comprehensive blood tests facilitate detection of different inflammations, allergies, diseases of the blood system, and the earliest signs of other illnesses.

Blood is a highly functional complex body fluid that serves as the principal transport medium of the body. It delivers oxygen, nutrients, vitamins and metabolites to vital parts of the body and as such is a fundamental part of the immune system.

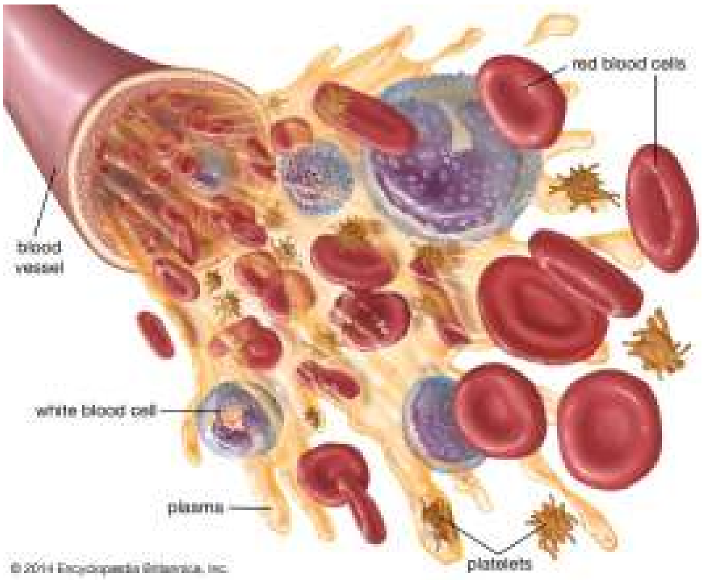

Figure 3-1 : Components of Blood.

In the human body, the amount of blood is around 7% of any person's total weight. Human blood consists of various components, among these red blood cells (RBC), white blood cells (WBC), and platelets suspended within plasma. Blood is, by volume, typically 45% red blood cells, 55% plasma and a very small amount of white blood cells. Plasma is composed predominantly of water (92%) and dissolved proteins and salts (8%). Red blood cells contain hemoglobin (HB), each molecule of which consists of four protein subunits which contain iron and are responsible for blood's characteristic red color. White blood cells defend the body against infection.

Platelets are involved in the formation of blood clots (thrombus), which consist of a solid mass of coagulated platelets and proteins (mainly fibrin).

When studying non-invasive tests to assess how the human body is affected by diseases, changes in blood's properties can be used to understand such impact. This comes from the fact that blood is a highly functional complex body that serves as the principal transport medium of the body. It delivers oxygen, nutrients, vitamins and metabolites to vital parts of the body and as such is a fundamental part of the immune system. The dielectric properties of blood are extremely important for various medical applications, such as microwave imaging, Analysis of blood plasma cells, hyperthermia and ablation.

Recently, terahertz (THz) technology has attracted interest as an effective analysis method to characterize the molecular dynamics of biomaterials, Therefore, by measuring the electric properties of blood one can obtain value information about evolution of some diseases, which affect modification of the local flow pattern and rheological properties of blood[81]. The dielectric properties of blood are extremely important for electromagnetic medical applications, dielectric properties are represented by the complex permittivity of the medium. These properties reveal various dynamic processes.

Moreover, reliable measurement and determination of safe limits for electromagnetic energy absorption by human body is not possible without precise knowledge of dielectric properties of blood, as terahertz frequency radiation (100 GHz – 10 THz) is highly absorbed by water, and water is one of the main constituents of blood, penetration depths in this frequency range are shallow[82].

3.3 Analysis of blood plasma cells at terahertz frequencies

Blood constants of qualitative and quantitative information about essential substances and waste products in the body can facilitate early diagnosis of several diseases. However, the study of THz spectroscopy to character blood cells has not been found widely in the literature. As THz radiation is highly absorbed by water which is one of the main constitutes of blood, the THz spectrum of blood are decided by water and not have any specific spectral feature useful for clinical application. Indeed, no significant difference in spectral between blood serum and water has been found between 50 – 650cm^{-1}.

Nevertheless, the researcher further investigated the spectroscopy features of various blood cells, attempting to find certain signatures for particular types of biological cells. The study showed that different blood cells have their spectroscopy features in the THz range. Early studies of the origin of contrast between healthy and diseased tissue in the THz region focused on changes in water content[83]. However, water content differences are not only limited to differences between healthy and diseased tissues, it is often seen that fat and muscle tissue have different THz optical properties, a difference that is dominated by their different water contents, Meanwhile, with the increasing interest and prospect on THz radiation for clinical application, we need to ensure that the energy absorption in human cells does not cause damage to cells.

Additionally, a recent study of bacteria found in infectious diseases observed significant differences in the THz spectrum of these cells, which was attributed to small changes in water content. However, the likelihood that water content variation is not the only cause of contrast has been highlighted in numerous studies. For example, showed that water does exclusively cause the differences observed in the refractive index and absorption coefficient between human tissues, In addition to structural changes, it is also likely that the molecular changes between diseased and healthy tissues could affect the THz response.

The spectroscopy of blood and its constituents is well known over many sections of the electromagnetic spectrum, As terahertz frequency radiation (100 GHz – 10 THz) is highly absorbed by water, and water is one of the main constituents of tissue, penetration depths in this frequency range are shallow, ranging from typically a few hundred microns in high water content tissues to centimeters in tissues with a high fat content[84]. One would expect the terahertz spectrum of blood to be dominated by water (over 50%) and thus not have any specific spectral feature useful for diagnostic purposes. However, the potential use of THz technology in the clinical environment for in vivo tissue diagnosis makes the knowledge of blood absorption spectrum and refractive index in the THz frequency range important.

3.4 Analysis Method in THz

3.4.1 Double Debye dielectric relaxation model

As terahertz frequency radiation (100 GHz – 10 THz) is highly absorbed by water and water is one of the main constituents of blood, penetration depths in this frequency range are shallow.

One would expect the terahertz spectrum of blood to be dominated by water and thus not have any specific spectral feature useful for diagnostic purposes. However, the potential use of THz technology in the clinical environment for in vivo tissue diagnosis makes the knowledge of blood absorption spectrum and refractive index in the THz frequency range important.

A typical blood model is Debye model, which is put forward on the basis of empirical formula, can meet the dielectric properties of composite materials well[81]. Theoretical calculation method of the dielectric properties may intend to discuss some of the empirical formula in systems.

The dependence of complex permittivity of various biomaterials up on frequency is often expressed in terms of the dielectric model of Debye, and its modifications.

The complex permittivity using the double Debye model is calculated using the formula [85]:

$$\hat{\varepsilon}(\omega)=\varepsilon_{\infty}+\sum_{j=1}^{n}\frac{\Delta\varepsilon_j}{1+j\omega\tau_j} \tag{3-1}$$

where $\Delta\varepsilon_j$, is the difference between static permittivity and permittivity at higher frequencies $\Delta\varepsilon = \varepsilon_j - \varepsilon_{j+1}$; here, ε_j are intermediate values of the dielectric constant at different time, ε_∞ is the real part of the dielectric constant at the high frequency limit, τ_j is the relaxation time, indicating the permittivity dispersion of the jth-Debye relaxation process, ω is the angular frequency.

The double Debye model, shown in equation (3-1) was first applied to describe the dielectric function of water, and then has been widely used for highly hydrated mixtures[85].

$$\hat{\varepsilon}(\omega)=\varepsilon_{\infty}-\frac{\Delta\varepsilon_1}{1+j\omega\tau_1}+\frac{\Delta\varepsilon_2}{1+j\omega\tau_2} \tag{3-2}$$

The double Debye coefficients in formula $\hat{\varepsilon}(\omega)$ at n = 1,j =1;2, τ_1 is the relaxation time of the slow process and τ_2 is the relaxation time of the fast process, ω is the angular frequency.

$\varepsilon_1 = \varepsilon_s$ is the low frequency permittivity, and ε_2 and ε_∞ is the permittivity at infinite frequency for whole blood and blood components such as blood cells and blood plasma are given in table 3-1.

The complex dielectric coefficient of a material is simply related to the complex refractive index $\hat{n}$ (ω) as described by (3-3), where ε' (ω) and ε'' (ω) are the real and imaginary parts of the complex dielectric coefficient (dielectric permittivity). The complex dielectric coefficient of a material can be determined simply from the measured values for absorption coefficient μ_a and refractive index n using (3-4) and (3-5), respectively[85].

$$\hat{\varepsilon}(\omega)=\hat{n}^2(\omega)=\varepsilon'(\omega)+i\varepsilon''(\omega) \tag{3-3}$$

$$\varepsilon'(\omega)=n^2(\omega)-\mu_a^2(\omega) \tag{3-4}$$

$$\varepsilon''(\omega)=2n(\omega)\mu_a(\omega) \tag{3-5}$$

The refraction index n and the absorption coefficient μ_a can be related to ε' (ω) and ε'' (ω) as described in equations (3-6), and (3-7), respectively.

$$n(\omega)=\left(\frac{\sqrt{\varepsilon'^{2}(\omega)+\varepsilon''^{2}(\omega)}+\varepsilon'(\omega)}{2}\right)^{\frac{1}{2}} \tag{3-6}$$

$$\mu_a(\omega)=\frac{2\omega}{c}\left(\frac{\sqrt{\varepsilon'^{2}(\omega)+\varepsilon''^{2}(\omega)}-\varepsilon'(\omega)}{2}\right)^{\frac{1}{2}} \tag{3-7}$$

We assumed that the temperature of biomaterials corresponds to the room temperature (22–25 °C) in our study. The final parameters of the double Debye model are shown in table 3-1.

Table 3-1:Double Debye coefficients for whole blood and blood components[85].

	ε_∞	ε_S	ε_2	**τ_1(ps)**	**τ_2(ps)**
Whole Blood	2.1	130	3.8	14.4	0.1
Blood Plasma	1.7	78.8	3.6	8.0	0.1
Blood Cells	3.4	2.5	23.8	410.8	1.8
Thrombus	2.2	130	3.7	16.1	0.1
Water	3.3	78.8	4.5	8.4	0.1

The permittivity of blood components was defined using the double Debye dielectric relaxation model (equation (3-2)).

Double Debye coefficients for whole blood, blood plasma, blood cells, thrombus and water are taken from the experimental results in table 3-1.The complex permittivity of the blood components are shown figure 3-2.

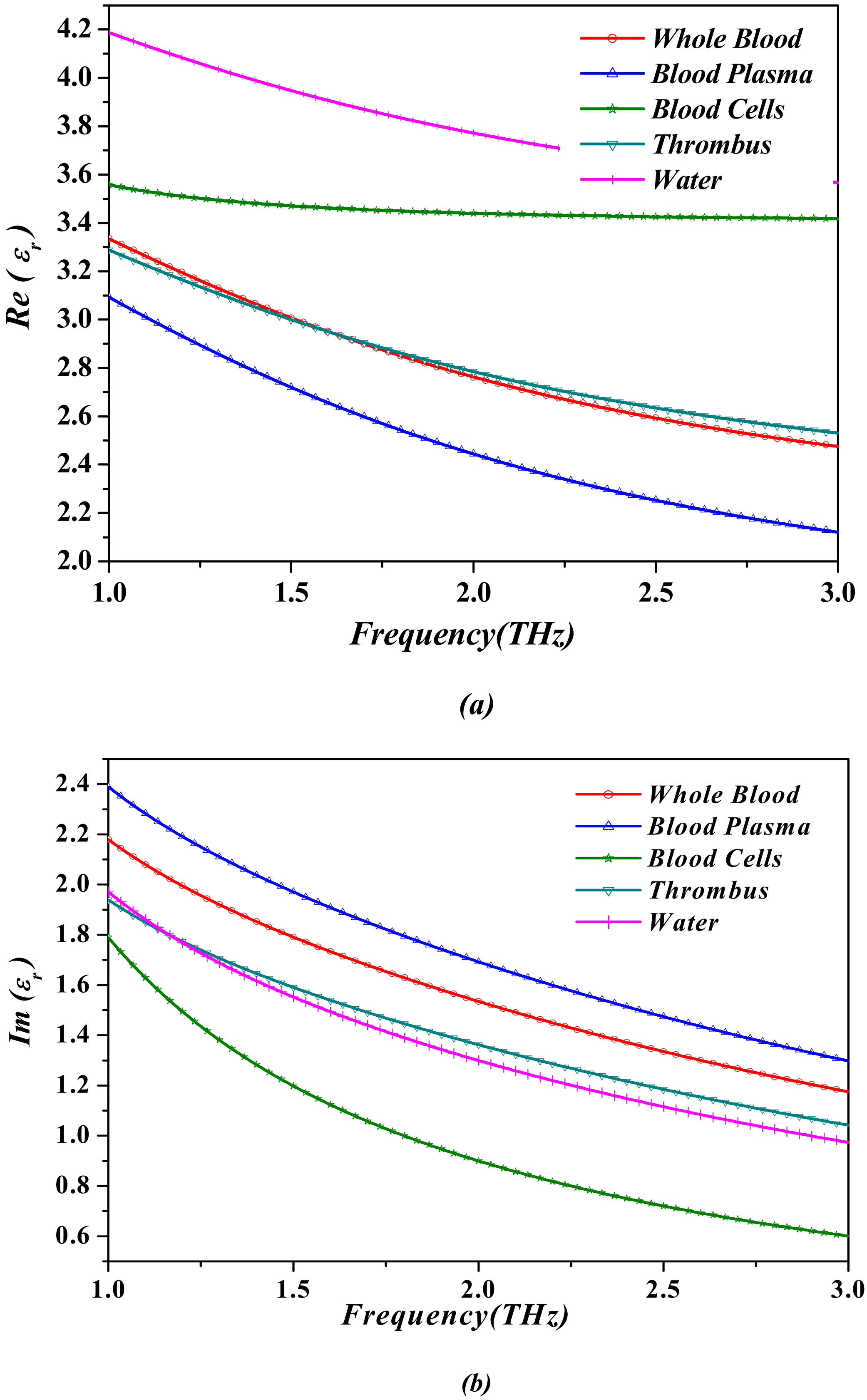

Figure 3-2 : (a) Real permittivity resulted for whole blood, blood plasma, blood cells, water, and a thrombus from double Debye equations, (b) Imaginary permittivity resulted for whole blood, blood plasma, blood cells, water, and a thrombus from double Debye equations.

The refractive index *n* and the absorption coefficient for whole blood and blood components are calculating using the equations (3-6), (3-7), and shown in figure 3-3, and figure 3-4, respectively.

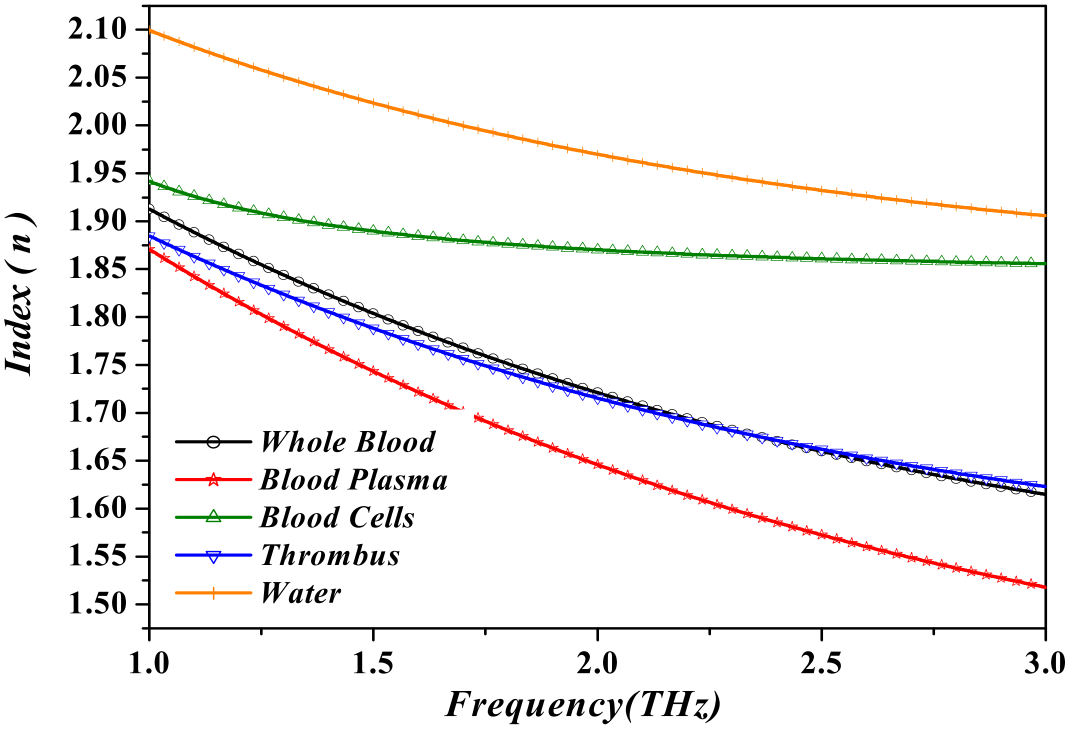

Figure 3-3 : The refractive index *n* for whole blood and blood components.

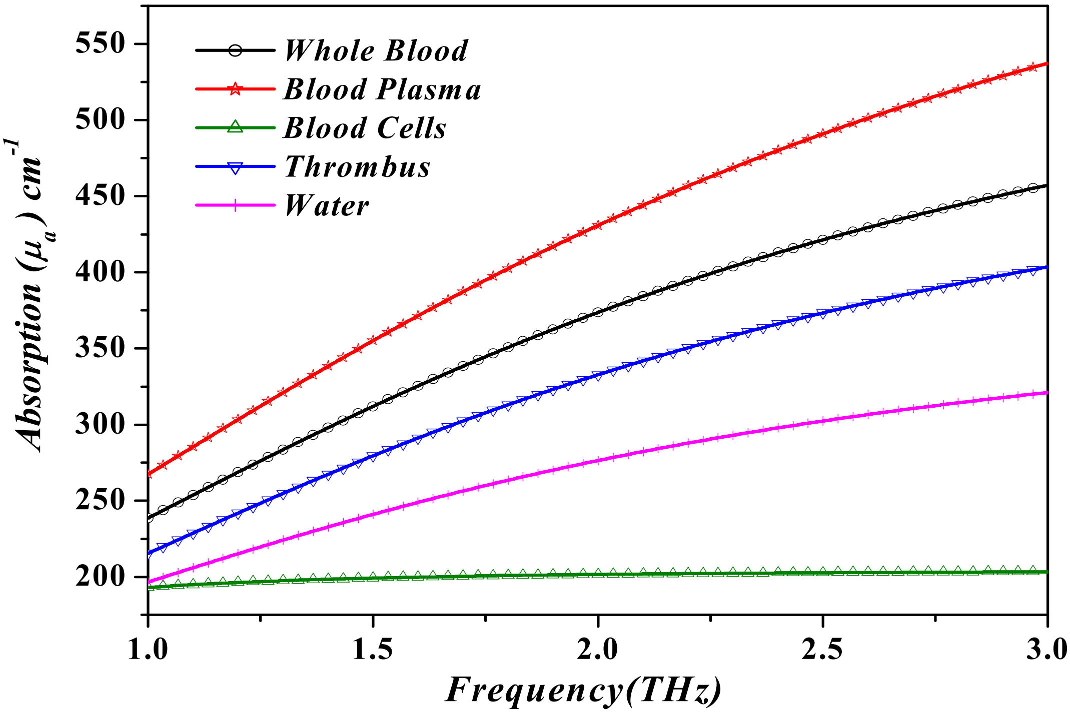

Figure 3-4: Absorption coefficient for whole blood, blood plasma, blood cells, water, and thrombus.

3.5 Analysis Method in GHz

3.5.1 Four-pole Debye model

After analyses the whole blood, blood plasma, blood cells, thrombus and water in the THz frequency range using double Debye model, we will now analyze the dielectric parameters of the whole blood on GHz frequency range (1 – 10 GHz) by using fourth-order Debye equations, which is more accurate than the double Debye model.

At the broad band of microwave frequencies, the fourth order Debye dispersive model as expressed in the following equation[86]:

$$\varepsilon_r(j\omega)=\varepsilon_r^{'}(j\omega)+\varepsilon_r^{''}(j\omega) \qquad (3\text{-}8)$$

$$\varepsilon_r(j\omega)=\varepsilon_\infty+\sum_{k=1}^{k}\frac{\Delta\varepsilon_k}{1+j\omega\tau_k}+\frac{\sigma_s}{j\omega\varepsilon_0} \qquad (3\text{-}9)$$

Where ω is the angular frequency, ε_0 is the free space permittivity, ε_r' and $\varepsilon_r'' = \sigma/\omega\varepsilon_0$ are the real part and the imaginary part of the complex relative permittivity (ε_r) of the Debye dispersive media.

σ: denotes the electric conductivity, ε_∞ is the permittivity at the infinite frequency, k is the number of Debye modes, $\Delta\varepsilon_k$ and τ_k are, respectively, the magnitude and the relaxation time of the *k-th* Debye dispersion mode, and σ_s is the static conductivity.

The experimental parameters of fourth-order Debye equations are described in table 3-2.

Table 3-2 : Parameters of the four-pole Debye model of human blood[86].

Parameters	ε_∞	$\Delta\varepsilon_1$	$\Delta\varepsilon_2$	$\Delta\varepsilon_3$	$\Delta\varepsilon_4$	τ_1 [rad/s]	τ_2 [rad/s]	τ_3 [rad/s]	τ_4 [rad/s]	σ_s[S/m]
Whole Blood	1.96E + 01	1.76E + 04	4.59E + 03	1.17E + 02	3.70E + 01	8.65E − 04	9.73E − 08	5.86E − 09	1.41E − 11	1.064

We use these experimental parameters to calculate the dielectric permittivity and conductivity of whole human blood in GHz frequency range. The simulation results are shown in figure 3-5, and figure 3-6.

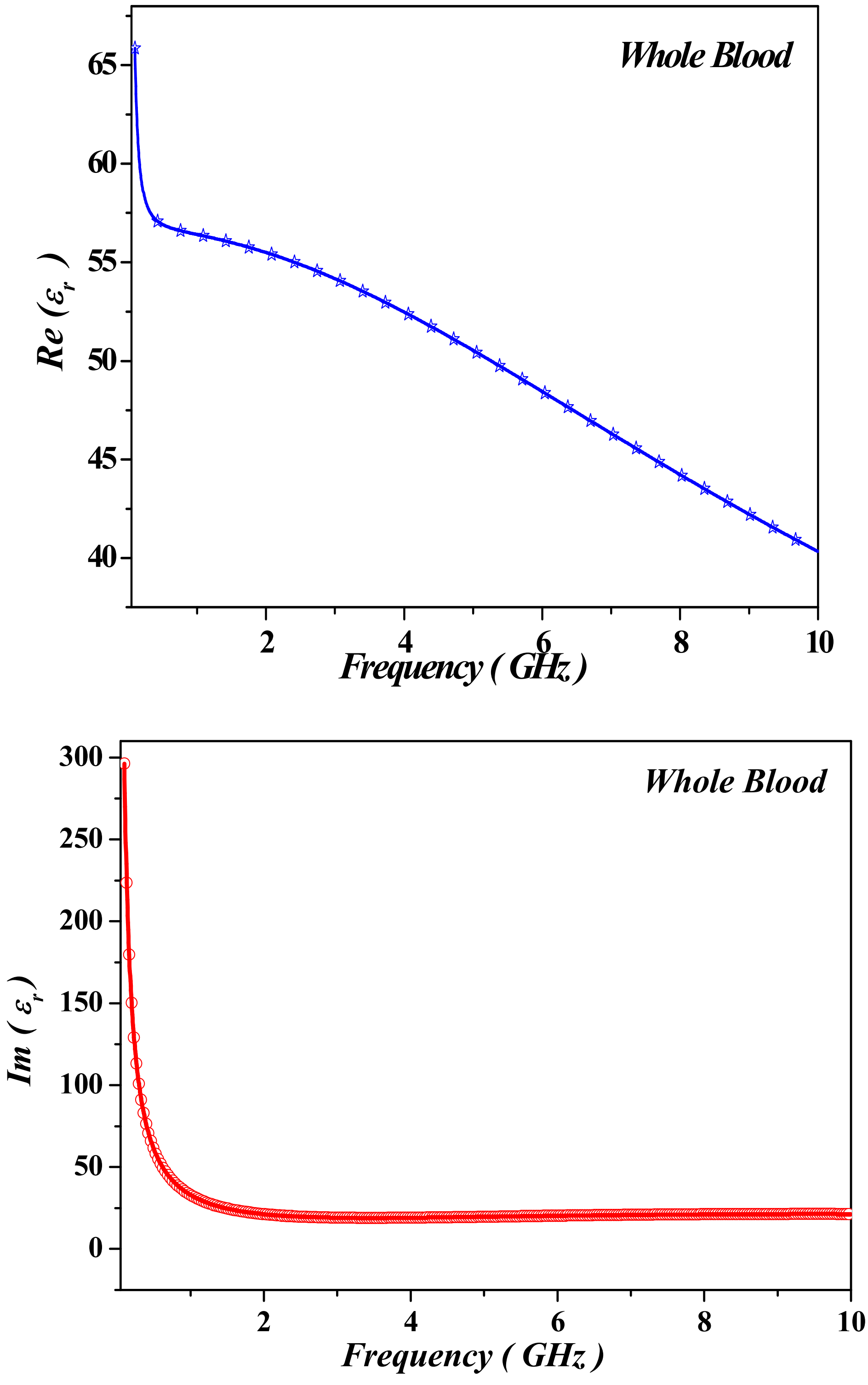

Figure 3-5:Real and imaginary part of the relative permittivity obtained from the four-pole Debye model of human blood.

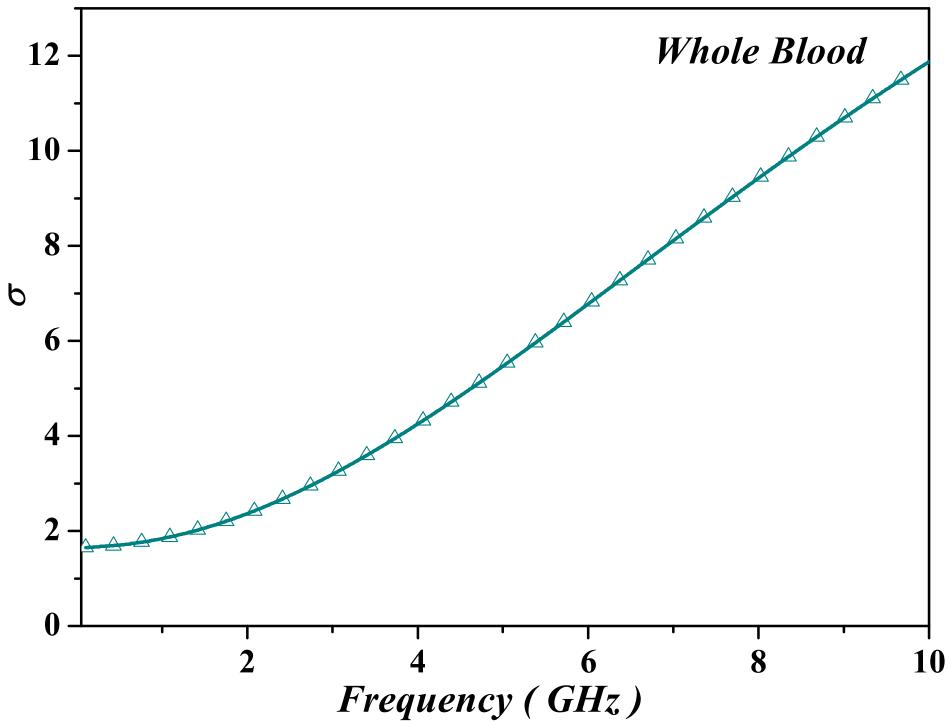

Figure 3-6: Conductivity of whole blood.

3.6 COVID-19 blood

It was reported from literature that dielectric permittivity of blood is decreased when the count of lymphocytes is increased[87][88]. Ermolina, et al [93] used different mixture formulas to conclude that the relationship between static dielectric permittivity of blood as functions of volume fraction of cells is almost linear from 0% to about 20% of cells volume fraction[92]. It was demonstrate that in most cases of COVID-19, lymphocyte percentage (LYM%) was reduced to lower than 5%[89][90][91][92]. Furthermore, when the immunoglobulin/antibody proteins are just started to produce by the immune system in response to the COVID-19 antigen, the dielectric permittivity is further lowered. This is because it was evidenced that the increase of IgG and IgM immunoglobulin's has led to the decreased capacitance and dielectric permittivity of blood[89][90][91][92].

The dielectric constant of COVID-19 patient (COVID-19 blood henceforth)shown in figure 3-7, and figure 3-8, was calculated based on their decrement by 5%compared to that of the normal blood at high frequency.

The fourth-order Debye parameters of COVID-19 blood are described in table 3-3.

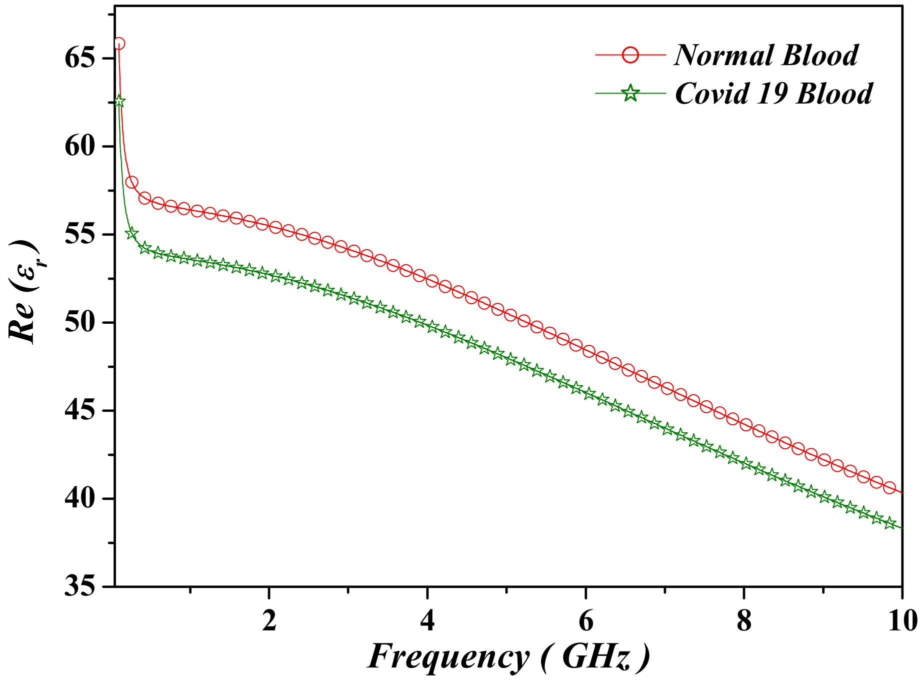

Figure 3-7 :Real part of the relative permittivity obtained from the four-pole Debye model of the Normal blood and COVID-19 Blood.

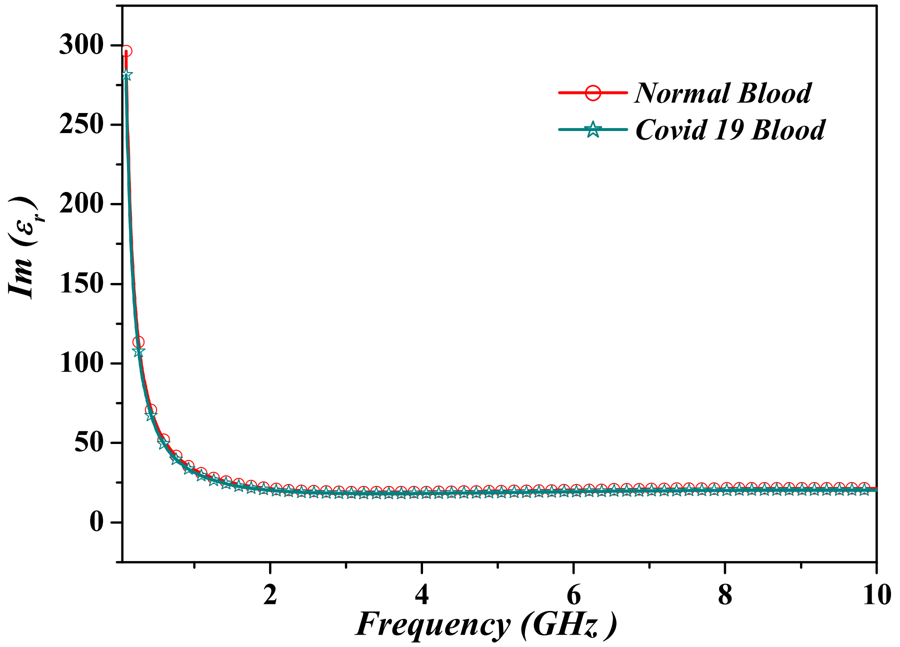

Figure 3-8 : Imaginary part of the relative permittivity obtained from the four-pole Debye model of the Normal blood and COVID-19 Blood.

Table 3-3: Parameters of the four-pole Debye model of human COVID-19 blood.

Parameters	ε_∞	$\Delta\varepsilon_1$	$\Delta\varepsilon_2$	$\Delta\varepsilon_3$	$\Delta\varepsilon_4$	τ_1 [rad/s]	τ_2 [rad/s]	τ_3 [rad/s]	τ_4 [rad/s]	σ_s[S/m]
COVID-19 Blood	1.86E +01	1.672E + 04	4.36E + 03	1.11E + 02	3.51E + 01	8.65E − 04	9.73E − 08	5.86E − 09	1.41E − 11	1.0108

3.7 Design of Biosensors antenna

We use the metamaterial unit cell to design a metamaterial super strate which are composed of 9 CLL's unit cells, as shown in figure 3-9.

The layout of the proposed biosensor antenna, composed of three layers, is shown in figure 3-9. On the top layer, a metamaterial super strate has been placed on the top of a microstrip antenna at a distance *h=8mm* from the patch. The metamaterials unit cell conductor is made of copper with a conductivity of 5.8 × 107 S/m, and thickness of 0.035 mm. The dielectric super strate is made of Rogers RO3010 substrate with a thickness of 1.27 mm. This sub strate has been chosen due to the low loss value.

The second layer is utilized as the sensor layer which is filled with blood samples under in vestigation. The bottom layer is representing our proposed microstrip patch antenna. This biosensor antenna was designed over the frequency range of 1 – 4 GHz (C-band),

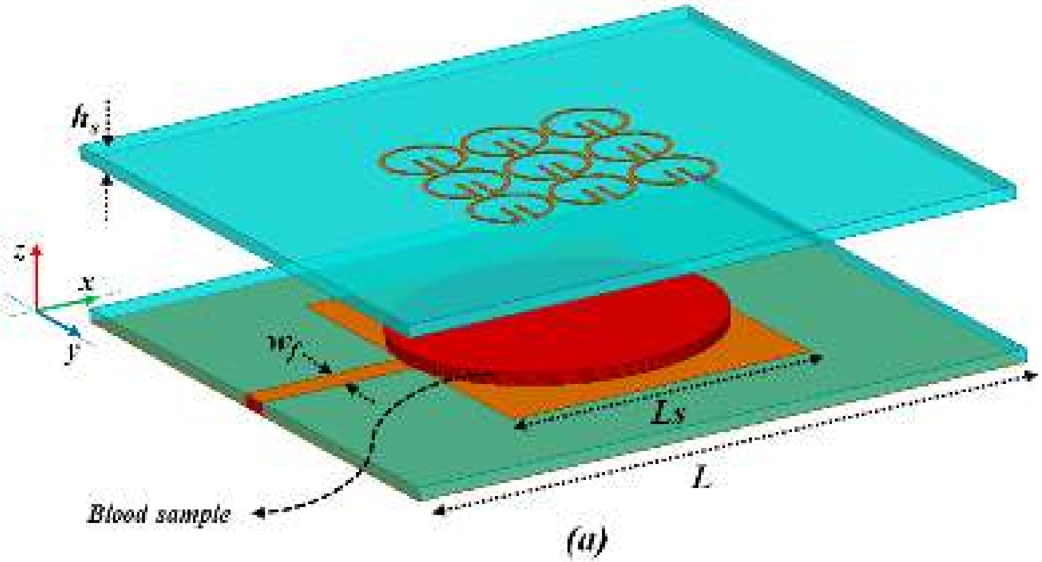

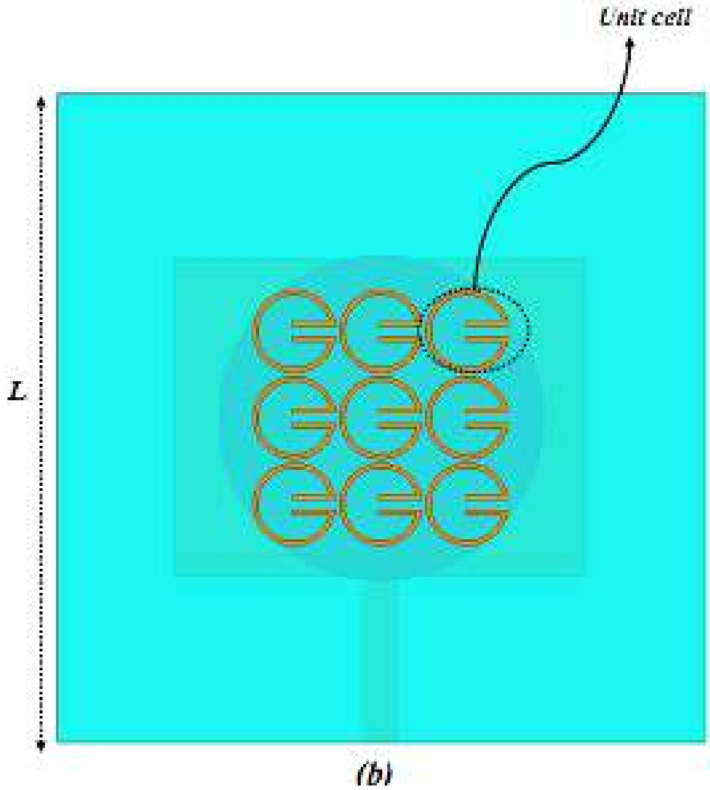

Figure 3-9 : Biosensors antenna, (a) side views, (b) top views, *L*=60 mm, *L*s= 29.4 mm, w_f=3 mm, *h*s=1.27 mm.

3.8 Characterization of metamaterial biosensors antenna

In the first step we use the copper as a metallic conductor of our metamaterials structure. The simulation results of the reflection coefficient (S_{11}) under different simple test (air, water, normal blood and COVID-19 blood) as shown in figure 3-10.

It can be seen from the results that there exist two minima peaks at there sonance frequencies of 1.81 GHz, 3.25 GHz for the normal blood sample, and 1.9 GHz, 3.25 GHz for the COVID-19 blood samples. The reflection coefficient of the sensor layer filled with COVID-19 blood showed a significant shift in the resonance frequency compared to that of air, water, and normal blood-filled sensor, as shown in figure 3-10. In the case of COVID-19 blood, the resonance frequency have shifted towards higher frequency by about 100 MHz compared to the normal blood-filled sensor as also clearly shown in figure 3-11. This suggests that the proposed structure can be highly sensitive for the detection of COVID-19. The magnitudes of the return loss are -17.13 dB, and -20.77 dB for the normal blood-filled sensor and COVID-19 blood-filled sensor, respectively. The maximum return loss contrast between the normal blood-filled sensor and COVID-19 blood-filled sensor is about 3.64 dB.

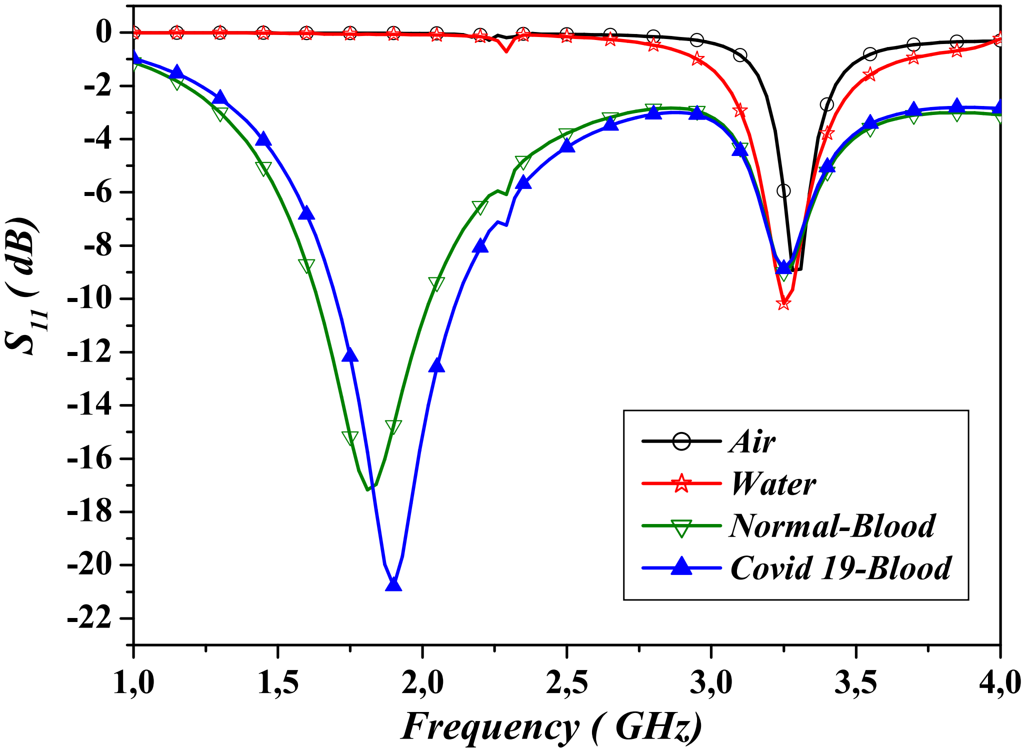

Figure 3-10 : Reflection coefficient (S_{11}) of the proposed biosensors antenna under different simple test (air, water, normal blood, and COVID-19 blood).

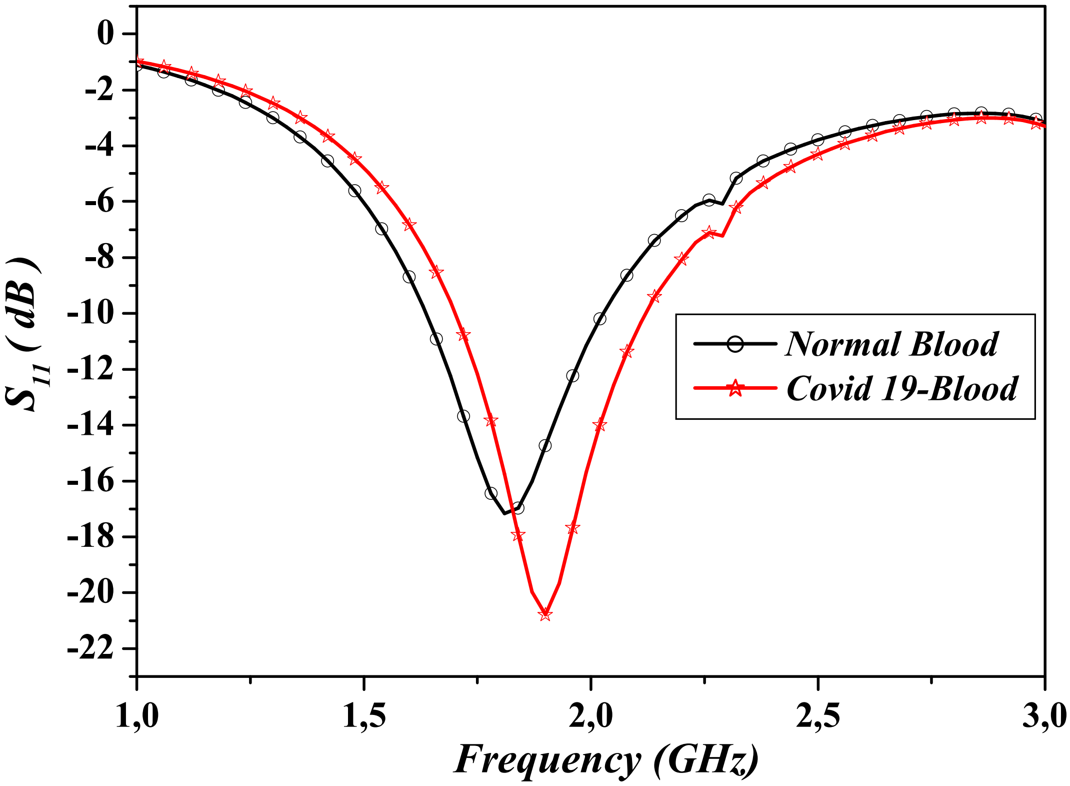

Figure 3-11 : Reflection coefficient (S_{11}) of the proposed biosensors antenna for the normal blood and COVID-19 blood filled sensor.

Figure 3-12, shows the distribution of electric field in biosensor antenna for the sample with a normal blood and COVID-19 Blood. The electric field mainly follows in the z-direction and is distributed strongly in the case of the biosensor antenna with COVID-19 blood filled sensor.

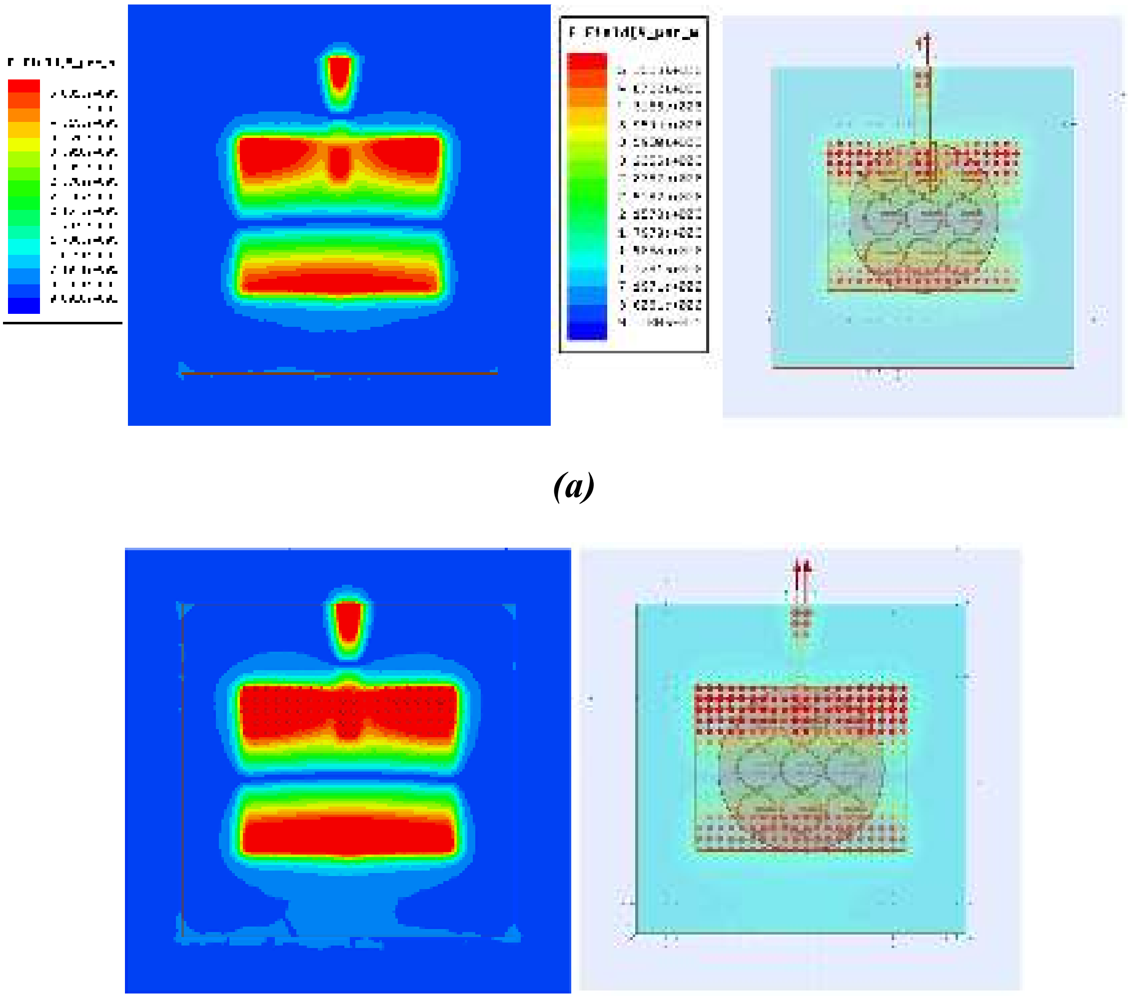

(a)

(b)

Figure 3-12 : Distribution of electric field in biosensor antenna for: (a)-Normal blood, (b)-COVID-19 Blood.

The 3D radiation pattern of the proposed biosensor antenna with a normal blood and COVID-19 blood filled sensor are shown in figure 3-13.

It can be seen from this figure that the realized gain are 5.75 dB, and 4.74 dB for the proposed biosensor antenna with a normal blood and COVID-19 blood filled sensor, respectively.

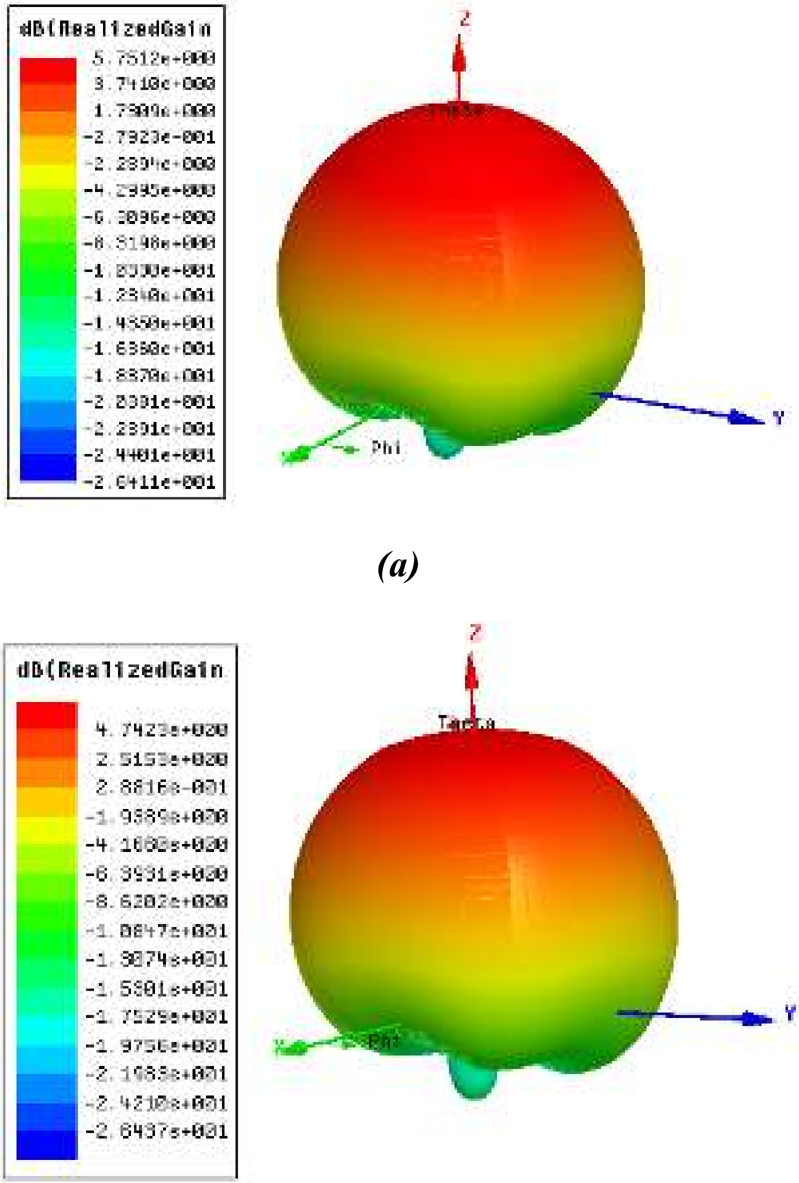

(a)

(b)

Figure 3-13 : 3D radiation pattern of biosensor antenna for a sample with: (a)-normal blood, (b)-COVID-19 blood.

3.9 Characterization of biosensors antenna based on graphene materials

We have seen in the chapter 1, that the graphene-based biosensors being fabricated, for the detection of specialized compounds such as COV-SARS2 virus. Graphene exhibits extremely superior electrical conductivity and good sensitivity by transforming chemical signals into electric current. Graphene is a flat hexagonal lattice of carbon atoms, just one atom thick. It is a form of carbon related to carbon nano tubes. It also depicts enhanced mechanical properties, including high tensile strength, flexibility, and elastic modulus. In spite of being atomically thin, it exhibits high absorbance, and is also thermally as well as chemically stable. In this section we use the graphene as a metallic conductor of our metamaterials structure (figure 3-14).

Graphene can be modeled as the infinitely thin surface of complex conductivity σ. It is represented by[94]:

$$\sigma(\omega)=\sigma_{\mathrm{int}ra}(\omega)+\sigma_{\mathrm{int}er}(\omega) \qquad (3\text{-}10)$$

Where:

$$\sigma_{\mathrm{int}ra}(\omega)\approx -j\,\frac{q_e^2 k_B T}{\pi\hbar(\omega-j2\Gamma)}\left(\frac{\mu_c}{k_B T}+2\ln\left(e^{\frac{-\mu_c}{k_B T}}+1\right)\right) \qquad (3\text{-}11)$$

$$\sigma_{\mathrm{int}er}(\omega)\approx -j\,\frac{q_e^2}{4\pi\hbar}\ln\left(\frac{2|\mu_c|-(\omega-j\tau^{-1})\hbar}{2|\mu_c|+(\omega-j\tau^{-1})\hbar}\right) \qquad (3\text{-}12)$$

$\sigma_{\mathrm{int}ra}(\omega)$ is intra band term, $\sigma_{\mathrm{int}er}(\omega)$ is the inter band term, q_e is the electron charge, $\hbar$ is the reduced Planck's constant, K_B is the Boltzman's constant,τ is the transport relaxation time, T is the temperature, ω is the operating angular frequency, the scattering rate $\Gamma=1/2\pi$ represents loss mechanism, and μ_c is the chemical potential.

The surface conductivity of graphene has been calculated using equations (3-10),(3-11), and (3-12), for T=300K and chemical potential μ_c=0.8 eV, τ=0.1s, as shown in figure 3-15.

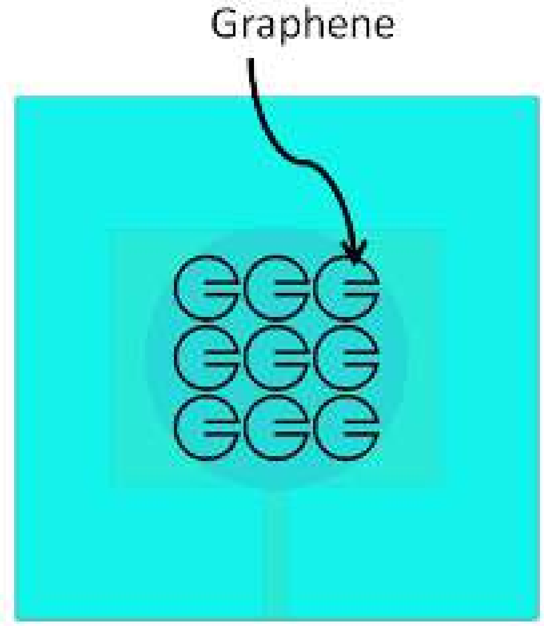

Figure 3-14:Biosensors antenna loaded with metamaterials based graphene materials.

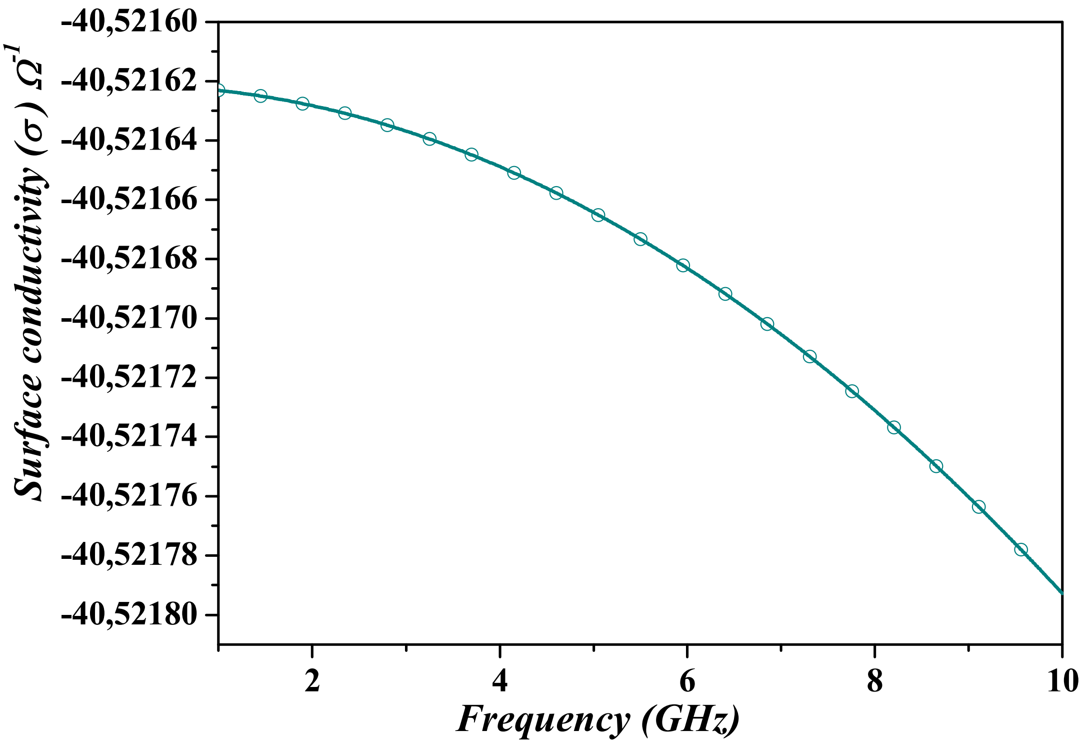

Figure 3-15: Surface conductivity of graphene for T=300K, $\mu_c = 0.8eV$, τ=0.1 s.

The simulation results of the reflection coefficient S_{11} and realized gain of the biosensors antenna loaded with graphene materials cells as shown in figure 3-16, and figure 3-17.

It is clear from the figure 3-16, that the reflection coefficient of the biosensor antenna filled with COVID-19 blood showed a shift in the resonance frequency compared to the normal blood-filled sensor. The resonance frequency has been shifted towards higher frequency by about 100 MHz compared to the normal blood-filled. The magnitudes of the return loss are -14.92 dB, and -21.7 dB for the normal blood and COVID-19 blood-filled sensor, respectively. There is a contrast of about 6.78 dB in the magnitude of the return loss between the normal blood and COVID-19 blood-filled sensor. This makes the biosensor antenna based graphene tobe efficiently used for COVID-19 diagnoses over this wide range of frequency (C-band).

The 3D radiation pattern of the proposed biosensor antenna based on graphene materials for the normal blood and COVID-19 blood filled sensor are shown in figure 3-17.

The maximum realized gain is 7.75 dB, and 6.74 dB for the proposed biosensor antenna with a normal blood and COVID-19 blood filled sensor, respectively.

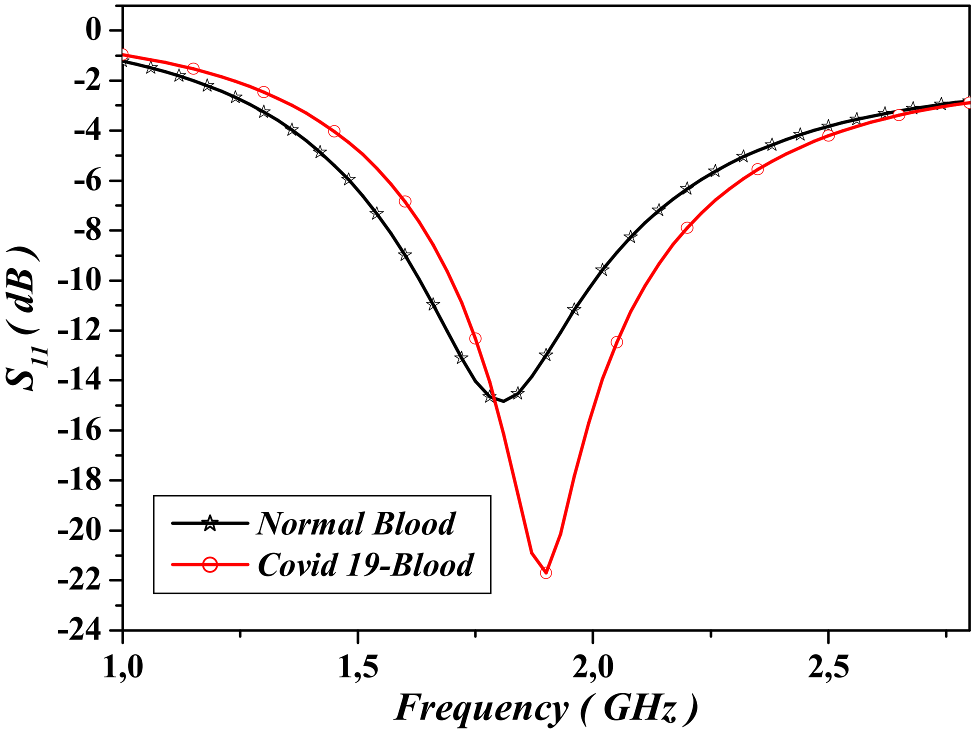

Figure 3-16 : Reflection coefficient (S_{11}) of the biosensors antenna based on graphene for the normal blood and COVID-19 blood filled sensor.

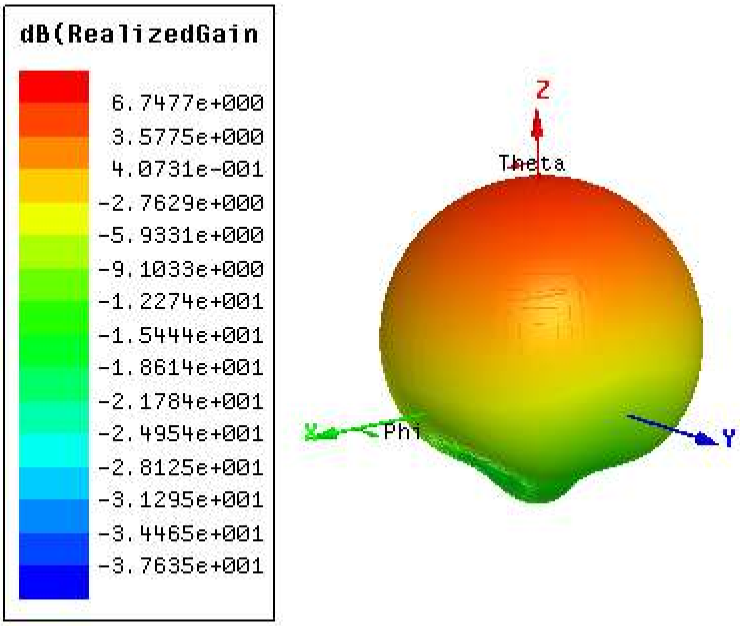

(a)

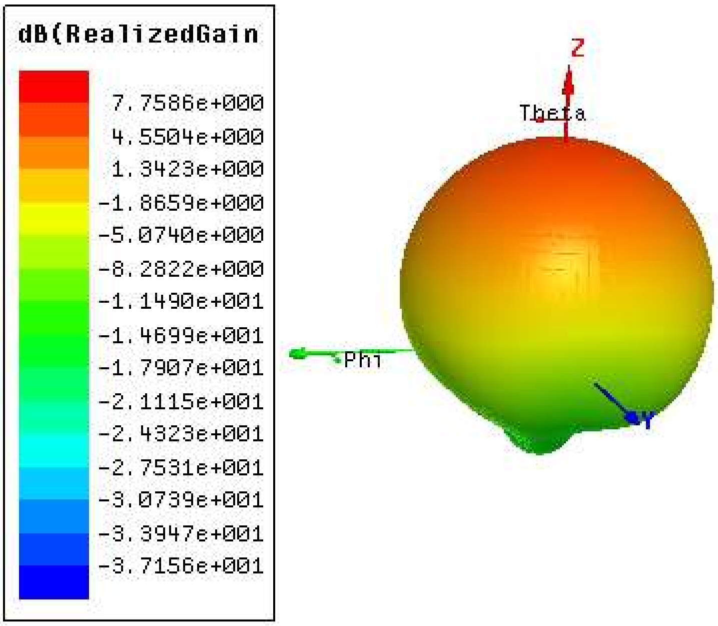

(b)

Figure 3-17 : 3D radiation pattern of biosensor antenna based on graphene for a sample with: (a)- normal blood, (b)- COVID-19 blood.

Table 3-4, are summarized the characteristics results of the biosensor antenna in the case of copper as a metallic conductor on the one hand, and graphene as a metallic conductor on the other.

It is clear from the comparison that the resonance frequency and the bandwidth of the biosensor antenna for both cases (copper and graphene) are remaining the same. The bandwidth is about 0.22in the case of COVID-19 blood, and 0.2 in normal blood filled sensor. However, for the biosensor antenna based on graphene we can see that there is a contrast of about 6.78 dB in the magnitude of the return loss between the normal blood and COVID-19 blood.

The presence of the graphene materials increases the antenna gain from 5.75 dB to 7.75 dB in the case of normal blood filled sensor. Witch corresponds to an enhancement of 2 dB.

These results demonstrate that graphene as a metallic conductor showed a good sensitivity in the magnitude of the return loss between normal blood and COVID-19 blood.

Table 3-4 : Characteristics of the biosensor antenna based on graphene and based on copper materials.

Materials	Samples	Bandwidth (BW)	f_r(GHz)	Return loss (dB)	Realized gain (dB)
Copper	Normal Blood	0.22	1.81	-17.13	5.75
	COVID-19 Blood	0.22	1.90	-20.77	4.74
	Air	0.04	3.28	-10.02	4.3
	Water	0.03	3.26	-10.26	4.5
Graphene	COVID-19 Blood	0.215	1.901	-21.7	6.74
	Normal Blood	0.2055	1.8	-14.92	7.75

3.10 Conclusion

In this chapter we design a metamaterials based biosensor antenna for the rapid diagnosis of COVID-19 virus. The proposed biosensor was successfully employed for tested the evaluating variations in the reflection coefficient (S_{11}) and the others parameters of our biosensor antenna such as the realized gain and the bandwidth.

The dielectric properties of normal whole blood and COVID-19 blood have been calculated using four-pole Debye model.

We used two different metallic conductor of our metamaterials structure for analyses the sensibility of our biosensor antenna devices. For the metamaterials based on copper as a metallic conductor, we show that in the case of COVID-19 blood, the resonance frequency shifted towards higher frequency band by about 100 MHz compared to the normal blood filled sensor. The maximum return loss contrast between the normal blood-filled sensor and COVID-19 blood-filled sensor is about 3.64 dB.

However, for the metamaterials based on graphene as a metallic conductor, there is a contrast of about 6.78 dB in the magnitude of the return loss between the normal blood and COVID-19 blood-filled sensor.

In conclusion, our proposed biosensor antenna can be achieved in order to operate in the terahertz frequency range because the graphene showed a good sensitivity in this frequency band.

Conclusion

The flared up of new coronavirus disease (COVID-19) throughout the globe has terrified people and attract more attention towards health, It made a challenge to the researchers in development of medicines and vaccines or advanced methods to prevent the spreading out of the virus and It is an urgent to develop a method to accurately identify the vast infected patients and asymptomatic viral carriers from the population.

The main goal of this work is to design a metamaterial biosensor antenna for rapid detection and diagnosis of COVID-19 through electromagnetic stimulated analysis of the blood drawn from the patient. The basic idea is based on tailored a metamaterials unit cell for which exhibits a resonant behavior. This metamaterial unit cell has been characterized to use after that for designing our biosensor antenna.

We adopted in our research of a metamaterial because it have shown great potential in sensing applications at different frequency ranges, and of their simplicity, portability, sensitivity, and cost effectiveness.

We have analyses the human blood in two different frequencies ranges (GHz and THz). The dielectric permittivity, the absorption, refractive index, and other parameters of whole human blood, and COVID-19 blood have been calculated over those frequency ranges using double Debye, and four-pole Debye model.

We have established the hypothesis that it is possible to detect changes in the dielectric permittivity of blood among COVID-19 patients by the use of electromagnetic inspired metamaterial based antenna sensors. The involvement of metamaterials (MTMs) in the construction of highly sensitive sensors has become a new trend.

On the practical side, the proposed antenna was simulated by using 3D full wave electromagnetic simulator high frequency structure (HFSS). The simulation results of COVID-19 blood sample showed a pronounced shift in the main resonant frequency about 1.81 GHz to 1.90 GHz compared to the normal blood sample, with maximum return loss contrast of about 3.64 dB between the normal blood and COVID-19 blood-filled sensor.

We used the graphene materials as a metallic conductor of our metamaterials structure for analyses the sensibility of our biosensor antenna devices. The metamaterials based graphene have been a prime interest of research and development communities where the discovery of graphene opened up a new era of sensor development due to its properties. graphene exhibits unique mechanical and electrochemical properties that make it ideal for the development of sensitive electrochemical sensors, so for evaluating the performance of graphene we have presented comparative analysis of graphene based antenna biosensor operating in the same frequency band with copper based antenna biosensor.

The results shows that, for the metamaterials biosensor antenna based on graphene as a metallic conductor, there is a contrast of about 6.78 dB in the magnitude of the return loss between the normal blood and COVID-19 blood-filled sensor. The graphene material increases the antenna gain from 5.75 dB to 7.75 dB in the case of normal blood filled sensor. Witch corresponds to an enhancement of 2 dB. The bandwidth of our biosensor antenna is 0.215 for COVID-19 blood, and 0.2055 for the normal blood-filled sensor.

Finally, our biosensor antenna operating in GHz frequency band is able to detect SARS-CoV-2 virus in human blood samples.

References

[1] Zhu, N. et al. A Novel Coronavirus from patients with pneumonia in China, 2019. N. Engl. J. Med. 382, 727–733 (2020).

[2] Gralinski, L. E. & Menachery, V. D. Return of the coronavirus: 2019-nCoV. Viruses 12, 135 (2020).

[3] Jiang, S., Du, L. & Shi, Z. An emerging coronavirus causing pneumonia outbreak in Wuhan, China: calling for developing therapeutic and prophylactic strategies. Emerg. Microbes Infect. 9, 275–277 (2020).

[4] Wu, Z. & McGoogan, J. M. Characteristics of and important lessons from the coronavirus disease 2019 (COVID-19) outbreak in china: summary of a report of 72314 cases from the Chinese Center for Disease Control and Prevention. JAMA 323, 1239–1242 (2020).

[5] Wu, F. et al. A new coronavirus associated with human respiratory disease in China. Nature 579, 265–269 (2020).

[6] National Health Commission of the People's Republic of China. Briefing on the latest situation of the novel coronavirus pneumonia epidemic. http://www.nhc.gov.cn/xcs/yqtb/list_gzbd.shtml (2020).

[7] Coronaviridae Study Group of the International Committee on Taxonomy of Viruses. The species severe acute respiratory syndrome-related coronavirus: classifying 2019-nCoV and naming it SARS-CoV-2. Nat. Microbiol. 5, 536–544 (2020).

[8] Fisher, D. & Heymann, D. Q&A: the novel coronavirus outbreak causing COVID-19. BMC Med. 18, 57 (2020).

[9] Dong, E., Du, H. & Gardner, L. An interactive web-based dashboard to track COVID-19 in real time. Lancet Infect. Dis. 20, 533–534 (2020).

[10] Li, Q. et al. Early transmission dynamics in Wuhan, China, of novel coronavirus-infected pneumonia. N. Engl. J. Med. 382, 1199–1207 (2020).

[11] Deslandes, A. et al. SARS-CoV-2 was already spreading in France in late December 2019. Int. J. Antimicrob. Agents 55, 106006 (2020).

[12] Bordi, L. et al. Differential diagnosis of illness in patients under investigation for the novel coronavirus (SARS-CoV-2), Italy, February 2020. Euro Surveill. 25, 2000170 (2020).

[13] Han, H., Luo, Q., Mo, F., Long, L. & Zheng, W. SARS-CoV-2 RNA more readily detected in induced sputum than in throat swabs of convalescent COVID-19 patients. Lancet Infect. Dis. 20, 655–656 (2020).

[14] Xie, X. et al. Chest CT for typical 2019-nCoV pneumonia: relationship to negative RT-PCR testing. Radiology 296, E41–E45 (2020).

[15] Nature Biosensors—Latest Research and Reviews. [(accessed on 17 July 2020)]; Available online: https://www.nature.com/subjects/biosensors

[16] Sanders, G.H.W.; Manz, A. Chip-based microsystems for genomic and proteomic analysis. Trends Anal. Chem. 2000, 19, 364–378

[17] Solinas Toldo, S.; Lampel, S.; Stilgenbauer, S.; Nickolenko, J.; Benner, A.; Dohner, H.;

Cremer, T.; Lichter, P. Matrix-based comparative genomic hybridization: Biochips to screen for genomic imbalances. Genes Chromosomes Cancer 1997, 20, 399–407.

[18] Michalet, X.; Kapanidis, A.N.; Laurence, T.; Pinaud, F.; Doose, S.; Pflughoefft, M.; Weiss, S. The power and prospects of fluorescence microscopies and spectroscopies. Annu. Rev. Biophys. Biomol. Struct. 2003, 32, 161–182.

[19] Webb, S.E.D.; Roberts, S.K.; Needham, S.R.; Tynan, C.J.; Rolfe, D.J.; Winn, M.D.; Clarke, D.T.; Barraclough, R.; Martin-Fernandez, M.L. Single-molecule imaging and fluorescence lifetime imaging microscopy show different structures for high- and low-affinity epidermal growth factor receptors in A431 cells. Biophys. J. 2008, 94, 803–819.

[20] Grifoni, A., Sidney, J., Zhang, Y., Scheuermann, R. H., Peters, B., & Sette, A. (2020). A sequence homology and bioinformatic approach can predict candidate targets for immune responses to SARS-CoV-2. Cell Host & Microbe, 27(4), 671–680.e672. doi: https://doi.org/10.1016/j.chom.2020.03.002.

[21] Zhang, Y.-Z., Holmes, E.C., 2020. A genomic perspective on the origin and emergence of SARS-CoV-2. Cell 181 (2), 223–227. https://doi.org/10.1016/j.cell.2020.03.035.

[22] Alifano, M., Alifano, P., Forgez, P., Iannelli, A., 2020. Renin-angiotensin system at the heart of COVID-19 pandemic. Biochimie 174, 30–33. https://doi.org/10.1016/j. biochi.2020.04.008.

[23] Guan,W.-J., Ni, Z.-Y., Hu, Y., Liang, W.-H., Ou, C.-Q., He, J.-X., … Zhong, N.-S. (2020). Clinical characteristics of coronavirus disease 2019 in China. New England Journal of Medicine, 382(18), 1708–1720. doi: https://doi.org/10.1056/NEJMoa2002032.

[24] Gu, J., Han, B., Wang, J., 2020. COVID-19: gastrointestinal manifestations and potential fecal–oral transmission. Gastroenterology 158 (6), 1518–1519. https://doi.org/ 10.1053/j.gastro.2020.02.054.

[25] Wang,W., Xu, Y., Gao, R., Lu, R., Han, K.,Wu, G., Tan,W., 2020a. Detection of SARS-CoV-2 in different types of clinical specimens. JAMA 323 (18), 1843–1844. https://doi.org/ 10.1001/jama.2020.3786.

[26] Augustine, S., Singh, J., Srivastava,M., Sharma,M., Das, A.,Malhotra, B.D., 2017. Recent advances in carbon based nanosystems for cancer theranostics. [10.1039/ C7BM00008A]. Biomaterials Science 5 (5), 901–952. https://doi.org/10.1039/ c7bm00008a.

[27] Kokkinos, C., 2019. Electrochemical DNA biosensors based on labeling with nanoparticles. Nanomaterials 9 (10). https://doi.org/10.3390/nano9101361.

[28] Ozer, T., Geiss, B.J., Henry, C.S., 2020. Review-chemical and biological sensors for viral detection. J. Electrochem. Soc. 167 (3), 037523. https://doi.org/10.1149/2.0232003jes.

[29] Layqah, L.A., Eissa, S., 2019. An electrochemical immunosensor for the corona virus associated with the Middle East respiratory syndrome using an array of gold nanoparticle-modified carbon electrodes. Microchim. Acta 186 (4), 224. https://doi.org/10.1007/s00604-019-3345-5.

[30] Ishikawa, F.N., Chang, H.-K., Curreli,M., Liao, H.-I., Olson, C.A., Chen, P.-C., ... Zhou, C., 2009. Label-Free, Electrical Detection of the SARS Virus N-Protein with Nanowire Biosensors Utilizing Antibody Mimics as Capture Probes. ACS Nano 3 (5), 1219–1224. https://doi.org/10.1021/nn900086c.

[31] Draz, M.S., Shafiee, H., 2018. Applications of gold nanoparticles in virus detection. Theranostics 8 (7), 1985–2017. https://doi.org/10.7150/thno.23856.

[32] Qiu, G., Gai, Z., Tao, Y., Schmitt, J., Kullak-Ublick, G.A.,Wang, J., 2020. Dual-functional plasmonic photothermal biosensors for highly accurate severe acute respiratory syndrome coronavirus 2 detection. ACS Nano https://doi.org/10.1021/acsnano.0c02439.

[33] Mahari, S., Roberts, A., Shahdeo, D., & Gandhi, S. (2020). eCovSens-ultrasensitive novel inhouse built printed circuit board based electrochemical device for rapid detection of nCovid-19 antigen, a spike protein domain 1 of SARS-CoV-2. bioRxiv, 2020.2004.2024.059204. doi: https://doi.org/10.1101/2020.04.24.059204.

[34] Xiang, J., Yan, M., Li, H., Liu, T., Lin, C., Huang, S., & Shen, C. (2020). Evaluation of enzymelinked immunoassay and colloidal gold-immunochromatographic assay kit for detection of novel coronavirus (SARS-Cov-2) causing an outbreak of pneumonia (COVID-19). medRxiv, 2020.2002.2027.20028787. doi: https://doi.org/10.1101/ 2020.02.27.20028787.

[35] Ma, Q., Wang, J., Li, Z., Lv, X., Liang, L., Yuan, Q., 2019. Recent progress in time-resolved biosensing and bioimaging based on lanthanide-doped nanoparticles. Small 15 (32), 1804969. https://doi.org/10.1002/smll.201804969.

[36] Chen, Z., Zhang, Z., Zhai, X., Li, Y., Lin, L., Zhao, H.,…Lin, G. (2020). Rapid and sensitive detection of anti-SARS-CoV-2 IgG, using lanthanide-doped nanoparticles-based lateral flow immunoassay. Analytical Chemistry. doi: https://doi.org/10.1021/acs. analchem.0c00784.

[37] Li, S.,Ma, L., Zhou,M., Li, Y., Xia, Y., Fan, X., ... Luo, H., 2020a. Newopportunities for emerging 2D materials in bioelectronics and biosensors. Current Opinion in Biomedical Engineering 13, 32–41. https://doi.org/10.1016/j.cobme.2019.08.016.

[38] Peña-Bahamonde, J., Nguyen, H.N., Fanourakis, S.K., Rodrigues, D.F., 2018. Recent advances in graphene-based biosensor technology with applications in life sciences. Journal of Nanobiotechnology 16 (1), 75. https://doi.org/10.1186/ s12951-018-0400-z.

[39] Seo, G., Lee, G., Kim, M. J., Baek, S.-H., Choi, M., Ku, K. B., … Kim, S. I. (2020). Rapid detection of COVID-19 causative virus (SARS-CoV-2) in human nasopharyngeal swab specimens using field-effect transistor-based biosensor. ACS Nano, 14(4), 5135–5142. doi: https://doi.org/10.1021/acsnano.0c02823.

[40] Lee, H.-J., Yook, J.-G, ‘‘Biosensing using split-ring resonators at microwave regime,’’ Appl.Phys. Lett. 92, 254103 (2008)

[41] O’Hara, J.F., Singh, R., Brener, I., Smirnova, E., Han, J., Taylor, A.J., Zhang, W, ‘‘Thin-film sensing with planar terahertz metamaterials: sensitivity and limitations,’’ Opt. Express 16,1786–1795 (2008).

[42] Yadgar I. Abdulkarim1,2, Halgurd N. Awl, et al, ‘Design and study of a coronavirus-shaped metamaterial sensor stimulated by electromagnetic waves for rapid diagnosis of covid-19’, arXiv preprint arXiv:2009.08862,2020

[43] Ermolina, I., et al., Study of normal and malignant white blood cells by time domain dielectric spectroscopy. IEEE Transactions on Dielectrics and Electrical Insulation, 2001. 8(2): p. 253-261.

[44] Walser RM (2001) Electromagnetic metamaterials. In: Lakhtakia A, Weiglhofer WS, Hodgkinson IJ (eds) Complex mediums II: beyond linear isotropic dielectrics, Proc. SPIE 4467, SPIE – International Society for Optical Engineering, San Diego, CA, USA, pp. 1–15Google Scholar.

[45] R.A. Shelby, D.R. Smith, S. Schultz Experimental verification of a negative index of refraction Science, 292 (2001), pp. 77-79.

[46] M. Bakir Electromagnetic-based microfluidic sensor applications J Electrochem Soc, 164 (2017), pp. B488-B494

[47] CloseS. Mukherjee, Z. Su, L. Udpa, S. Udpa, A. Tamburrino Enhancement of microwave imaging using a metamaterial Lens IEEE Sens J, 19 (13) (2019), pp. 4962-4971.

[48] WJ, Antenna properties improvement by means of modern technology—Metamaterials as a modified substrate and/or superstrate. In: 20th M&RW, MIKON 2014, 20th International Conference on Microwave, Radar and Wireless Communications. Vol. 2. Gdansk, Poland: MIKON; 2014. pp. 637-640. ISBN 978-83-931525-2-0

[49] PrathabanMookiah, and Kapil R. Dandekar “Metamaterial substrate antenna array for MIMO communication system,” IEEE transactions on antennas and propagation, vol. 57, no. 10, October 2009

[50] ShridharE.Mendhe and Yogeshwar Prasad Kosta, ‘‘Metamaterial properties and applications,’’ International journal of information technology and knowledge management January-June 2011, Volume 4, No. 1, pp. 85-89

[51] S. Raghavan and V. Rajeshkumar, ‘‘An overview of metamaterials in biomedical applications,’’ Piers Proceedings, Taipei, March 25-28, 2013

[52] T. J.Cui , D.R.S mith, R.Liu, ‘‘Metamaterials Theory Design and Applications,’’ Springer.2010.

[53] N. Engheta, R. W. Ziolkowski, ‘‘Metamaterials Physics and engineering explorations,’’ IEEE.2006.

[54] Steven M. Anlage, ‘‘The physics and applications of superconducting metamaterials,’’ Journal of Optics, Volume 13, Number 2

[55] Shamonina, E., Solymar, L, ‘‘Properties of magnetically coupled metamaterial elements. ,’’ J.Magn. Magn.Mater. 300, 38–43 (2006).

[56] Syms, R.R.A., Shamonina, E., Kalinin, V., Solymar, L, ‘‘A theory of metamaterials based on periodically loaded transmission lines: interaction between magneto inductive and electromagnetic waves,’’ J. Appl. Phys. 97, 064909 (2005).

[57] Baena, J.D., Jelinek, L., Marques, R., Mock, Gollub, J., Smith, D.R, ‘‘Isotropic frequency selective surfaces made of cubic resonators,’’Appl Phys. Lett. 91, 191105 (2007).

[58] Alu, A., Engheta, N, ‘‘Achieving transparency with plasmonic and metamaterial coatings,’’ Phys. Rev. E 72, 016623 (2005).

[59] Milton, G.W., Nicorovici, N.P, ‘‘On the cloaking effects associated with anomalous localized resonance,’’ Proc. R. Soc. A 462, 3027–3059 (2006).

[60] Leonhardt, U, ‘‘Optical conformal mapping,’’ Science 312, 1777–1780 (2006)

[61] Pendry, J.B., Schurig, D., Smith, D.R, ‘‘Controlling electromagnetic fields,’’ Science 312,1780–1782 (2006).

[62] Greenleaf, A., Lassas, M., Uhlmann, G, ‘‘non-uniqueness for Calder´on’s inverse problem,’’ Math. Res. Lett. 10, 685–693 (2003)

[63] Cummer, S.A., Popa, B.-I., Schurig, D., Smith, D.R., Pendry, J, ‘‘Full-wave simulations of electromagnetic cloaking structures,’’ Phys. Rev. E 74, 036621 (2006)

[64] Schurig, D., Mock, J.J., Justice, B.J., Cummer, S.A., Pendry, J.B., Starr, A.F.S., Smith, D.R, ‘‘Metamaterial electromagnetic cloak at microwave frequencies,’’ Science 314, 977–980 (2006).

[65] Liang, Z., Yao, P., Sun, X., Jiang, X, ‘‘The physical picture and the essential elements of the dynamical process for dispersive cloaking structures,’’ Appl. Phys. Lett. 92, 131118 (2008).

[66] Valentine, J.; Zhang, S.; Zentgraf, T.; Ulin-Avila, E.; Genov, D.A.; Bartal, G.; Zhang, X. Three dimensional optical metamaterial exhibiting negative refractive index. Nature 2008, 455, 376–379.

[67] Von Hippel, and R. Arthur, “Dielectrics and Waves,” Cambridge, MA: MIT Press, 1954.

[68] Engheta, N., and R. Ziolkowski, (eds.), “Metamaterials Physics and Engineering Explorations,” New York: John Wiley & Sons, 2006.

[69] www.wave-scattering.com/negative.html.

[70] Lamb, H., ‘‘On Group-Velocity,’’ Proc. London Math.Soc. 1, 1904, pp. 473--479.

[71] Veselago, V. G., and E. E. Narimanov, ‘‘The Left Hand of Brightness: Past, Present andFuture of Negative Index Materials,’’ Nature Materials 5, 2006, pp. 759—762

[72] Sihvola, A., ‘‘Metamaterials in Electromagnetics,’’ Metamaterials, Vol. 1, Issue 1, 2007,pp. 2--11.

[73] Shamonina, E., and L. Solymar, ‘‘Metamaterials: How the Subject Started,’’ Metamaterials, Vol. 1, Issue 1, 2007, pp. 12--18.

[74] Smith DR, Schultz S, Markos P, Soukoulis CM. Determination of effective permittivity and permeability of metamaterials from reflection and transmission coefficients. Phys Rev B 2002;65:195104.10.1103/PhysRevB.65.195104

[75] Li, Z., K. Aydin, and E. Ozbay, "Determination of the effective constitutive parameters of bianisotropic metamaterials from reflection and transmission coeffcients, " Phys. Rev. E, Vol.79, 026610-1-7, 2009.

[76] Constantine, A. B, "Advanced Engineering Electromagnetics," John Wiley & Sons, 1989.

[77] U. C. Hasar and J J. Barroso, "Retrieval approach for determination of forward and backward wave impedances of bianisotropic metamaterials," Progress In Electromagnetics Research, Vol. 112, 109-124, 2011

[78] Barroso, J. J. and U. C. Hasar, "Resolving phase ambiguity in the inverse problem of transmission/reflection measurement methods," Int. J. Infrared Milli. Waves, Vol. 32, 857-866, 2011.

[79] D Bensafieddine, F Djerfaf, F Chouireb, D Vincent, "Design of tunable microwave transmission lines using metamaterial cells," Applied Physics A 123 (4), 248

[80] Yadgar I. Abdulkarim,Lianwen Deng, Muharrem Karaaslan, Olcay Altıntaş, et al., ," Novel Metamaterials-Based Hypersensitized Liquid Sensor Integrating Omega-Shaped Resonator with Microstrip Transmission Line," Sensors 2020, 20(3), 943; https://doi.org/10.3390/s20030943

[81] C. Mackin et al., "Chemical sensor systems based on 2D and thin film materials," 2D Mater., vol. 7, no. 2, Feb. 2020, Art. no. 022002, doi: 10.1088/2053-1583/ab6e88.

[82] C. B. Reid, G. Reese, A. P. Gibson and V. P. Wallace, IEEE Journal of Biomedical and Health Informatics, 2013, 3, 363–367.

[83] P. C. Ashworth, E. Pickwell-MacPherson, S. E. Pinder, E. Provenzano, A. D. Purushotham, M. Pepper, V. P. Wallace, and Ieee, Terahertz spectroscopy of breast tumors, 2007.

[84] C. Gabriel, Compilation of the Dielectric Properties of Body Tissues at RF and Microwave Frequencies, RadiofrequencyRadiation Division, Brooks Air Force Base, San Antonio,TX, USA, 1996, http://www.dtic.mil/cgi-bin/GetTRDoc?AD=ADA309764.

[85] Caroline B. Reid, George Reese, Adam P. Gibson, and Vincent ,'' Terahertz Time-Domain Spectroscopy of Human Blood,'' IEEE journal OF biomedical and health informatics, VOL. 17, NO. 4, july 2013.

[86] Ammar Guellab, Qun Wu, " Modeling Human Body Using Four-Pole Debye Model in Piecewise Linear Recursive Convolution FDTD Method for the SAR Calculation in the Case of Vehicular Antenna," International Journal of Antennas and Propagation,Volume 2018, Article ID 2969237, 9 pages, https://doi.org/10.1155/2018/2969237.

[87] Dawsmith, W., et al., Microwave Frequency Dependent Dielectric Properties of Blood as a Potential Technique to Measure Hydration. IEEE Access, 2020.

[88] Garyfallou, G.-Z., et al., Electrochemical detection of plasma immunoglobulin as a biomarker for Alzheimer's disease. Sensors, 2017. 17 (11): p. 2464.

[89] Abdulkarim, Y.I., et al., The Detection of Chemical Materials with a Metamaterial-Based Sensor Incorporating Oval Wing Resonators. Electronics, 2020. 9(5): p. 825.

[90] Karatepe, A., et al., Multipurpose chemical liquid sensing applications by microwave approach. PloS one, 2020. 15(5): p. e0232460.

[91] Abdulkarim, Y.I., et al., Novel metamaterials-based hypersensitized liquid sensor integrating omega-shaped resonator with microstrip transmission line. Sensors, 2020. 20(3): p. 943.

[92] Tan, L., et al., Lymphopenia predicts disease severity of COVID-19: a descriptive and predictive study. Signal transduction and targeted therapy, 2020. 5(1): p. 1-3.

[93] Ermolina, I., et al., Study of normal and malignant white blood cells by time domain dielectric spectroscopy. IEEE Transactions on Dielectrics and Electrical Insulation, 2001. 8(2): p. 253-261.

[94] F. Yavari and N. Koratkar, "Graphene-based chemical sensors," J. Phys. Chem. Lett., vol. 3, no. 13, pp. 1746–1753, Jul. 2012, doi: 10.1021/jz300358t.